# Self-Assembly of Block Copolymers in Solution Controlled by the Intermolecular Interactions

A Doctoral Thesis

by

**Rintaro Takahashi**

Submitted to
the Graduate School of Science, Osaka University

August, 2016

## ACKOWLEDGEMENTS

This study was carried out from April 2014 to July 2016 at Department of Macromolecular Science, Osaka University under the supervision of Professor Takahiro Sato. I express my gratitude for his kind guidance and numerous invaluable comments. Professor Akihito Hashidzume (Osaka University) gave many advices and reviewed this thesis. Associate Professor Ken Terao (Osaka University) instructed the SAXS measurements and reviewed this thesis. The polymer samples of PIPOZ-*b*-PNIPAM (used in Chapter 4) was synthesized by Professor Françoise M. Winnik (University of Montreal) and Doctor Xing-Ping Qiu (University of Montreal). Professor Winnik made many fruitful comments on this study. The polymer samples of ionic-neutral block copolymers, PM and PA (used in Chapters 2 and 3), were kindly provided by Associate Professor Shin-ichi Yusa (University of Hyogo), and he allowed me to use the TEM apparatus. Professor Tadashi Inoue (Osaka University) reviewed this thesis. Fluorescence lifetime measurement was performed at Horiba, Ltd., coordinated by Doctor Yasushi Nakata. SAXS experiments were conducted on SPring-8 under the approval by the JASRI (Proposal No. 2010G080, 2011B1068, 2014B1715, 2014B1087, 2015A1804, and 2015B1674) with the help by Doctor Noboru Ohta (Japan Synchrotron Radiation Research Institute; JASRI), and on KEK-PF under the approval by the PF-PAC (Proposal No. 2013G516). This work was financially supported in part by Grant-in-Aid for JSPS Fellows (Grant No. 16J00359). I appreciate very much the supports from them.

Rintaro Takahashi

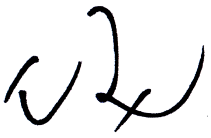

Grenoble
July 2016

## CONTENTS

# Chapter 1. General Introduction

## 1. 1. Main Purpose of This Thesis

Block copolymers can form various morphologies of micelles in selective solvents and attract much attention. Because such block copolymers are expected to be used as drug delivery systems, the attention is not limited to be in academic field. When micelles are injected into the blood vessel in a drug delivery system, it must be stable and not be dissociated into unimers, so that the critical micelle concentration (cmc) must be very low. Polymer micelles are superior to small molecular micelles due to their stability and much lower cmc. However, the stability of the polymer micelle makes the inclusion of drugs difficult. To include drugs into the polymer micelle effectively, drugs may be added (under stirring) to a physiological saline solution where the block copolymer is molecularly dispersed, and then the block copolymer is forced to form the micelle by changing some external conditions. Stimulus responsive block copolymers are therefore suitable for drug delivery systems.

The formation and dissociation of the micelle, as well as the morphology of the micelle, are governed by the intermolecular interaction of block copolymer chains. In spite of the importance, the relation between the intermolecular interaction and micellization and also micellar morphology has not been established. The main purpose of this thesis is to establish the relation to control the micellization behavior by the intermolecular interactions.

## 1. 2. Intermolecular Interactions and Self-Assembly Morphology in Block Copolymer Solutions

Intermolecular interactions play important roles in the self-assembly behavior of block copolymers in solution. Intermolecular interactions in a solution of a diblock copolymer composed of A and B monomers dissolved in a solvent (S) are specified by three interaction parameters between the A monomer unit and S, $\chi_{AS}$, between the B monomer unit and S, $\chi_{BS}$, and between the A and B monomer units, $\chi_{AB}$, as shown in Figure 1-1. If the solvent S is a good solvent to the A (B) block chain, $\chi_{AS}$ ($\chi_{BS}$) is close to zero, and if S is poor to the A (B) block chain, $\chi_{AS}$ ($\chi_{BS}$) is a larger value. Similarly, $\chi_{AB}$ increases with decreasing the affinity between the A and B monomer units. The interaction parameters $\chi_{AS}$ and $\chi_{BS}$ can be changed by the solvent conditions, e.g., by changing the solvent composition in a mixed solvent, or by

changing temperature for block copolymers where the A or B block chain is a thermosensitive polymer.

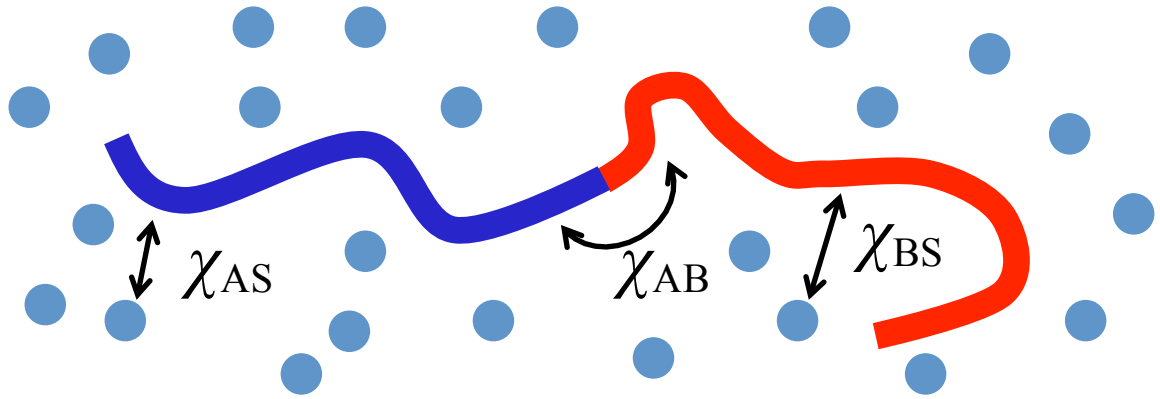


**Figure 1-1.** Schematic illustration of a diblock copolymer in solution and the three interaction parameters.

It is well known that polymer micelles can take three different morphologies, the spherical micelle, the cylindrical micelle, and bilayer vesicle (cf. Figure 1-2a-c). The micellar morphology depends on the ratio of the degrees of polymerization of the A and B block chains, and also by other external conditions mentioned below.

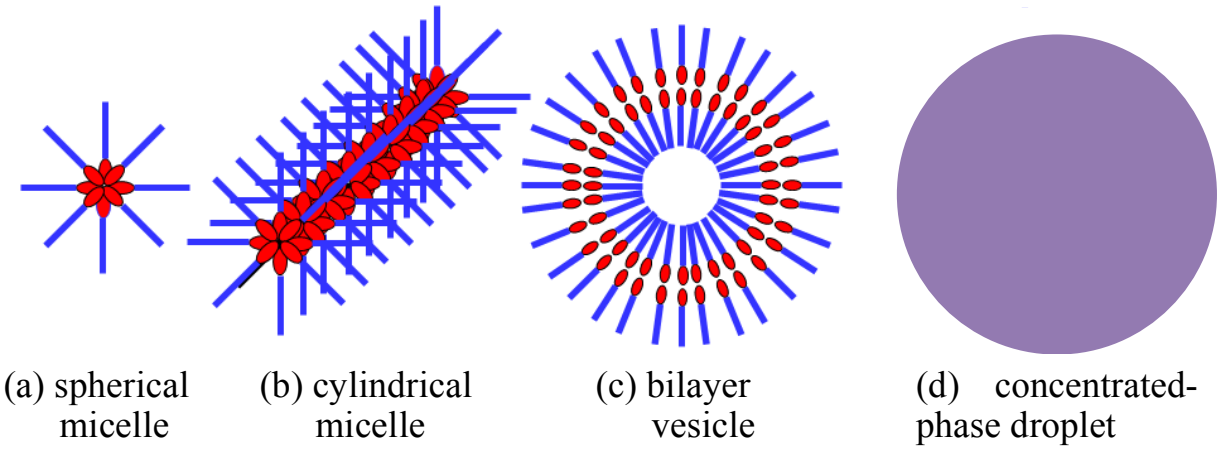


**Figure 1-2.** Various types of the self-assembly morphology of block copolymers in solution.

Recently, Takahashi et al. [1] and Sato et al. [2] found that when the amphiphilicity of the block copolymer is weak, i.e., $\chi_{AS}$ and $\chi_{BS}$ is not so much different, the block copolymer did not form any micelles but the block copolymer solution underwent a liquid-liquid phase separation. When the interfacial tension between the coexisting dilute and concentrated

phases is high enough, ten to hundred nanometer sized concentrated-phase droplets exist in the phase-separating block copolymer solution (Figure 1-2d). It is important to understand how the interaction parameters control the micellization and phase separation in block copolymer solutions. The following two sections deal with this problem theoretically.

## 1. 3. Phase Separation in Block Copolymer Solutions

According to the Flory-Huggins theory [3], the mixing Gibbs energy density (per unit cell of the lattice) $\Delta g_h$ for a homogeneous solution of the molecularly dispersed block copolymer is given by

$$\frac{\Delta g_h}{k_B T} = \phi_S \ln \phi_S + \frac{\phi_P}{P} \ln \phi_P + \bar{\chi} \phi_S \phi_P \tag{1-1}$$

where $k_B$ is the Boltzmann constant, $T$ is the absolute temperature, $\phi_S$ and $\phi_P$ are the volume fractions of the solvent and copolymer, respectively ($\phi_S + \phi_P = 1$), and $P$ is the number of segments per copolymer chain. In the last term of the above equation, $\bar{\chi}$ is the average interaction parameter defined by

$$\bar{\chi} \equiv x_A \chi_{AS} + x_B \chi_{BS} - x_A x_B \chi_{AB} \tag{1-2}$$

Here, $x_A$ and $x_B$ are the mole fractions of A and B segments in the copolymer chain. When the numbers of A and B segments per chain are denoted as $P_A$ and $P_B$ ($P = P_A + P_B$), $x_A = P_A / P$ and $x_B = P_B / P$.

When the solvent S is good for both A and B block chains, the magnitude of $\bar{\chi}$ is small and the plot of $\Delta g_h$ against $\phi_P$ provides a curve convex downward. If the solvent S becomes poor for A or B block chain or for both chains, $\bar{\chi}$ increases and the plot of $\Delta g_h$ vs. $\phi_P$ exhibits a bump as shown by the solid curve in Figure 1-3 (where $P = 100$, $x_B = 0.5$, and $\bar{\chi} = 0.8$), and one can draw a common tangent as indicated by the red broken line. Let the copolymer volume fractions at two points of contact D and C of the common tangent denote as $\phi_{P,d}$ and $\phi_{P,c}$, respectively. Then, the copolymer solution with $\phi_P$ between $\phi_{P,d}$ and $\phi_{P,c}$ undergoes the phase separation into the dilute phase with $\phi_{P,d}$ and the concentrated phase with $\phi_{P,c}$, because the mixing Gibbs energy density of the phase-separating solution is lower than that of the homogeneous solution, as indicated by the points F and E, respectively, in Figure 1-3.

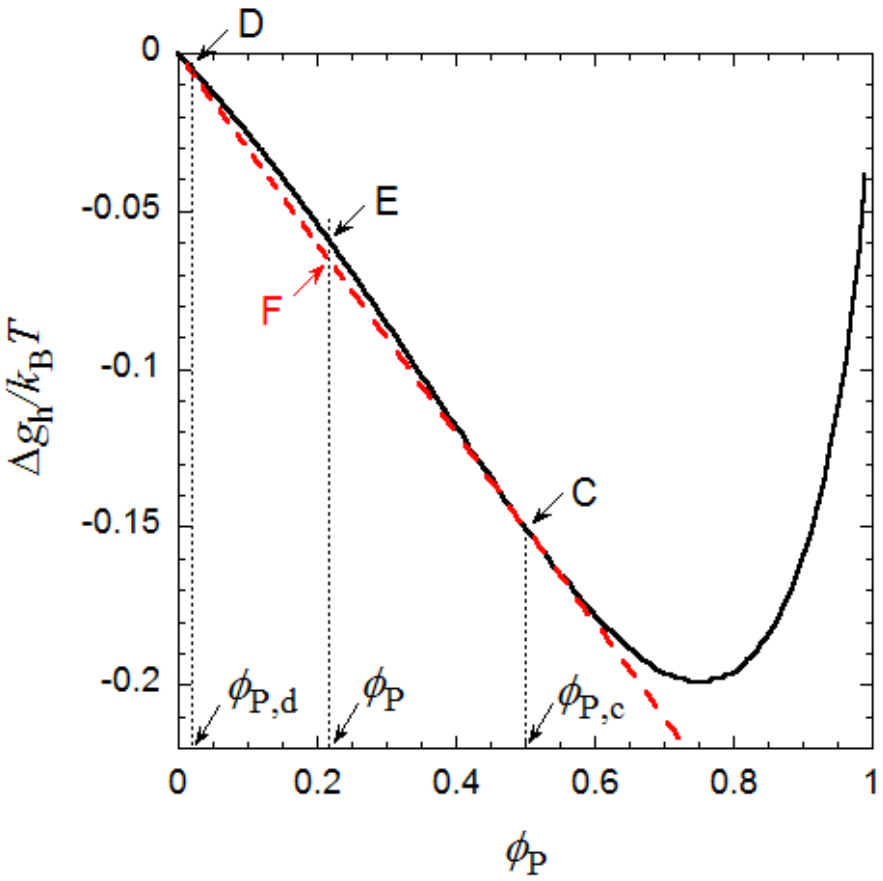


**Figure 1-3.** Plot of $\Delta g_h$ against $\phi_P$ for a homogeneous solution of the molecularly dispersed block copolymer, where $P = 100$, $x_B = 0.5$, and $\bar{\chi} = 0.8$.

## 1. 4. Micellization in Block Copolymer Solutions

If the solvent S is a selective solvent for the A-B block copolymer, the block copolymer may form a micelle. This micellization behavior can be treated by extending the Flory-Huggins theory. Let us regard the spherical micelle formed by the block copolymer chain as a thermodynamical phase with the concentration profile illustrated in Figure 1-4. In what follows, we consider an aqueous block copolymer solution where the solvent S is water or aqueous salt solution, the A block chain is hydrophilic, and the B block chain is hydrophobic. Then, the micelle has the hydrophobic core region consisting of B block chains and the hydrophilic shell region consisting of A block chains.

The volume fractions of the B chain and the solvent S in the hydrophobic core are denoted as $\phi_B$ and $\phi_{S,core}$ (= 1 − $\phi_B$), and the volume fractions of the A chain and the solvent S as $\phi_A$ and $\phi_{S,shell}$ (= 1 − $\phi_A$), respectively. The radii of the hydrophobic core $R_{core}$ and of the whole micelle $R$ may be given by

$$R_{\mathrm{core}} = aP_{\mathrm{B}}{}^{\alpha}, \quad R = a\left(P_{\mathrm{A}}{}^{\alpha} + P_{\mathrm{B}}{}^{\alpha}\right) \tag{1-3}$$

where $a$ is the size of the unit lattice cell and $\alpha$ is the scaling exponent. It is known that the exponent $\alpha$ is 1/2 in the weak segregation limit and 2/3 in the strong segregation limit. (Strictly speaking, the two scaling exponents in the core and shell regions may be different, but here we neglect the difference.) The average volume fraction $\phi_{\mathrm{P}}$ of the copolymer in the micellar phase is calculated by

$$\phi_{\mathrm{P}} = \frac{3PN_{\mathrm{P}}a^3}{4\pi R^3} \tag{1-4}$$

with the aggregation number $N_{\mathrm{P}}$ of the micelle. Using this $\phi_{\mathrm{P}}$, $\phi_{\mathrm{B}}$ and $\phi_{\mathrm{A}}$ are given by

$$\phi_{\mathrm{B}} = \frac{x_{\mathrm{B}}R^3}{R_{\mathrm{core}}{}^3}\phi_{\mathrm{P}}, \quad \phi_{\mathrm{A}} = \frac{x_{\mathrm{A}}R^3}{R^3 - R_{\mathrm{core}}{}^3}\phi_{\mathrm{P}} \tag{1-5}$$

The mean-field lattice theory gives us the mixing enthalpy density in the micellar phase $\Delta h_{\mathrm{m}}$ as

$$\frac{\Delta h_{\mathrm{m}}}{k_{\mathrm{B}}T} = \left(\chi_{\mathrm{AS}}x_{\mathrm{A}}\phi_{\mathrm{S,shell}} + \chi_{\mathrm{BS}}x_{\mathrm{B}}\phi_{\mathrm{S,core}} - \chi_{\mathrm{AB}}x_{\mathrm{A}}x_{\mathrm{B}}\right)\phi_{\mathrm{P}} \tag{1-6}$$

By extending the Flory-Huggins theory, one can count the number of ways $\omega_i$ in which the $i$-th copolymer chain ($1 \le i \le N_{\mathrm{P}}$) is inserted in the micellar phase:

$$\omega_i = \frac{27x_{\mathrm{B}}\phi_{\mathrm{P}}}{\pi P_{\mathrm{B}}{}^{\alpha}\phi_{\mathrm{B}}}\frac{(z-1)^{P-3}}{P_{\mathrm{A}}P_{\mathrm{B}}}\left[1 - \frac{\phi_{\mathrm{A}}}{N_{\mathrm{P}}}(i-1)\right]^{P_{\mathrm{A}}}\left[1 - \frac{\phi_{\mathrm{B}}}{N_{\mathrm{P}}}(i-1)\right]^{P_{\mathrm{B}}} \tag{1-7}$$

where $z$ is the coordination number of the lattice. In the micellar phase, the interface between the core and shell regions acts as the reflecting barrier for the A and B block chains. This restriction has been taken into account in the above equation, using the theory of Hoeve [4]. The mixing entropy density $\Delta s_{\mathrm{m}}$ in the micellar phase can be calculated from $\omega_i$ given by eq 1-7, just like the Flory-Huggins theory. The result is given by

$$\frac{\Delta s_{\mathrm{m}}}{k_{\mathrm{B}}} = -\frac{\phi_{\mathrm{P}}}{P}\left(\ln\varsigma + \ln\phi_{\mathrm{P}}\right) - \frac{R^3 - R_{\mathrm{core}}^3}{R^3}\phi_{\mathrm{S,shell}}\ln\phi_{\mathrm{S,shell}} - \frac{R_{\mathrm{core}}^3}{R^3}\phi_{\mathrm{S,core}}\ln\phi_{\mathrm{S,core}} \tag{1-8}$$

where $\varsigma$ is defined as

$$\varsigma = \frac{4\pi^2}{81}x_{\mathrm{A}}x_{\mathrm{B}}^{1-2\alpha}\left(x_{\mathrm{A}}^{\alpha} + x_{\mathrm{B}}^{\alpha}\right)^6 P^{2-4\alpha} \tag{1-9}$$

At last, the micellar phase has also the interfacial Gibbs energy density $\Delta g_{\mathrm{I}}$. According to Noolandi and Hong [5], $\Delta g_{\mathrm{I}}$ is written as

$$\frac{\Delta g_{\mathrm{I}}}{k_{\mathrm{B}}T} = \frac{x_{\mathrm{B}}\phi_{\mathrm{P}}}{\phi_{\mathrm{B}}P_{\mathrm{B}}{}^{\alpha}}\left[3\left(\phi_{\mathrm{A}} + \phi_{\mathrm{B}}\right)\Delta f_{12}\right]^{1/2} \tag{1-10}$$

where $\Delta f_{12}$ is given by

$$\Delta f_{12} = \tfrac{1}{4}\left[\chi_{AB}\phi_A\phi_B + \left(\chi_{BS}\phi_B - \chi_{AS}\phi_A\right)\left(\phi_B - \phi_A\right)\right]$$
$$+\frac{1}{2}\left[\left(1-\frac{1}{2}\phi_A-\frac{1}{2}\phi_B\right)\ln\left(1-\frac{1}{2}\phi_A-\frac{1}{2}\phi_B\right)-(1-\phi_A)\ln(1-\phi_A)-(1-\phi_B)\ln(1-\phi_B)\right] \quad (1\text{-}11)$$

The total mixing Gibbs energy density $\Delta g_m$ of the micellar phase is given as the sum

$$\Delta g_m = \Delta h_m - T\Delta s_m + \Delta g_I \quad (1\text{-}12)$$

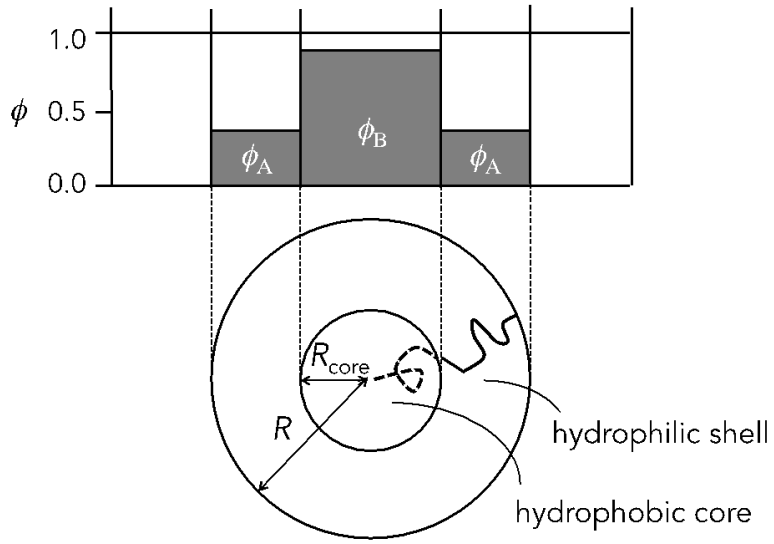


**Figure 1-4.** Concentration profile of the spherical micelle in solution.

Under the suitable condition, the micellar phase coexists with the dilute phase of the block copolymer solution. The phase equilibrium condition is just the same as in the case of the liquid-liquid phase separation explained in the above section. Figure 1-5 illustrates the plot of $\Delta g_m/k_BT$ against $\phi_P$ for the micellar phase (the red dotted and solid curves), along with the plot for the homogeneous solution (the black solid curve), which is the same curve as shown by the solid curve in Figure 1-3. The same values of $P$ (= 100), $x_B$ (= 0.5), and $\bar{\chi}$ (= 0.8) were chosen for the micellar phase and homogeneous solution, the value of $\chi_{AB}$ was fixed to be 0.3, as an example, and $\alpha$ was chosen to be 1/2. Because $\phi_B$ must be less than unity, $\phi_P$ cannot exceed 0.25 (cf. eq 1-5) for the curves of $\Delta g_m/k_BT$.

When S is the non-selective solvent where $\chi_{AS} = \chi_{BS}$ (= 0.875), the red dotted curve of the micellar phase is above the common tangent (the thin black broken line, the same line as the red broken line in Figure 1-3) for the solid curve for the homogeneous solution over whole the $\phi_P$ range. This indicates that the liquid-liquid phase separation is thermodynamically more stable than the formation of the micellar phase at any $\phi_P$ (< 0.25). However, with increasing the amphiphilicity of the copolymer, i.e., when $\chi_{BS}$ becomes considerably larger than $\chi_{AS}$ (e.g., $\chi_{BS}$ = 1.3 and $\chi_{AS}$ = 0.45), the red solid curve of the micellar phase goes down

at higher $\phi_P$, one can draw the common tangent (the thin black solid line) below the common tangent for the solid curve for the homogeneous solution. This demonstrates that the micellar phase with $\phi_P = \phi_{P,m}$ coexists with the dilute solution with $\phi_P = \phi'_{P,d}$, and the micellar phase formation becomes thermodynamically more stable than does the liquid-liquid phase separation at $\phi'_{P,d} < \phi_P < \phi_{P,m}$, as seen from the points G and F' in Figure 1-5.

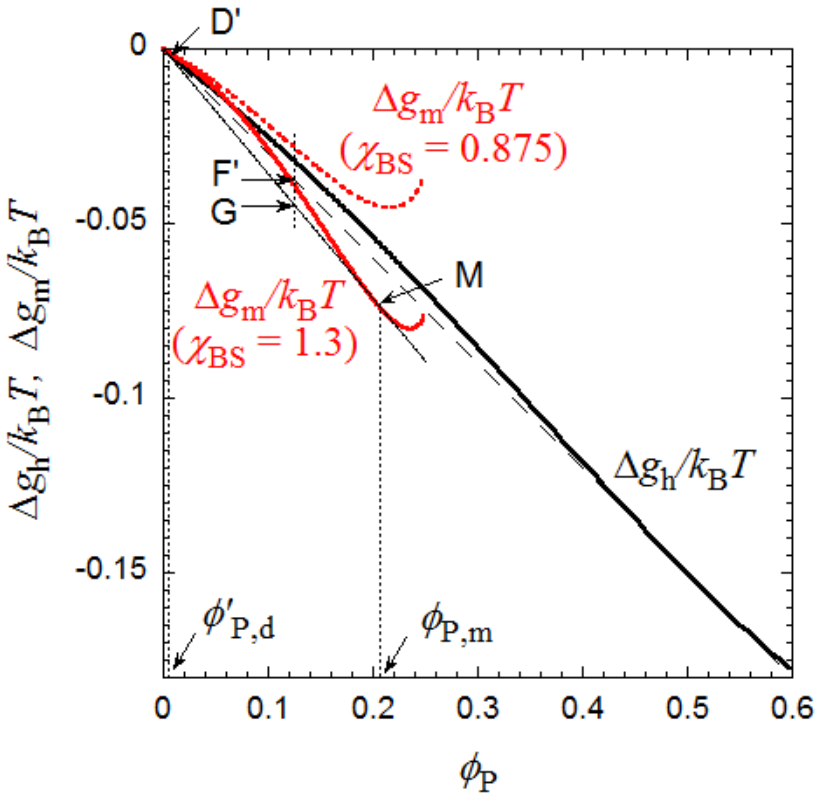


**Figure 1-5.** Plots of $\Delta g_m$ and $\Delta g_h$ against $\phi_P$ where $P = 100$, $x_B = 0.5$, and $\bar{\chi} = 0.8$. The black solid curve and dashed line are the same as the black solid curve and the red dashed line in Figure 1-3.

## 1. 5. Packing Parameter and the Micellar Morphology

The micellar morphology of various diblock copolymers in a selective solvent has been extensively investigated [6–13]. The morphology is related to the packing parameter $\lambda$, proposed by Israelachvili et al. [14,15], defined as

$$\lambda = \frac{v}{a_0 l_c} \tag{1-13}$$

where $v$, $l_c$, and $a_0$ denote the effective volume and effective length of the hydrophobic part of the block copolymer chain, and the effective area of the hydrophobic–hydrophilic part interface of the chain, respectively. As shown in Figure 1-6, when the hydrophobic part is viewed as a corn, $\lambda$ = 1/3, and when the hydrophobic part is viewed as a cylinder, $\lambda$ = 1. If corn-like hydrophobic parts of block copolymer chains aggregate, a spherical micelle is formed, and if cylindrical hydrophobic parts aggregate, a plate-like bilayer micelle is formed. Therefore, we may expect the spherical micelle at $\lambda \approx 1/3$, the bilayer disk-like micelle or vesicle at $\lambda \approx 1$, and the cylindrical micelle at an intermediate $\lambda$. $\lambda$ can be changed by changing not only the ratio of the block length but also the intermolecular interaction [6–13]. The transition of the micellar morphology may occur by the change in $a_0$ (through the repulsion among coronal block chains) or the change in $v$ (thorough the interaction between the chains in the micellar core) with varying the solvent composition.

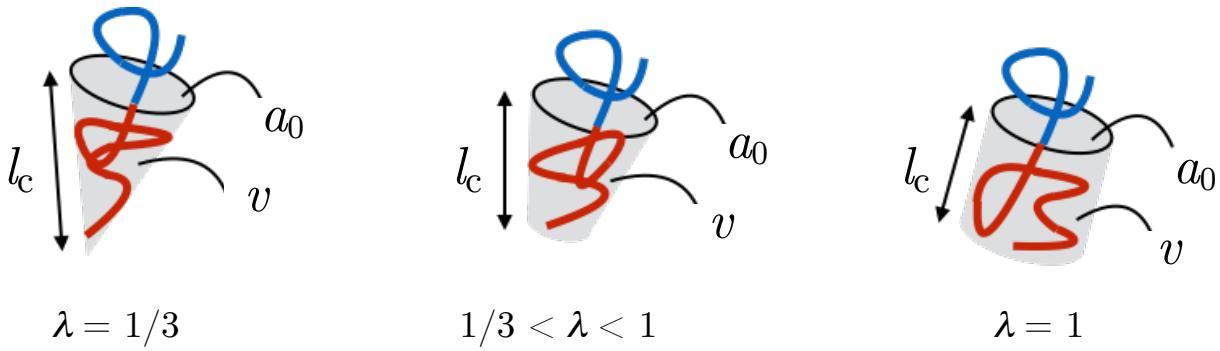


**Figure 1-6.** Schematic representation of the packing shapes of block copolymers.

## 1. 6. How to Change the Intermolecular Interaction: Stimuli-Sensitive Block Copolymers

Although there are several methods to vary the $\chi$ parameters of block copolymers, this thesis deals with the following two types of block copolymers: (i) Mixture of an anionic–neutral block copolymer and a cationic–neutral block copolymer and (ii) Thermo-sensitive block copolymers. A lot of excellent reviews and text books on the other types of polymers have been published [16–22].

**Mixture of an anionic–neutral block copolymer and a cationic–neutral block copolymer.** In 1995, Harada and Kataoka [47] first demonstrated that a mixture of an anionic–neutral block copolymer and a cationic–neutral block copolymer forms a micelle driven by the electrostatic attraction between the anionic and cationic block chains in aqueous

solution. They referred to such a micelle as “polyion complex micelle”. There have been many studies on the polyion complex formation, and such micelles are considered as good candidates for drug carriers [48–52].

Recently, Sakamoto et al. [53] investigated the morphology of the polyion complex micelle formed of a block copolymer (AP) composed of poly[sodium 2-(acrylamido)-2-methylpropanesulfonate] (PAMPS; A) and poly[2-(methacryloyloxy)ethyl phosphorylcholine] (PMPC; P) and a block copolymer (MP) consisting of poly{[3-(methacryloylamino)propyl]trimethylammonium chloride} (PMAPTAC; C) and PMPC (cf. Chart 1-1) with the different block length ratio in aqueous solution containing 0.1 M NaCl. They found that the micellar morphology is changed from the spherical micelle to the cylindrical micelle and finally to the vesicle (cf. Figure 1-2a-c) by increasing the ratio of the ionic block chain (A and M) lengths to the neutral block chain (P) lengths. The relation between the block length ratio and the morphology agrees with that of conventional micelles which assemble driven by hydrophobic interaction, as investigated by Eisenberg et al. [6].

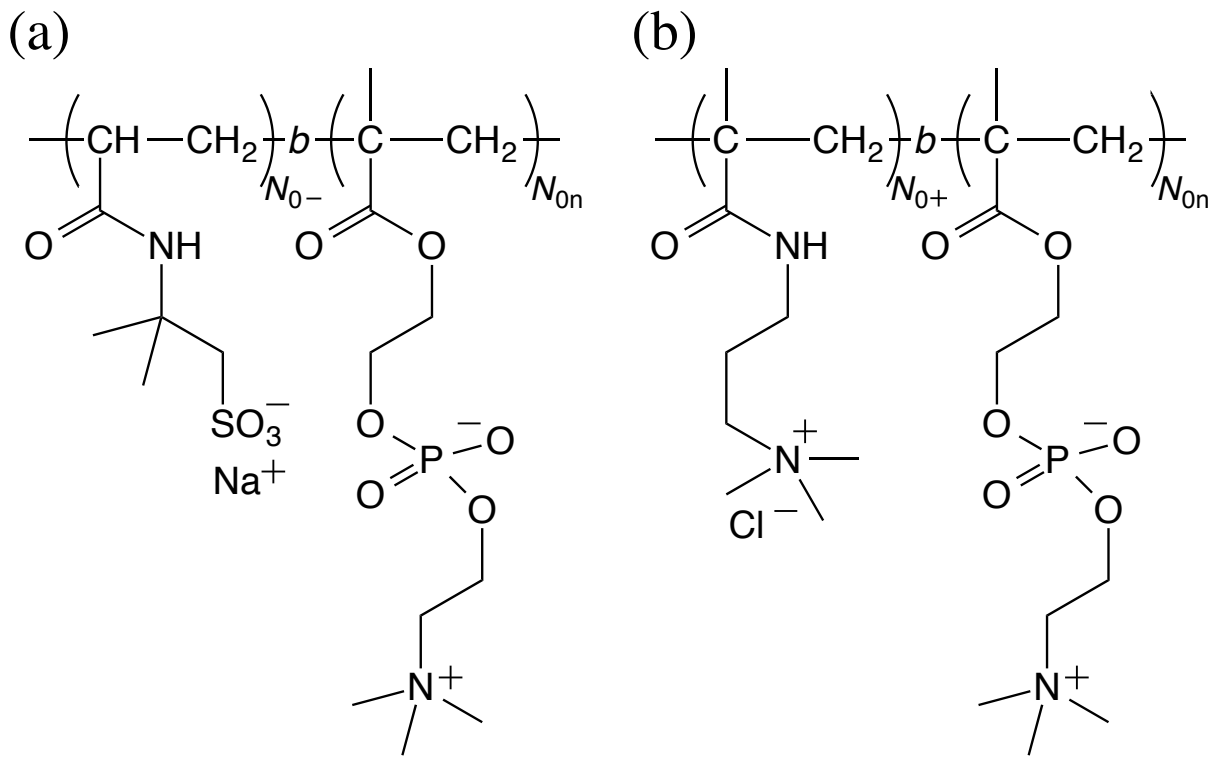


**Chart 1-1.** Chemical Structures of AP (a) and MP (b).

There are many external conditions which control the intermolecular interactions among ionic and neutral block chains in the above block copolymer mixture system, and then the self-assembly morphology of the block copolymer mixture. For example, the added salt

concentration controls the electrostatic interaction between the anionic and cationic block chains to change the affinity between the solvent water and the polyion complex formed. Hence, the salt-induced morphology transition of the micelle may take place. The mixing ratio of the two ionic-neutral block copolymers is another experimentally changeable parameter. The mixing ratio may change the composition of the polyion complex micelle formed and then the net charge of the micelle, which can affect the micellar morphology.

**Thermosensitive block copolymers.** Poly(*N*-isopropylacrylaide) (PNIPAM) [23–38] and poly(2-isopropyl-2-oxazoline) (PIPOZ) [1,24,39–46] (see Chart 1-2) are typical thermosensitive polymers which undergo the phase separation in aqueous solution upon heating. The phase separation behavior has been extensively investigated and is caused by that the water molecules dehydrate from the polymer chain with the thermal agitation.

If the block copolymer consisting of a thermosensitive polymer block and a hydrophilic polymer block, the block copolymer exists as single chains in solution at a temperature lower than the phase separation temperature. By increasing the solution temperature, the block copolymer is expected to form the micelle, because the thermosensitive block is changed from hydrophilic to hydrophobic, i.e. the amphiphilicity is increased with increasing temperature (cf. Section 1.4). There have been a lot of studies on such micellization behavior. However, most of them merely reported that the change in the hydrodynamic radius with increasing the temperature. The detail morphology or structure depending on temperature (i.e. the amphiphilicity) is far from clear, in spite of the importance in their applications.

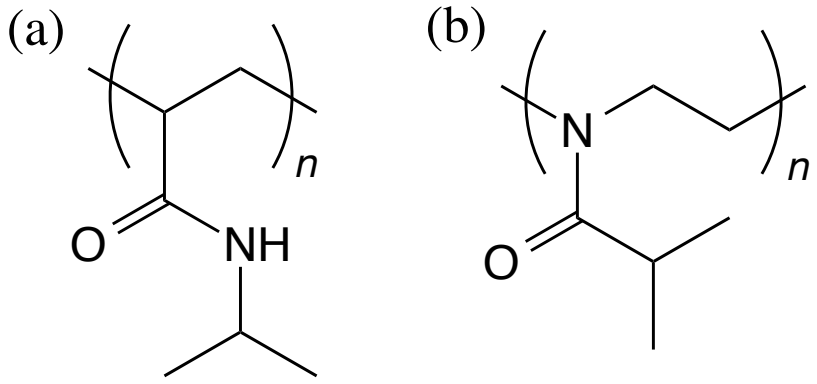


**Chart 1-2.** Chemical structures of (a) Poly(*N*-isopropylacrylaide) (PNIPAM) and (b) poly(2-isopropyl-2-oxazoline) (PIPOZ).

## 1. 7. Scope of This Work

The goal of this study is to establish the relation between the intermolecular interaction and the morphology of self-assemblies formed by block copolymers in solution. Two block copolymer systems have been chosen in this work: (i) the mixture of the anionic−neutral block copolymer (AP) and cationic−neutral block copolymer (MP) shown in Chart 1-1 and (ii) the thermosensitive block copolymer composed of PNIPAM and PIPOZ block chains shown in Chart 1-2.

Chapter 2 deals with the added salt concentration dependence of the self-assembly morphology formed by the mixture of MP and AP with an almost stoichiometric mixing ratio. As mentioned above, by changing the salt concentration the affinity between the solvent water and the polyion complex formed by M and A block chains varies, and thus the amphiphilicity of the complex of the two block copolymers MP and AP. When the ionic block chains lose their charges due to the neutralization at the complex formation, the affinity to water and then the amphiphilicity of the block copolymer complex can be drastically changed, which may strongly affect the self-assembly morphology of the complex.

In Chapter 3, the mixing ratio of the two ionic-neutral block copolymers MP and AP was changed from the stoichiometric one. This change brought about the variation in the composition of the block copolymer complex and in the electrostatic energy of the complex. As the result, a reversible micellar morphology transition was observed by addition of a solution of MP or AP to the MP-AP mixture solution. It is noted that all four morphologies depicted in Figure 1-2 were observed in aqueous solutions of the MP-AP mixture of different salt concentration and mixing ratios.

Chapter 4 is concerned with the self-assembly of the thermosensitive block copolymer PNIPAM-*b*-PIPOZ in mixtures of water and methanol. Both PNIPAM and PIPOZ are thermosensitive, and the phase separation temperatures of their aqueous solutions are almost identical. Thus, we may not expect the amphiphilicity of this block copolymer in aqueous solution. However, the phase separation temperature of PNIPAM decreases and that of PIPOZ increases in water-methanol mixtures with increasing the methanol content. Therefore, the interaction parameters $\chi_{AS}$ and $\chi_{BS}$ can be controlled by changing the methanol content and temperature, and the self-assembly behavior of PNIPAM-*b*-PIPOZ in mixtures of water and methanol was investigated at different methanol contents and temperatures.

The main results and conclusions obtained in this work are summarized in Chapter 5.

**References**


[1] T. Takahashi, T Sato, X.-P. Qiu, F. M. Winnik, Macromolecules **45,** 6111 (2012).

[2] T. Sato, K. Tanaka, A. Toyokura, R. Mori, R. Takahashi, K. Terao, S. Yusa, Macromolecules (2013).

[3] P. J. Flory, Principles of Polymer Chemistry, Cornell University Press, New York, 1953.

[4] J. Hoeve, Chem. Phys. **43,** 3007 (1965).

[5] J. Noolandi, K. M. Hong, Macromolecules **16,** 1443 (1983).

[6] Y. Mai, A. Eisenberg, Chem. Soc. Rev. **41,** 5969 (2012).

[7] L. Zhang, A. Eisenberg, Macromolecules **32,** 2239 (1999).

[8] Y.-Y. Won, A. K. Brannan, H. T. Davis, F. S. Bates, J. Phys. Chem. B **106,** 3354−3364 (2002).

[9] S. Jain, F. S. Bates, Macromolecules **37,** 1511 (2004).

[10] J. Bang, S. Jain, Z. Li, T. P. Lodge, J. S. Pedersen, E. Kesselman, Y. Talmon, Macromolecules **39,** 1199 (2006).

[11] P. Bhargava, J. X. Zheng, P. Li, R. P. Quirk, F. W. Harris, S. Z. D. Cheng, Macromolecules **39,** 4880 (2006).

[12] E. Di Cola, C. Lefebvre, A. Deffieux, T. Narayanan, R. Borsali, Soft Matter **5,** 1081 (2009).

[13] R. Lund, V. Pipich, L. Willner, A. Radulescu, J. Colmenero, D. Richter, Soft Matter **7,** 1491 (2011).

[14] J. N. Israelachvili, D. J. Mitchell, B. W. Ninham, J. Chem. Soc., Faraday Trans. 2 **72,** 1525 (1976).

[15] J. N. Israelachvili, Intermolecular and Surface Forces, 3rd ed., Academic Press, Waltham, MA, 2011.

[16] S. Mura, J. Nicolas, P. Couvreur, Nature Mater. **12,** 991 (2013).

[17] D. Schmaljohann, Adv. Drag Deliv. Rev. **58,** 1655 (2006).

[18] I. Szleifer, V. V. Tsukruk, M. Urban, F. M. Winnik, S. Zauscher, I. Luzinov, S. Minko, Nature Mater. **9,** 101 (2010).

[19] Y. Zhao, Macromolecules **45,** 3647 (2012).

[20] P. Schattling, F. D. Jochuma, P. Theato, Polym. Chem. **5,** 25 (2014).

[21] H.-J. Schneider, eds., Chemoresponsive Materials: Stimulation by Chemical and Biological Signals; RSC Smart Meterials 14, Royal Society of Chemistry, Cambridge, (2015).

[22] Reineke, ACS Macro Lett. **5,** 14 (2016).

[23] H. G. Schild, Prog. Polym. Sci. **17,** 163 (1992).

[24] V. Aseyev, H. Tenhu, F. M. Winnik, Adv. Polym. Sci. **242,** 29 (2011).

[25] A. Halperin, M. Kröger, F. M. Winnik, Angew. Chem. Int. Ed. **54,** 15342 (2015).
[26] S. J. Scarpa, D. D. Mueller, I. M. Klotz, J. Am. Chem. Soc. **89,** 6024 (1967).
[27] M. Heskins, J. E. Guillet, J. Macromol. Sci. Chem. **A2,** 1441 (1968).
[28] F. M. Winnik, Macromolecules **23,** 233 (1990).
[29] C. Wu, X. Wang, Phys. Rev. Lett. **80,** 4092 (1998).
[30] F. Afroze, E. Nies, H. Berghmans, J. Mol. Struct. **554,** 55 (2000).
[31] Y. Maeda, T. Higuchi, I. Ikeda, Langmuir **16,** 7503 (2000).
[32] K. V. Durme, G. V. Assche, B. V. Mele, Macromolecules **37,** 9596 (2004).
[33] V. Aseyev. S. Hietala, A. Laukkanen, M. Nuopponen, O. Confortini, F. E. D. Prez, H. Tenhu, Polymer **46,** 7118 (2005).
[34] Y. Ono, T. Shikata, J. Am. Chem. Soc. **128,** 10030 (2006).
[35] X. Zhou, J. Li, C. Wu, B. Zheng, Macromol. Rapid Commun. **29,** 1363 (2008).
[36] T. Kawaguchi, K. Kobayashi, M. Osa, T. Yoshizaki, J. Phys. Chem. B **113,** 5440 (2009).
[37] M Philipp, R. Aleksandrova, U. Müller, M. Ostermeyer, R. Sanctuary, P. Müller-Buschbauma, J. K. Krüger, Soft Matter **10,** 7297 (2014).
[38] M.Philipp, K. Kyriakos, L. Silvi, W. Lohstroh, W. Petry, J. K. Krüger, C. M. Papadakis, P. Müller-Buschbaum, J. Phys. Chem. B **118,** 4253 (2014).
[39] K. Aoi, M. Okada, Prog. Polym. Sci. **21,** 151 (1996).
[40] R. Hoogenboom, Angew. Chem. Int. Ed. **48,** 7978 (2009).
[41] H. Schlaad, C. Diehl, A. Gress, M. Meyer, A. L. Demirel, Y. Nur, A. Bertin, Macromol. Rapid Commun **31,** 511 (2010).
[42] H. Uyama, S. Kobayashi, Chem. Lett. **21,** 1643 (1992).
[43] C. Diab, Y. Akiyama, K. Kataoka, F. M. Winnik, Macromolecules **37,** 2556 (2004).
[44] A. L. Demirel, M. Meyer, H. Schlaad, Angew. Chem. Int. Ed. **46,** 8622 (2007).
[45] J. Zhao, R. Hoogenboom, G. V. Assche, B. V. Mele, Macromolecules **43,** 6853 (2010).
[46] Y. Katsumoto, A. Tsuchiizu, X.-P. Qiu, F. M. Winnik, Macromolecules **45,** 3531 (2012).
[47] A. Harada, K. Kataoka, Macromolecules **28,** 5294 (1995).
[48] M. A. Cohen Stuart, B. Hofs, I. K. Voets, A. de Keizer, Curr. Opin. Colloid Interface Sci. **10,** 30 (2005).
[49] I. K. Voets, A. de Keizer, M. A. Cohen Stuart, Adv. Colloid Interface Sci. **147–148,** 300 (2009).
[50] Y. Lee, K. Kataoka, Soft Matter **5,** 3810 (2009).
[51] N. Lefèvre, C.-A. Fustin, J.-F. Gohy, Macromol. Rapid Commun. **30,** 1871 (2009).
[52] D. V. Pergushov, A. H. E. Müller, F. H. Schacher, Chem. Soc. Rev. **41,** 6888 (2012).

[53] S. Sakamoto, Y. Sanada, M. Sakashita, K. Nishina, K. Nakai, S. Yusa, K. Sakurai, Polym. J. **46,** 617 (2014).

# Chapter 2. Salt Concentration Dependence of Self-Assembly of a Mixture of Anionic−Neutral and Cationic−Neutral Block Copolymers in Aqueous Solution

## 2.1. Introduction

Intermolecular interactions of block copolymers are a key factor for their self-assembly in solution [1]. For diblock copolymers, the intermolecular interactions in solution are characterized in terms of three interaction parameters: $\chi_{AS}$ between the solvent S and block chain A, $\chi_{BS}$ between the solvent S and block chain B, and $\chi_{AB}$ between the block chains A and B. Recently, Sato et al. [2−4] observed the thermally induced macroscopic phase separation and the micellization in dilute aqueous solutions of nonionic thermosensitive block copolymers [poly(2-isopropyl-2-oxazoline)-*b*-poly(2-ethyl-2-oxazoline) [2], poly(*N*-isopropylacrylamide)-*b*-poly(*N*-vinyl-2-pyrrolidone) [3], and poly(*N*-isopropylacrylamide)-*b*-poly(2-isopropyl-2-oxazoline)] [4], where the affinity of one block chain (say the block chain B) to the solvent becomes suddenly worse upon heating. When $\chi_{BS}$ increases upon heating, the average interaction parameter of the copolymer defined by $\bar{\chi} = x_A\chi_{AS} + x_B\chi_{BS} - x_Ax_B\chi_{AB}$ ($x_A$, $x_B$: the mole fractions of the A and B monomer units in the copolymer chain) also increases, and the macroscopic phase separation may take place. However, if $\chi_{BS}$ is sufficiently larger than $\chi_{AS}$, the amphiphilicity of the copolymer is so strong that the copolymer tends to form micelles. Therefore, the macroscopic phase separation and micellization occur in block copolymer solutions by a delicate balance of the interaction parameters.

In the present study, we have investigated the self-assembly behavior in aqueous solutions of anionic−neutral and cationic−neutral block copolymers mixtures, changing the intermolecular interactions by the added NaCl concentration *C*s. The block copolymers we have chosen are an anionic−neutral (AP) block copolymer composed of poly[sodium 2-(acrylamido)-2-methylpropanesulfonate] (PAMPS) and poly[2-(methacryloyloxy)ethyl phosphorylcholine] (PMPC) and an cationic−neutral (MP) block copolymer consisting of poly{[3-(methacryloylamino)propyl]trimethylammonium chloride} (PMAPTAC) and PMPC (cf. Chart 1-1), both of which were recently synthesized by Yusa et al. [5]. Here, the neutral block PMPC is an amphoteric water-soluble polymer with high biocompatibility, and its interaction parameter in aqueous solution is almost independent of the ionic strength [6]. For the aqueous solution of the copolymer mixture, we have six interaction parameters ($\chi_{AS}$, $\chi_{MS}$, $\chi_{PS}$, $\chi_{AP}$, $\chi_{MP}$, and $\chi_{AM}$) to characterize its thermodynamic properties. Here, the

subscripts A, M, P, and S represent the anionic, cationic, and neutral blocks and the solvent (aqueous NaCl), respectively. At a sufficiently high *C*s, the electrostatic attraction between the A and M block chains is screened out, and if all A, M, and P chains are hydrophilic, both AP and MP block copolymers may be molecularly dispersed in the aqueous solution. When *C*s is decreased, the electrostatic attraction between the A and M chains becomes strong (i.e., $\chi_{AM}$ becomes strongly negative), and the A and M chains form a neutral complex. Moreover, since charges of the A and M chains become neutralized, the hydrophilicity of the A and M chains reduces, which increases $\chi_{AS}$ and $\chi_{MS}$ and then decreases the solubility of the AP and MP copolymers [7−9]. However, when $\chi_{AS}$ and $\chi_{MS}$ are much larger than $\chi_{PS}$, the amphiphilicity of the AP and MP block copolymers is strong to form a micelle (polyion complex micelle or polyelectrolyte complex coacervate core micelle). When the micelle is formed, possibilities of contacts between the A or M chain and solvent are reduced, and the interaction parameters $\chi_{AS}$ and $\chi_{MS}$ do not play important roles in the micellar solution. This effect increases the solubility of the polyion complex micelle. Therefore, we can change the solubility and amphiphilicity of the AP and MP block copolymers by changing *C*s.

Furthermore, when *C*s in the solution decreases, the electrostatic attraction between the A and M chains becomes strong, and the neutral complex formed by the A and M chains squeezes more water out. As a result, the neutral complex shrinks in the aqueous solution by decreasing *C*s. If the AP and MP copolymer mixture forms a micelle in the solution, the hydrophobic part (comprising the neutral complex) of the micelle shrinks with decreasing *C*s, which may change the morphology of the micelle. Therefore, we can also expect some morphological transition of the polyion complex micelle by changing *C*s. The self-assembly in aqueous solutions of anionic−neutral and cationic−neutral block copolymer mixtures has been extensively studied for ca. two decades [10−27]. However, the competition of the macroscopic phase separation and micellization as well as the morphological transition of the micelle in such block copolymer mixture solutions by changing the ionic strength has not been investigated so far, although the self-assembly behavior of such polyion complexes is a basically important issue when they are applied to drug delivery systems [26,27].

Recently, Sakamoto et al. [20] investigated the morphological transition of micelles formed by mixtures of the AP and MP copolymers in 0.1 M aqueous NaCl with changing the ratio of the charged to the neutral block lengths for AP and MP. They found the morphological transition of the spherical micelle → cylindrical micelle → bilayer vesicle with increasing the relative lengths of the charged A and M block chains to that of the neutral P block chain. This is the same trend as amphiphilic block copolymers in selective solvents, as reported by Eisenberg et al. [1].

In the present study, we have selected a pair of AP and MP copolymer samples with A and M block chains much longer than the P block chain, expecting the formation of the vesicle at $C_S$ = 0.1 M, which is the same $C_S$ as Sakamoto et al. studied. We have studied the self-assembly behavior in aqueous AP and MP mixture solutions over a wide $C_S$ range from 0 to 2 M, by direct observation, optical and electron microscopies, and small-angle X-ray scattering (SAXS).

## 2. 2. Experimental Section

**Materials.** The AP and MP copolymer samples used in this study were synthesized, and their molecular weights were determined by Dr. Yusa at University of Hyogo. The procedures for the sample synthesis and characterization is described in ref. 5. Table 2-1 lists molecular characteristics of the AP and MP samples. Since the same neutral block chain was used as the precursor of both AP and MP samples, the weight-average degrees of polymerization $N_{0,P}$ of the neutral block chains of the two samples were identical to each other. Weight-average degrees of polymerization $N_{0,A}$ and $N_{0,M}$ of the anionic and cationic block chains were considerably higher than $N_{0,P}$. The molecular-weight dispersity of the anionic block chain was considerably wider than those of the cationic and neutral block chains. The water was purified by using a Millipore Milli-Q system.

**Table 2-1. Molecular Weight Characteristics of the AP and MP Samples**

| sample | $M_{n1}$[a] | $M_{w1}/M_{n1}$[b] | $M_{w1}$[c] | $M_{w1,P}$[d] | $M_{w1,A}$[d] | $M_{w1,M}$[d] | $N_{0,P}$[e] | $N_{0,A}$[e] | $N_{0,M}$[e] |
|---|---|---|---|---|---|---|---|---|---|
| PMPC | 6210 | 1.03 | 6400 | | | | | | |
| AP | 47200 | 1.56 | 73600 | 6400 | 67200 | | 21.7 | 293 | |
| MP | 49300 | 1.09 | 53700 | 6400 | | 47300 | 21.7 | | 215 |

[a]Number-average molecular weight determined by $^1$H NMR. [b]Dispersity index determined by SEC. [c]Weight-average molecular weight calculated from $M_{w1}/M_{n1}$ and $M_{n1}$. [d]Weight-average molecular weight of the neutral block chain $M_{w1,P}$, the anionic block chain $M_{w1,A}$, or the cationic block chain $M_{w1,M}$ calculated from $M_{w1}$ of the PMPC, AP, or MP samples. [e]Weight-average degree of polymerization of each block chain using the monomer-unit molar mass $M_{0,P}$ = 295, $M_{0,A}$ = 229, or $M_{0,M}$ = 220.5.

**Preparation of Test Solutions.** The MP and AP samples were separately dissolved in pure water, and then the MP solution was poured into the AP solution slowly and the mixture solution was shaken by a vortex mixer. An hour before the following experiments, solid NaCl was added into the copolymer mixture solution and stirred immediately. The salt concentration is specified by the molar concentration $C_S$ of NaCl. The X-ray scattering intensity of the mixture solution did not change with time at least for 50 h after adding NaCl.

Preliminary transmittance electron microscopic observations indicated that stable vesicles were formed at the mole fraction $x_+$ of cations borne by MP in the total charges borne by AP and MP to be 0.6. Thus, in the present study, the mixing ratio of AP and MP was fixed at $x_+ = 0.6$. This mixing ratio corresponds to 0.599 of the weight fraction $w_{MP}$ of MP in the total copolymer mixture.

**Optical and Electron Microscopy.** Solutions of MP−AP mixtures were observed at 25 °C by using a BX53 optical microscope (Olympus Corporation, Tokyo) and a transmittance electronmicroscope (TEM) (JEM-2100, JEOL Ltd., Tokyo). Samples for the TEM observation were prepared as follows: a drop of the test solution (the total polymer mass concentration $c = 0.005$ g/cm$^3$) was placed on a copper grid which was coated with Formvar film and plasma-irradiated, and then the drop was blotted. The sample was stained by an aqueous solution of sodium phosphotungstate (0.2wt%), and the excess solution was also blotted. The stained sample was dried under vacuum to make the TEM observation.

**Small-Angle X-ray Scattering.** SAXS experiments were conducted at 25 °C on two facilities at SPring-8, Hyogo, Japan, and the photon factory (PF) of KEK, Ibaraki, Japan. The BL40B2 beamline in SPring-8 equipped with an imaging plate detector R-AXIS VII (Rigaku Corporation, Tokyo) was chosen for this study. The incident X-ray was polarized, and the wavelength was 0.1 nm. The camera length and the accumulation time were 4.17 m and 180 s, respectively. We used the BL-10C beamline in PF equipped with a PILATUS3 2M detector (Dectris Ltd., Baden). The incident beam was polarized, and the wavelength was chosen to be 0.1488 nm, while the camera length and the accumulation time were 2.05 m and 180 s, respectively. No significant difference was observed on the SAXS profiles for identical solutions measured in the two beamlines. It was checked that SAXS intensity profiles were not changed by irradiations (180 s) repeated twice, indicating no sample damages by at least one irradiation. Scattering intensities were measured down to lower scattering angles in SPring-8 than in KEK-PF because of the different camera lengths and the size of the beam stoppers. A capillary cell with a 1.9 mm diameter was used for each measurement. The test solutions with different $C_S$ were prepared by addition of NaCl to the fresh salt-free copolymer solution at each time to reduce the sample damage by irradiation.

The excess scattering intensity $I_\theta$ over that of the solvent was transformed to the excess Rayleigh ratio $R_\theta$ using aqueous solutions of poly(ethylene glycol) (PEG) as the standard sample (cf. eq 2-A1 in the Appendix 2). The total polymer mass concentration $c$ in the solution was fixed at 0.005 g/cm$^3$.

## 2. 3. Results and Discussion

**Macroscopic Liquid−Liquid Phase Separation.** At $C$s = 2 and 1 M, aqueous dilute solutions of the mixture of MP and AP with $x_+ = 0.6$ were almost transparent, but we observed liquid−liquid phase separations in aqueous dilute solutions of the MP−AP mixture of $x_+ = 0.6$ at 1 M > $C_S$ > 0.4 M. Figure 2-1a shows a photograph of a macroscopically phase-separating solution with $C_S$ = 0.6 M and $c$ = 0.01 g/cm$^3$ in a tube. The separating upper and bottom phases are the coexisting dilute and concentrated phases. We observed the phase separation in the copolymer mixture solutions also by optical microscopy, as shown in Figure 2-1b, where spherical objects are phase-separating concentrated-phase droplets.

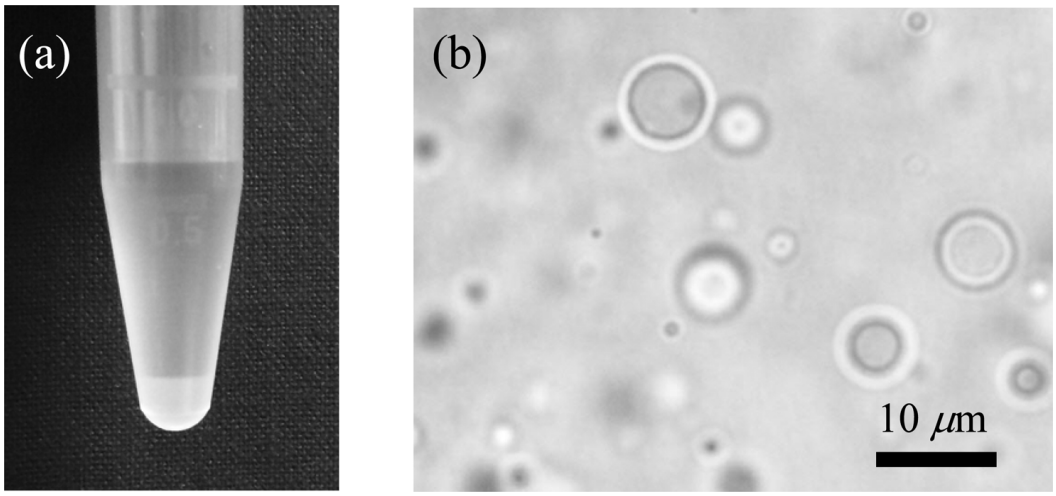


**Figure 2-1.** (a) Photograph and (b) optical micrograph of phase separating aqueous solutions of a MP−AP mixture with $x_+ = 0.6$ at $C_S$ = 0.6 M; the total copolymer concentration $c$ = 0.01 g/cm$^3$ in panels a and $c$ = 0.005 g/cm$^3$ in panel b.

From the existence of spherical objects in optical micrograph images, we judged whether the solution is in one-phase or two-phase region. Figure 2-2 shows the phase diagram, where the total mass concentration $c$ of the copolymer mixture and the molar concentration $C_S$ of NaCl are selected as the horizontal and vertical axes, respectively, and

filled and unfilled circles indicate the two-phase and one-phase, respectively. From this phase diagram, we can say that the mixture solution with $c$ = 0.005 g/cm$^3$ (as indicated by the vertical dashed line) is in the two-phase region at 1.0 M > $C_S$ > 0.4 M.

At a sufficiently high $C_S$, the electrostatic attraction between the A and M block chains is screened out, and if all A, M, and P block chains are hydrophilic, both AP and MP block copolymers may dissolve in the solution. When $C_S$ is decreased, the electrostatic attraction between the A and M block chains becomes strong enough to form a neutral complex, and the neutralization of the A and M block chains weakens the hydrophilicity of the two block copolymers to decrease their solubility [9]. However, if the amphiphilicity of the AP and MP block copolymers becomes strong with further decreasing $C_S$, AP and MP block copolymers may form polyion complex micelle. The solubility of the micelle formed in aqueous solution should increase because the hydrophobic neutral complexes of the A and M blocks are covered by the hydrophilic P block chains in the micelle. This may be the reason for the reentrant phase behavior shown in Figure 2-2.

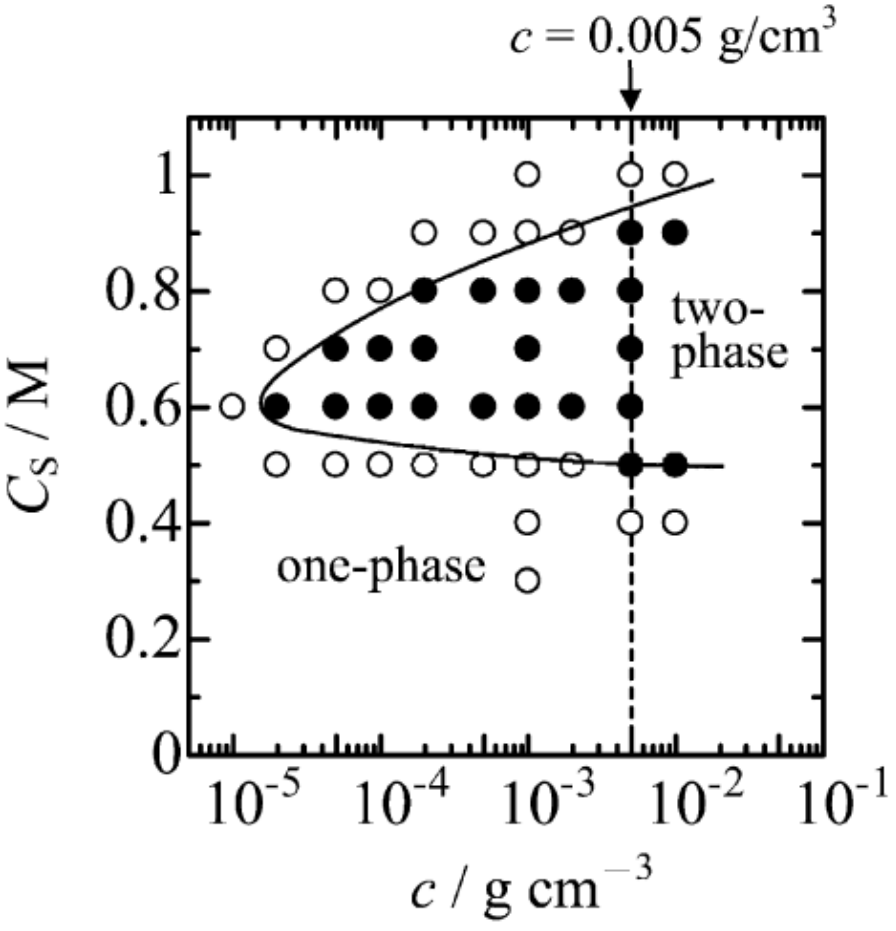


**Figure 2-2.** Phase diagram for the aqueous NaCl solution of the AP−MP mixture ($x_+$ = 0.6). Unfilled and filled circles denote one- and two-phase (macroscopically), respectively.

To examine the role of the neutral block PMPC chain in the phase behavior, we have made the same experiment for aqueous solutions of the PAMPS and PMAPTAC homopolymer mixture with $c$ = 0.005 g/cm$^3$ and $x_+$ = 0.6. (The weight-average molecular weights of the homopolymer samples used were both ca. 2.4 × 10$^4$, and the dispersity indices of PAMPS and PMAPTAC were 1.17 and 1.02, respectively, determined by SEC.) The biphasic region started at $C_S$ = 1.5 M for the homopolymer mixture solutions, considerably higher than for the copolymer mixture solutions, in spite of the lower molecular weights of the homopolymers. Thus, the neutral block PMPC chain appreciably increases the hydrophilicity of the block copolymer complex to reduce $C_S$ of the solubility limit to ca. 1 M, although the PMPC chain length is much shorter than the charged A and M block chains.

Yusa et al. [5] reported monotonous decreases of hydrodynamic radius with increasing $C_S$ from 0 to 1 M for aqueous solutions of three AP−MP mixtures with $N_{0,A}/N_{0,P} \sim N_{0,M}/N_{0,P} < 1$. This indicates that no phase separation takes place in their AP−MP mixture solutions. Yusa et al.'s [5] AP and MP samples have longer P block chains, so that the solubility of their AP and MP samples does not so much decrease after neutralization. Therefore, the neutral P block chain plays an important role in the solubility of the AP−MP neutral complex.

**SAXS Profiles of AP−MP Mixture Solutions at Different $C_S$.** Figure 2-3 compares SAXS profiles for aqueous solutions of the AP−MP mixture ($x_+$ = 0.6) with $c$ = 0.005 g/cm$^3$ at different NaCl molar concentrations $C_S$. In the ordinate, $K_e$ is the optical constant defined by

$$K_e = N_A a_e^2 \gamma_{av}^2 \tag{2-1}$$

with the Avogadro constant $N_A$, the classical electron radius $a_e$ (= 2.82 × 10$^{-13}$ cm), and the average contrast factor $\gamma_{av}$ (calculated from the measured or literature value [28] of the partial specific volume; see eq 2-A4). $k$ in the abscissa denotes the magnitude of the scattering vector. At $C_S$ = 2 M, the profile shows essentially no angular dependence at $k < 0.2$ nm$^{-1}$, indicating that no large self-assemblies are formed in the mixture solution. With decreasing $C_S$ from 2 M, both angular dependence and intensity itself of the profile at $k < 0.2$ nm$^{-1}$ become stronger remarkably, which demonstrates the formation of large self-assemblies of the AP−MP mixture in the solutions of the lower ionic strength. Furthermore, the profile at $C_S$ = 0.01 M has a weaker $k$ dependence ($R_\theta/K_e c \propto k^{-1}$) than that at $C_S$ = 0.1 M ($R_\theta/K_e c \propto k^{-2}$) in a low $k$ region ($k < 0.06$ nm$^{-1}$), implying different morphologies of self-assemblies at the two $C_S$. It is noted that the profiles at $C_S$ = 0.1 and 0.01 M have small broad peaks around $k$ = 0.35 and 0.25 nm$^{-1}$, respectively. (The profile at $C_S$ = 0.7 M was taken on a beamline of a shorter camera length, so that data were not obtained at $k < 0.07$ nm$^{-1}$.)

**Contribution from Neutral Complexes and Free Chains to SAXS Profiles for Biphasic Solutions.** If the AP and MP block copolymer chains exist independently in the mixture solution, the excess Rayleigh ratio for the mixture can be expressed by [29]

$$\frac{R_\theta}{K_e c} = \sum_{i=\mathrm{MP,AP}} \frac{w_i M_i P_i(k)}{1 + 2A_{2,i} M_i P_i(k) c w_i} \tag{2-2}$$

where $w_i$, $M_i$, $P_i(k)$, and $A_{2,i}$ are the weight fraction, the molar mass, the intramolecular interference factor, and the second virial coefficient of the component $i$ (= MP and AP) ($w_{\mathrm{MP}} = 1 - w_{\mathrm{AP}} = 0.599$ at $x_+ = 0.6$). The molecular parameters for the AP and MP block copolymer samples including in eq 2-2 were determined from the scattering functions of the two individual samples in 1 and 0.1 M aqueous NaCl (see Table 2-A1).

The purple solid curve for the mixture at $C_S = 2$ M in Figure 2-3 indicates the value calculated by eq 2-2, with the molecular parameters of the AP and MP samples at $C_S = 1$ M (listed in Table 2-A1). We have assumed that the molecular parameters at $C_S = 2$ M are identical with those at $C_S = 1$ M. The theoretical curve agrees with the experimental data at $C_S = 2$ M, and we can say that the AP and MP block copolymer chains are molecularly dispersed at $C_S$ as high as 2 M, where the electrostatic attraction between A and M block chains are screened out by the added salt. The scattering function for $C_S = 0.7$ M in Figure 2-3 could not be fitted by eq 2-2 using the molecular parameters for the AP and MP samples at $C_S = 1$ M, indicating the polyion complex formation by the A and M block chains due to stronger electrostatic interaction at $C_S = 0.7$ M. As mentioned in the Appendix 2, the electrophoretic light scattering (ELS) experiment indicated that the complex of AP and MP formed at $C_S = 0.1$ M was almost neutral and adsorbed a tiny amount of the excess MP in the solution with $x_+ = 0.6$, when the Henry equation [30] for the charged sphere was applied. Here, we assume that the complex of AP and MP formed at $C_S \leq 1$ M is neutral. If the mole fraction of free AP in the total AP is denoted as $x_{\mathrm{AP}}^{\mathrm{E}}$, the weight fractions of the free MP, the free AP, and the neutral complex (NC) are given by eq 2-A10. When $x_{\mathrm{AP}}^{\mathrm{E}} = 0$, all AP forms the neutral complex, and when $x_{\mathrm{AP}}^{\mathrm{E}} = 1$, no neutral complex is formed.

If the three components, AP, MP, and NC, exist independently in the solution, we have the following equation [29,31]

$$\frac{R_\theta}{K_e c} = \sum_{i=\mathrm{MP,AP}} \frac{w_i^{\mathrm{E}} M_i P_i(k)}{1 + 2A_{2,i} M_i P_i(k) c w_i^{\mathrm{E}}} + w_{\mathrm{NC}} M_{\mathrm{NC}} P_{\mathrm{NC}}(k) \tag{2-3}$$

where $w_{\mathrm{NC}}$, $M_{\mathrm{NC}}$, and $P_{\mathrm{NC}}(k)$ are the weight fraction, the weight-average molar mass, and the z-average particle scattering function, respectively, for the neutral complex. The

intermolecular interference effect for the neutral complex was neglected because of its electroneutrality.

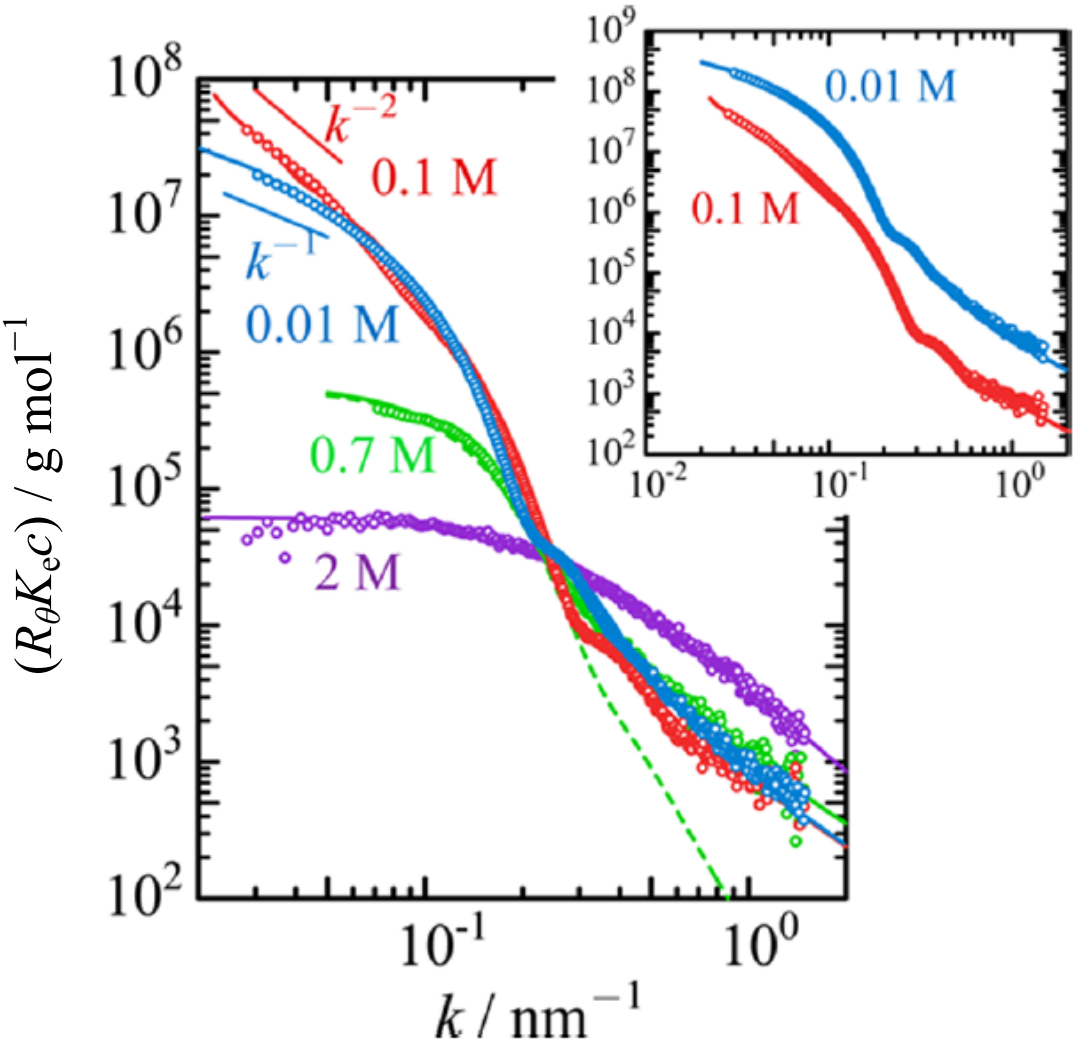


**Figure 2-3.** SAXS profiles for the AP−MP mixture in aqueous NaCl ($c$ = 0.005 g/cm$^3$, $x_+$ = 0.6) at $C_S$ = 2, 0.7, 0.1, and 0.01 M. Upper right panel: comparison of SAXS profiles at $C_S$ = 0.1 and 0.01 M (the profile at $C_S$ = 0.01 M is shifted vertically by the factor 10 for viewing clarity). Solid and dashed curves: theoretical curves explained in the text.

As seen from the phase diagram in Figure 2-2, the solution of the AP−MP mixture with $c$ = 0.005 g/cm$^3$ and $C_S$ = 0.7 M is within the biphasic region, and the polyion complex of the AP and MP block copolymers may form spherical droplets of the coexisting concentrated phase. The molar mass $M$ of the spherical droplets of the NC may not be uniform but has a dispersity. Assuming the log-normal molar mass distribution, we can express $M_{NC}P_{NC}(k)$ as

$$M_{\mathrm{NC}}P_{\mathrm{NC}}(k) = \frac{1}{\sqrt{2\pi \ln Đ_{\mathrm{NC}}}} \int P_M(k) \exp\left[ -\frac{\ln^2\left(\sqrt{Đ_{\mathrm{NC}}}\, M/M_{\mathrm{NC}}\right)}{2\ln Đ_{\mathrm{NC}}} \right] \mathrm{d}M \tag{2-4}$$

with the dispersity index $Đ_{\mathrm{NC}}$ ($\equiv M_{\mathrm{w}}/M_{\mathrm{n}}$) of the neutral complex and the particle scattering function $P_M(k)$ for the neutral complex of the molar mass $M$. The scattering functions $\mathrm{P}_M(k)$ for the spherical particle of the uniform density is given by eqs 2-A16−18.

If the molecular parameters for free AP and MP chains given in Table 2-A1 at $C_{\mathrm{S}}$ = 1 M are used, there remain $x_{\mathrm{AP}}^{\mathrm{E}}$, $M_{\mathrm{NC}}$, $Đ_{\mathrm{NC}}$, and the concentration $c_{\mathrm{c}}$ within the concentrated phase droplet as adjustable parameters in eq 2-3. Among the parameters, $M_{\mathrm{NC}}$ and $c_{\mathrm{c}}$ mainly determine the absolute value and the $k$ dependence of $R_\theta/K_{\mathrm{e}}c$ at low $k$, respectively, and $x_{\mathrm{AP}}^{\mathrm{E}}$ mainly determines the absolute value of $R_\theta/K_{\mathrm{e}}c$ at high $k$; the dispersity index $Đ_{\mathrm{NC}}$ slightly modifies the $k$ dependence of $R_\theta/K_{\mathrm{e}}c$ at low $k$. However, the best fit at $C_{\mathrm{S}}$ = 0.7 M was obtained by using $w_{\mathrm{NC}}$ slightly smaller than that calculated from $x_{\mathrm{AP}}^{\mathrm{E}}$ with eq 2-A10, probably because a part of concentrated-phase droplets went out from the scattering volume in the SAXS measurement by sedimentation. The green solid curve for $C_{\mathrm{S}}$ = 0.7 M in Figure 2-3 shows the fitting results using the parameters listed in Table 2-2. The green dashed curve for $C_{\mathrm{S}}$ = 0.7 M in Figure 2-3 indicates theoretical values of the NC contribution $w_{\mathrm{NC}}M_{\mathrm{NC}}P_{\mathrm{NC}}(k)$. The deviation of the dashed curve from the data points at $k > 0.3$ nm$^{-1}$ is the clear evidence for the existence of the free AP and MP chains in the solution. We have made SAXS measurements for biphasic solutions of the AP−MP mixture at 1 M $\geq C_{\mathrm{S}} \geq$ 0.6 M, other than 0.7 M, and the results have been fitted by eq 2-3 in the same way (cf. Figure 2-A2). Table 2-2 lists also fitting results at those $C_{\mathrm{S}}$. In Table 2-2, $x_{\mathrm{AP}}^{\mathrm{E}}$ decreases with decreasing $C_{\mathrm{S}}$ because the electrostatic attraction between the A and M block chains becomes strong. Moreover, the concentration $c_{\mathrm{c}}$ of the concentrated phase decreases with decreasing $C_{\mathrm{S}}$ from 1 to 0.6 M and seems to approach $c_{\mathrm{c}}$ ($\sim 10^{-2}$ g/cm$^3$) for aqueous solutions of polyion complexes formed by oppositely charged homopolyelectrolytes ($C_{\mathrm{S}}$ = 0 M) [7,8]. Because the SAXS profiles in Figures 2-3 and 2-A2 at $C_{\mathrm{S}}$ = 1 M $\geq C_{\mathrm{S}} \geq$ 0.6 M are smooth functions without any bumps and peaks, there may be no higher-order structure (any microphase separation structures) inside the concentrated-phase droplet, probably due to the weak amphiphilicity of the NC.

**Fitting the SAXS Profiles of AP−MP Complex Assemblies in the Micellar Solutions.** Although we did not observe macroscopic phase separation in aqueous solutions of the AP−MP mixture with $c$ = 0.005 g/cm$^3$ and $C_{\mathrm{S}} \leq$ 0.5 M, the SAXS profiles at $C_{\mathrm{S}}$ = 0.1 and 0.01 M in Figure 2-3 indicate the formation of large self-assemblies. Sakamoto et al. [20] demonstrated that the AP−MP complex at $C_{\mathrm{S}}$ = 0.1 M is a spherical micelle, cylindrical

micelle, and bilayer vesicle when $N_{0,A}/N_{0,P} \sim N_{0,M}/N_{0,P} = 0.27-1$, 4.7, and 9.5, respectively. Since our AP and MP samples have $N_{0,A}/N_{0,P} \sim N_{0,M}/N_{0,P} \sim 10$, we can expect that the NC of our AP and MP samples at $C_S = 0.1$ M takes bilayer vesicle (cf. Figure 2-4a), and the small peak at $k \sim 0.35$ nm$^{-1}$ (cf. the inset in Figure 2-3) may correspond to the thickness $D$ of the hydrophobic shell in the bilayer vesicle.

**Table 2-2. Parameters Used in Fitting of SAXS Profiles for Biphasic Solutions at $C_S$ = 1−0.6 M**

| $C_S$ (M) | $x_{AP}^E$ | $w_{AP}^E$ [a] | $w_{MP}^E$ [a] | $w_{NC}$ [b] | $M_{NC}$ ($10^5$ g mol$^{-1}$) | $Đ_{NC}$ | $c_c$ (g cm$^{-3}$) |
|---|---|---|---|---|---|---|---|
| 1 | 0.63 ± 0.03 | 0.25 | 0.45 | 0.27 ± 0.02 (0.30[c]) | 3 ± 0.5 | >7 | 0.2 ± 0.02 |
| 0.9 | 0.47 ± 0.03 | 0.18 | 0.38 | 0.4 ± 0.02 (0.44[c]) | 9 ± 0.2 | >7 | 0.2 ± 0.02 |
| 0.8 | 0.4 ± 0.03 | 0.16 | 0.36 | 0.38 ± 0.02 (0.48[c]) | 10 ± 3 | >5 | 0.15 ± 0.02 |
| 0.7 | 0.18 ± 0.02 | 0.07 | 0.27 | 0.52 ± 0.04 (0.66[c]) | 8 ± 0.2 | 2 ± 0.4 | 0.09 ± 0.01 |
| 0.6 | 0.03 ± 0.03 | 0.01 | 0.21 | 0.7 ± 0.05 (0.78[c]) | 10 ± 3 | 1.8 ± 0.4 | 0.09 ± 0.01 |

[a]Weight fractions of the free AP and free MP, calculated from $x_{AP}^E$ (the second column) by eq 2-A10. [b]Weight fraction of the NC in the total copolymer. [c]Values of $w_{NC}$ calculated by eq 2-A10 with the $x_{AP}^E$ value given in the second column.

Since the electrostatic attraction between the A and M block chains is stronger at $C_S$ = 0.1 M than at $C_S \geq 0.6$ M, we can expect $x_{AP}^E = 0$ from the results in Table 2-2 and that the minor component AP at $x_+ = 0.6$ is all included into the NC. Although free MP chains (the major component) remain in the mixture solution at $C_S = 0.1$ M, it turns out that their contribution to $R_\theta/K_e c$ is negligibly small, when compared the experimental $R_\theta/K_e c$ with that calculated by eq 2-3 with the molecular parameters of the MP chain at $C_S = 0.1$ M (cf. Table 2-A1). Therefore, we consider only the NC contribution $w_{NC}M_{NC}P_{NC}(k)$ in eq 2-3 , i.e.

$$\frac{R_\theta}{K_e c} = w_{NC} M_{NC} P_{NC}(k) \tag{2-3′}$$

In a first approximation, we assume the bilayer vesicle with a uniform hydrophobic layer thickness $D$, which is characterized by five parameters ($M_{NC}$, $Đ_{NC}$, $D$, the mass concentration

$c_{core}$ within the hydrophobic layer, and the height $H$ of the hydrophilic layer) and other structural parameters are calculated from the five parameters (cf. the Appendix 2). It is noted that the absolute values of the excess Rayleigh ratio $R_\theta$ were determined, and the contrast factors for the hydrophilic and hydrophobic parts of the vesicle were calculated from the partial specific volumes of the block chains and solvent (cf. eq 2-A20), so that they were not adjustable parameters in our fittings. The particle scattering function $P_{NC}(k)$ of the bilayer vesicle can be calculated by eq 2-4 along with eqs 2-A19−23, and the weight fraction $w_{NC}$ is calculated by eq 2-A10 with $x_{AP}^{E} = 0$. Among the structural parameters, $D$ almost uniquely determines the small peak position ($k \sim 0.35$ nm$^{-1}$) of the scattering function, $M_{NC}$ and $c_{core}$ mainly determine the absolute value and the $k$ dependence of $R_\theta/K_e c$ at low $k$, $H$ mainly determines the $k$ dependence of $R_\theta/K_e c$ at high $k$, and $Đ_{NC}$ slightly modifies the $k$ dependence of $R_\theta/K_e c$ at low $k$. Because the theoretical value of $R_\theta/K_e c$ is insensitive to $Đ_{NC}$, we have assumed $Đ_{NC}$ to be 2. Then, we can almost uniquely determine the four adjustable parameters by fitting the theoretical $R_\theta/K_e c$ to the experimental data. However, the theoretical scattering function has a too sharp peak at $k \sim 0.35$ nm$^{-1}$ (cf. the red solid curve in Figure 2-A2d). When $N_{0,A}$ and $N_{0,M}$ of the ionic block chains have some dispersities, $D$ has also a dispersity, which makes the peak broader. Thus, we have considered the dispersity in $D$ by eq 2-A24 using the parameter $\sigma_D$, though the smearing effect [32] at SAXS measurements may contribute more or less to $\sigma_D$.

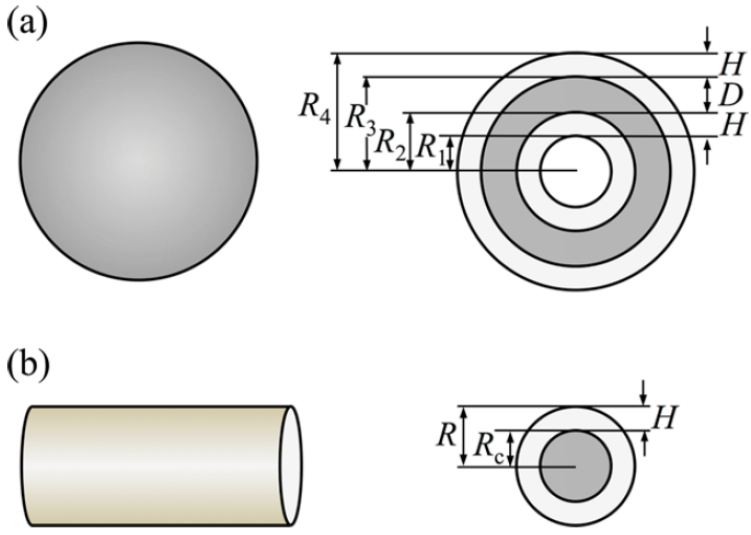


**Figure 2-4.** Schematic diagrams of the bilayer vesicle (a) and the cylindrical micelle (b).

The fitting curve at $C_S = 0.1$ M slightly disagrees with experimental data at high $k >$ 0.5 nm$^{-1}$ (cf. the green solid curve in Figure 2-A2d). This is because eq 2-A19 does not

consider the scattering contribution from individual chains in the hydrophilic layer part. When calculating this contribution according to Pedersen and Gerstenberg [32,33] (eq 2-A29), we obtain the red solid curve for $C_S$ = 0.1 M in Figure 2-3 (and also the blue solid curve in Figure 2-A2d), which perfectly fits the experimental data points. The parameters determined by this fitting are listed in Table 2-3. The average diameter $2R_4$ (cf. Figure 2-4a) calculated from eqs 2-A21 and 2-A23 with $D$ = 19 nm (the average $\langle D \rangle$ in Table 2-3) and $M = M_N$ is 200 nm.

**Table 2-3. Characteristics of the Bilayer Vesicle Formed at $C_S$ = 0.5−0.05 M**

| $C_S$ / M | $x_{AP}^E$ ($w_{NC}$ [a]) | $M_{NC}$ / $10^8$ g mol$^{-1}$ | $Đ_{NC}$ | $c_{core}$ /g cm$^{-3}$ | $\langle D \rangle$/nm | $\sigma_D$/nm | $H$/nm |
|---|---|---|---|---|---|---|---|
| 0.1 | 0 (0.71) | 7 ± 4 | 2 [b] | 0.42 ± 0.03 | 19 ± 0.5 | 3.5 ± 0.5 | 2 |
| 0.5–0.05 | 0 (0.71) | 7 ± 4 | 2 [b] | 0.42 ± 0.03 – 0.35 ± 0.03 | 19 ± 0.5 | 3.5 ± 0.5 | 2 |

[a] Values calculated from $x_{AP}^E$ by eq 2-A10 in the Appendix, and used for the fitting. [b] Assumed value.

Additional SAXS profiles at 0.5 M ≥ $C_S$ ≥ 0.05 M are shown in Figure 2-A2b. The profiles are almost identical each other and can be fitted by the equations for the bilayer vesicle with the parameter values same as those at $C_S$ = 0.1 M, although a slight variation of $c_{core}$ gave us a better fitting (see Table 2-3).

As mentioned above, the scattering profile at $C_S$ = 0.01 M is different from that at $C_S$ = 0.1 M, and it could not be fitted by the scattering function for the bilayer vesicle. The $k^{-1}$ dependence of the scattering function at $C_S$ = 0.01 M in the lowest $k$ region is the character of the cylindrical micelle. The different morphologies are observed also in TEM images of particles dried from an aqueous solution of the AP−MP mixture at 0 and 0.1 M, shown in Figure 2-5 and Figure 2-A4. The TEM image in Figure 2-5a implies the existence of the cylindrical micelle at $C_S$ = 0 M.

To fit the profile at $C_S$ = 0.01 M, we have assumed that the NC exists as a mixture of the bilayer vesicle and cylindrical micelle (cf. Figure 2-4). As in the case of $C_S$ = 0.1 M, we assume $x_{AP}^E$ (= $w_{AP}$) = 0 and calculate $R_\theta/K_e c$ by eq 2-3′ with

$$w_{NC} M_{NC} P_{NC}(k) = w_{ves} M_{ves} P_{ves}(k) + w_{cyl} M_{cyl} P_{cyl}(k) \tag{2-5}$$

where the subscripts ves and cyl denote the vesicle and cylinder, respectively, and the scattering function $M_{cyl}P_{cyl}(k)$ for the cylindrical micelle is calculated by eq 2-4 where $P_M(k)$ is given by eqs 2-A25−27. From the $k^{-1}$ dependence of $R_\theta/K_ec$ at low $k$, the contribution of the vesicle in eq 2-5 should be minor at $C_S$ = 0.1 M, and we have approximated $M_{ves}P_{ves}(k)$ by that at $C_S$ = 0.5 − 0.05 M (calculated using the parameters listed in Table 2-3). Furthermore, according to the theory of the cylindrical micelle [34], the aggregation number distribution of the micelle was assumed to obey the most probable distribution, i.e., $Đ_{cyl}$ = 2. We have therefore the five parameters $w_{cyl}$, $M_{cyl}$, $c_{core}$, $R_c$, and $H$ to be determined. Among them, $R_c$ almost uniquely determines the small peak position ($k \sim 0.25$ nm$^{-1}$) of the scattering function, $M_{cyl}$ and $c_{core}$ mainly determine the absolute value and the $k$ dependence of $R_\theta/K_ec$ at low $k$, $H$ mainly determines the $k$ dependence of $R_\theta/K_ec$ at high $k$, and $w_{cyl}$ shifts vertically the scattering function. We can almost uniquely determine all the adjustable parameters by fitting the theoretical $R_\theta/K_ec$ to the experimental data.

As in the case of the vesicle fitting at $C_S$ = 0.1 M, the peak corresponding to $R_c$ (at $k \sim 0.25$ nm$^{-1}$) was too sharp and the scattering function at high $k$ decays too steep at the above fitting. These disagreements were adjusted using eq 2-A28 (the $R_c$ dispersity correction with the additional adjustable parameter $\sigma_R$) and eq 2-A29 (the contribution of individual chains in the hydrophilic coronal part). The solid curve for $C_S$ = 0.01 M in Figure 2-3 shows the fitting result, and Table 2-4 lists the parameters selected. Similar fittings were made on the scattering functions at $C_S$ = 0.02 and 0 M (cf. Figure 2-A2c), and fitting parameters are listed in Table 2-4.

**Table 2-4. Characteristics of Cylindrical Micelles Formed at $C_S$ = 0.02−0 M**[a]

| $C_S$ / M | $w_{NC}$ [b] | $w_{ves}$, $w_{cyl}$ | $M_{cyl}$ / $10^8$ g mol$^{-1}$ | $Đ_{cyl}$ | $c_{core}$ /g cm$^{-3}$ | $\langle R_c \rangle$/nm | $\sigma_R$/nm | $H$/nm |
|---|---|---|---|---|---|---|---|---|
| 0.02 | 0.71 | 0.25 ± 0.03, 0.46 ± 0.03 | 1.4 ± 0.6 | 2 [c] | 0.43 ± 0.03 | 16.5 ± 0.5 | 3.5 ± 0.5 | 2 |
| 0.01 | 0.71 | 0.19 ± 0.03, 0.52 ± 0.03 | 1.4 ± 0.6 | 2 [c] | 0.45 ± 0.03 | 18 ± 0.5 | 3.5 ± 0.5 | 2 |
| 0 | 0.71 | 0.05 ± 0.03, 0.61 ± 0.03 | 1.4 ± 0.6 | 2 [c] | 0.45 ± 0.03 | 19.5 ± 0.5 | 3.0 ± 0.5 | 2 |

[a] Parameters for the vesicle were the same as those at $C_S$ = 0.5−0.05 M listed in Table 3. [b] Values calculated from $x_{AP}^E = 0$ by eq 2-A10 in the Appendix. [c] Assumed value.

The length $L$ of the cylindrical micelle estimated by SAXS at $C_S$ = 0 M is calculated by eq 2-A27 (with $M = M_{w,cyl}$ and $R_c = \langle R_c \rangle$ in Table 2-4) to be 280 nm, which is much shorter than that of the TEM image in Figure 2-5a. Because the length of the cylindrical micelle is dependent on the amphiphile concentration [34], the micelle may grow and coagulate during the dry process in the sample preparation for the TEM experiment. Although the micellar image bends in Figure 2-A4a, the flexibility effect may not be important at fitting the SAXS profiles because the cylinder length is short in the solution, and the flexibility effect is not appreciable except at very low $k$.

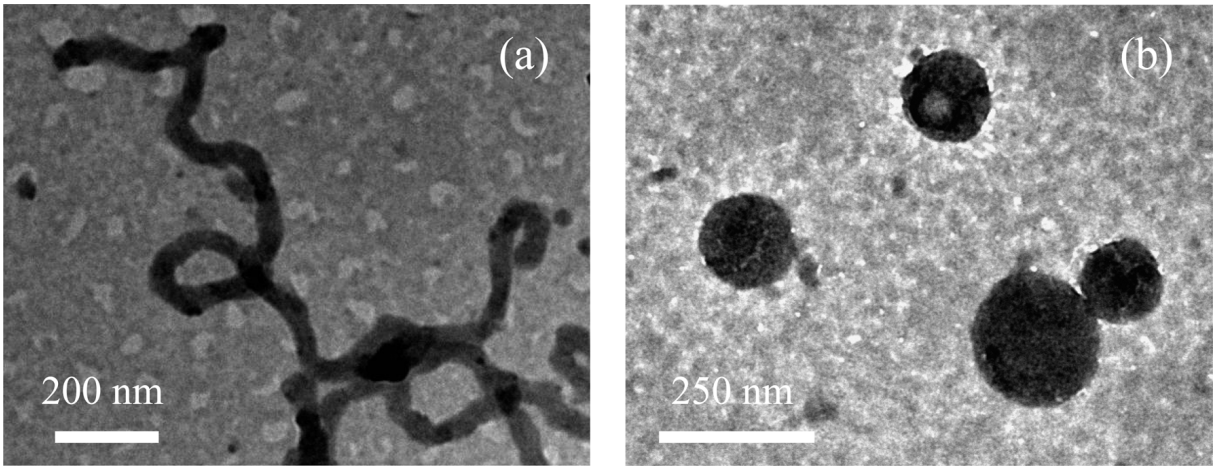


**Figure 2-5.** TEM images of MP−AP mixtures with $x_+$ = 0.6 at $C_S$ = 0 M (a) and 0.1 M (b).

**Salt-Induced Morphological Transition of the Polyion Complex Micelle.** The weight fraction $w_{cyl}$ of the cylindrical micelle estimated by fitting increases with decreasing $C_S$. According to Israelachvili et al. [35,36], the micellar morphology is related to the packing parameter $\lambda$ defined by

$$\lambda \equiv \frac{v}{a_0 l_c} \tag{2-6}$$

where $v$ is the effective volume of the hydrophobic chain, $a_0$ is the area per chain of the hydrophobic−hydrophilic domains interface, and $l_c$ is the length of the hydrophobic chain in the hydrophobic domain. Their prediction is that the cylindrical micelle is formed at $1/3 < \lambda < 1/2$ and bilayer vesicle at $1/2 < \lambda < 1$. When $C_S$ is decreased, the electrostatic attraction between AP and MP becomes stronger. This indicates that the hydrophobic domain formed by the polyanion and polycation chains of AP and MP becomes more compact, which reduces $v$ and then $\lambda$. In fact, $c_{core}$ increases slightly with decreasing $C_S$ (cf. Tables 2-3 and 2-4). Therefore, the preference of the cylindrical micelle with decreasing $C_S$ is consistent with the prediction of Israelachvili et al. It is worth noting that their prediction is also consistent with

Sakamoto et al.'s finding [20] that AP and MP form the cylindrical micelle instead of the vesicle at $C_S$ = 0.1 M, when $N_{0+}/N_{0\pm} \sim N_{0+}/N_{0\pm}$ decreases from 9.5 to 4.7.

Van der Gucht et al. [21] found the salt-induced spherical micelle to cylindrical micelle transition in the polyion complex system of poly(*N*-methyl-2-vinylpyridinium)-*b*-poly(ethylene oxide) and short poly(acrylic acid) homopolymer in aqueous solution. This can be also explained by the increase in $\lambda$ through $v$ with increasing $C_S$. Zhang et al. [37] reported a morphology transition from the vesicle, cylindrical, to spherical micelle in aqueous solution of polystyrene-*b*-poly(acrylic acid) with decreasing $C_S$. This transition may be explained by the increase of $a_0$ through the electrostatic repulsion among coronal poly(acrylic acid) chains with decreasing $C_S$, which decreases $\lambda$ (cf. eq 2-6). Similar morphological transitions from the vesicle, cylindrical, to spherical micelle for block copolymer micelles were observed in many aqueous and organic solvent systems, by changing the solvent composition [1,37−41].

In Tables 2-3 and 2-4, the diameter $2\langle R_c \rangle$ of the cylindrical micelle core is about twice as large as the thickness $\langle D \rangle$ of the hydrophobic layer of the vesicle. This corresponds to the shift of the small peak in the SAXS profiles at $C_S$ = 0.1 and 0.01 M in Figure 2-3. In the solvent-composition-induced morphological transition for block copolymer micelles, the thickness of the solvophobic domain generally increases in order "the vesicle → cylindrical → spherical micelle" [37−41]. Our result agrees with this general tendency.

The volume $V_{core}$ and interfacial area $A_{core}$ of the solvophobic domain in the micelle are related by

$$A_{core} = \frac{2(3-d)V_{core}}{D} \tag{2-7}$$

where $D$ and $d$ are the thickness and dimensionality of the solvophobic domain ($D = 2R_c$ for the cylindrical micelle and $d$ = 0, 1, and 2 for the spherical, cylindrical, and disk-like micelles, respectively). Eq 2-7 indicates that $A_{core}$ abruptly increases with the morphological transition from the disk (or vesicle; $d$ = 2), cylinder ($d$ = 1), to sphere ($d$ = 0). To reduce the penalty of this interfacial energy, $D$ may increase along with the morphological or dimensional transition of the micelle.

## 2. 4. Conclusion

We have investigated the self-assembly in dilute aqueous solutions of a mixture of the anionic−neutral block copolymer (AP) and cationic−neutral block copolymer (MP) by

changing the added NaCl concentration $C_S$ or the electrostatic interaction among oppositely charged blocks at a fixed total copolymer concentration (= 0.005 g/cm$^3$). The ratio of the charged to neutral block chain lengths was ca. 10, and the mixing ratio (the mole fraction of the MP charge unit in the total charge units) of AP and MP was fixed to be 0.6.

At a sufficiently high $C_S$ (= 2 M), the electrostatic interaction is almost screened out, and AP and MP are dissolved independently in the aqueous solution. With decreasing $C_S$, the neutral complex of AP and MP starts forming, and the neutralization of the charged blocks reduces the affinity of the complex to water, which increases the average interaction parameter for the AP−MP complex in aqueous solution. As the result, a macroscopic phase separation takes place at 1 M $\geq C_S \geq$ 0.6 M.

Further decreasing $C_S$, the electrostatic attraction between the oppositely charged blocks becomes stronger to squeeze out more water from polyion complex domain. Thus, the interaction parameter between the charged blocks and the solvent water increases to enhance amphiphilicity of AP and MP chains, the AP−MP complex forms micelles, and the solution returns to the one-phase region. Moreover, the micelle morphology changes with $C_S$. At 0.5 M $\geq C_S \geq$ 0.05 M, the micelle is the bilayer vesicle, while at $C_S \leq$ 0.02 M the cylindrical micelle appears and becomes the major component in salt-free solution where the attraction between the oppositely charged blocks is maximum. This morphological transition and the change of the hydrophobic domain thickness along with the transition were explained in terms of the packing parameter of Israelachvili et al. [35,36] and the interfacial energy penalty, respectively.

**References**

[1] Y. Mai, A. Eisenberg, Chem. Soc. Rev. **41,** 5969 (2012).

[2] R. Takahashi, T. Sato, K. Terao, X.-P. Qiu, F. M. Winnik, Macromolecules **45,** 6111 (2012).

[3] T. Sato, K. Tanaka, A. Toyokura, R. Mori, R. Takahashi, K. Terao, S. Yusa, Macromolecules **46,** 226 (2013).

[4] R. Takahashi, X.-P. Qiu, N. Xue, T. Sato, K. Terao, F. M. Winnik, Macromolecules **47,** 6900 (2014).

[5] K. Nakai, M. Nishiuchi, M. Inoue, K. Ishihara, Y. Sanada, K. Sakurai, S. Yusa, Langmuir **29,** 9651 (2013).

[6] Y. Matsuda, M. Kobayashi, M. Annaka, K. Ishihara, A. Takahara, Langmuir **24,** 8772 (2008).

[7] K. Ueno, H. Ueno, T. Sato, Polym. J. **44,** 59 (2012).
[8] H.-D. Liu, T. Sato, Chin. J. Polym. Sci. **31,** 39 (2013).
[9] J. Qin, D. Priftis, R. Farina, S. L. Perry, L. Leon, J. Whitmer, K. Hoffmann, M. Tirrell, J. J. de Pablo, ACS Macro Lett. **3,** 565 (2014).
[10] M. A. Cohen Stuart, B. Hofs, I. K. Voets, A. de Keizer, Curr. Opin. Colloid Interface Sci. **10,** 30 (2005).
[11] I. K. Voets, A. de Keizer, M. A. Cohen Stuart, Adv. Colloid Interface Sci. **147−148,** 300 (2009).
[12] Y. Lee, K. Kataoka, Soft Matter **5,** 3810 (2009).
[13] D. V. Pergushov, A. H. E. Müller, F. H. Schacher, Chem. Soc. Rev. **41,** 6888 (2012).
[14] A. Harada, K. Kataoka, Macromolecules **28,** 5294 (1995).
[15] S. Schrage, R. Sigel, H. Schlaad, Macromolecules **36,** 1417 (2003).
[16] A. Koide, A. Kishimura, K. Osada, W.-D. Jang, Y. Yamasaki, K. Kataoka, J. Am. Chem. Soc. **128,** 5988 (2006).
[17] A. Kishimura, A. Koide, K. Osada, Y. Yamasaki, K. Kataoka, Angew. Chem., Int. Ed. **46,** 6085 (2007).
[18] M. Burkhardt, N. Martinez-Castro, S. Tea, M. Drechsler, I. Babin, I. Grishagin, R. Schweins, D. V. Pergushov, M. Gradzielski, A. B. Zezin, A. H. E. Müller, Langmuir **23,** 12864 (2007).
[19] W.-F. Dong, A. Kishimura, Y. Anraku, S. Chuanoi, K. Kataoka, J. Am. Chem. Soc. **131,** 3804 (2009).
[20] S. Sakamoto, Y. Sanada, M. Sakashita, K. Nishina, K. Nakai, S. Yusa, K. Sakurai, Polym. J. **46,** 617 (2014).
[21] H. M. van der Kooij, E. Spruijt, I. K. Voets, R. Fokkink, M. A. Cohen Stuart, J. van der Gucht, Langmuir **28,** 14180 (2012).
[22] M. Lemmers, I. K. Voets, M. A. Cohen Stuart, J. van der Gucht, Soft Matter **7,** 1378 (2011).
[23] D. V. Krogstad, S.-H. Choi, N. A. Lynd, D. J. Audus, S. L. Perry, J. D. Gopez, C. J. Hawker, E. J. Kramer, M. V. Tirrell, J. Phys. Chem. B **118,** 13011 (2014).
[24] D. V. Krogstad, N. A. Lynd, S.-H. Choi, J. M. Spruell, C. J. Hawker, E. J. Kramer, M. V. Tirrell, Macromolecules **46,** 1512 (2013).
[25] D. V. Krogstad, N. A. Lynd, D. Miyajima, J. Gopez, C. J. Hawker, E. J. Kramer, M. V. Tirrell, Macromolecules **47,** 8026 (2014).
[26] A. Harada, K. Kataoka, Prog. Polym. Sci. **31,** 949 (2006).
[27] A. Kishimura, Polym. J. **45,** 892 (2013).

[28] R. Hagino, J. Yashiro, M. Sakata, T. Norisuye, Polym. J. **38,** 861 (2006).
[29] B. H. Zimm, J. Chem. Phys. **16,** 1093 (1948).
[30] D. C. Henry, Proc. R. Soc. London, Ser. A **133,** 106 (1931).
[31] J.-F. Berret, Macromolecules **40,** 4260 (2007).
[32] J. S. Pedersen, Adv. Colloid Interface Sci. **70,** 171 (1997).
[33] J. S. Pedersen, M. C. Gerstenberg, Macromolecules **29,** 1363 (1996).
[34] T. Sato, Langmuir **20,** 1095 (2004).
[35] J. N. Israelachvili, D. J. Mitchell, B. W. Ninham, J. Chem. Soc., Faraday Trans. 2 **72,** 1525 (1976).
[36] J. N. Israelachvili, Intermolecular and Surface Forces, 3rd ed.; Academic Press: Waltham, MA, 2011.
[37] L. Zhang, A. Eisenberg, Macromolecules **32,** 2239 (1999).
[38] J. Bang, S. Jain, Z. Li, T. P. Lodge, J. S. Pedersen, E. Kesselman, Y. Talmon, Macromolecules **39,** 1199 (2006).
[39] P. Bhargava, J. X. Zheng, P. Li, R. P. Quirk, F. W. Harris, S. Z. D. Cheng, Macromolecules **39,** 4880 (2006).
[40] Y.-Y. Won, A. K. Brannan, H. T. Davis, F. S. Bates, J. Phys. Chem. B **106,** 3354 (2002).
[41] S. Jain, F. S. Bates, Macromolecules **37,** 1511 (2004).

**Appendix 2.**

**Analysis of the SAXS intensity.** The excess scattering intensity $I_\theta$ over that of the solvent at the scattering angle $\theta$ was transformed to the excess Rayleigh ratio $R_\theta$ using aqueous solutions of polyethylene glycol (PEG) with the polymer mass concentration $c_{\mathrm{ref}}$ as reference materials by

$$R_\theta = N_{\mathrm{A}} a_{\mathrm{e}}^{\,2} \left( \frac{\bar{\upsilon}_{\mathrm{ref}} \Delta\rho_{\mathrm{ref}}}{N_{\mathrm{A}}} \right)^2 \frac{c_{\mathrm{ref}} M_{\mathrm{ref}}}{1 + 2A_{2,\mathrm{ref}} M_{\mathrm{ref}} c_{\mathrm{ref}}} \frac{I^{\circ}_{\mathrm{ref}}}{I_{0,\mathrm{ref}}} \frac{I_\theta}{I^{\circ}} \tag{2-A1}$$

where $N_{\mathrm{A}}$ is the Avogadro constant, $a_{\mathrm{e}}$ is the classical radius of electron (= 2.82 × $10^{-13}$ cm), $I^{\circ}_{\mathrm{ref}}$ and $I^{\circ}$ are the intensities of incident beam at measurements of the reference and test solutions, respectively, and $I_{0,\mathrm{ref}}$, $M_{\mathrm{ref}}$, $A_{2,\mathrm{ref}}$, $\bar{\upsilon}_{\mathrm{ref}}$, and $\Delta\rho_{\mathrm{ref}}$ are the excess scattering intensity at $\theta$ = 0, the molar mass, the second virial coefficient, the partial specific volume, and the excess electron density, respectively, of the reference solution. The values of $M_{\mathrm{ref}}$ (= 5050) and $A_{2,\mathrm{ref}}$ (= 2.4 × $10^{-3}$ $\mathrm{cm^3 mol/g^2}$) were determined by light scattering, the value of $\bar{\upsilon}_{\mathrm{ref}}$ (= 0.838 $\mathrm{cm^3/g}$) by densitometry (using an Anton Paar DMA 5000 densitometer), and the contrast factor $\bar{\upsilon}_{\mathrm{ref}} \Delta\rho_{\mathrm{ref}}/N_{\mathrm{A}}$ was calculated by

$$\frac{\bar{\upsilon}_{\mathrm{ref}}\Delta\rho_{\mathrm{ref}}}{N_{\mathrm{A}}} = \frac{n_{0,\mathrm{ref}}}{M_{0,\mathrm{ref}}} - \frac{\bar{\upsilon}_{\mathrm{ref}} n_{\mathrm{e,H_2O}}}{\upsilon_{\mathrm{H_2O}} M_{\mathrm{H_2O}}} \tag{2-A2}$$

with the number of electrons $n_{0,\mathrm{ref}}$ (= 24) and the molar mass $M_{0,\mathrm{ref}}$ (44 g/mol) of the monomer unit of PEG, the number of electrons $n_{\mathrm{e,H_2O}}$ (= 10) and the molar mass $M_{0,\mathrm{H_2O}}$ (= 18 g/mol) of a water molecule, and the specific volume $\upsilon_{\mathrm{H_2O}}$ (= 1.003 $\mathrm{cm^3/g}$) of water.

The optical constant $K_{\mathrm{e}}$ is defined by

$$K_{\mathrm{e}} = N_{\mathrm{A}} a_{\mathrm{e}}^2 \gamma_{\mathrm{av}}^2 \tag{2-A3}$$

with the average contrast factor $\gamma_{\mathrm{av}}$ of the polymer. For the mixture of the AP and MP copolymers dissolved in aqueous NaCl, $\gamma_{\mathrm{av}}$ was calculated by

$$\gamma_{\mathrm{av}} \equiv \frac{\bar{\upsilon}_{\mathrm{AP}}\Delta\rho_{\mathrm{AP}}}{N_{\mathrm{A}}} w_{\mathrm{AP}} + \frac{\bar{\upsilon}_{\mathrm{MP}}\Delta\rho_{\mathrm{MP}}}{N_{\mathrm{A}}} w_{\mathrm{MP}} \tag{2-A4}$$

where $\bar{\upsilon}_i$, $\Delta\rho_i$, and $w_i$ are the partial specific volume, the excess electron density, and the weight fraction of the copolymer $i$ ($i$ = AP and MP), respectively. The contrast factor $\gamma_i$ ($\equiv \bar{\upsilon}_i \Delta\rho_i / N_{\mathrm{A}}$) of each component $i$ is calculated by

$$\gamma_i = \frac{n_{\mathrm{e},i}}{M_i} - \left(\frac{\bar{\upsilon}\rho_{\mathrm{e}}}{N_{\mathrm{A}}}\right)_{\mathrm{solv}} \tag{2-A5}$$

with

$$\left(\frac{\bar{\upsilon}\rho_{\mathrm{e}}}{N_{\mathrm{A}}}\right)_{\mathrm{solv}} \equiv \frac{\bar{\upsilon}_i}{\upsilon_{\mathrm{solv}}}\left[\frac{n_{\mathrm{e,H_2O}}}{M_{\mathrm{H_2O}}}\left(1 - w_{\mathrm{NaCl}}\right) + \frac{n_{\mathrm{e,NaCl}}}{M_{\mathrm{NaCl}}} w_{\mathrm{NaCl}}\right] \tag{2-A6}$$

where $n_{\mathrm{e},i}$, $n_{\mathrm{e,H_2O}}$, and $n_{\mathrm{e,NaCl}}$ are numbers of electrons of copolymer $i$, $H_2O$ molecule, and NaCl, respectively, $M_i$, $M_{\mathrm{H_2O}}$, and $M_{\mathrm{NaCl}}$ are molar masses of copolymer $i$, $H_2O$ and NaCl, respectively, $\upsilon_{\mathrm{solv}}$ is the specific volume of the solvent (aqueous NaCl), and $w_{\mathrm{NaCl}}$ is the weight fraction of NaCl in aqueous NaCl. It should be noticed that $(\bar{\upsilon}\rho_{\mathrm{e}}/N_{\mathrm{A}})_{\mathrm{solv}}$ depends on the polymer through $\bar{\upsilon}_i$ in eq 2-A6. For the block copolymer of AM or MP, $n_{\mathrm{e},i}/M_i$ and $\bar{\upsilon}_i$ are calculated by

$$\frac{n_{\mathrm{e},i}}{M_i} = \frac{n_{\mathrm{e0,P}} N_{0,\mathrm{P}} + n_{\mathrm{e0,A}} N_{0,\mathrm{A}}}{M_{\mathrm{AP}}} \text{ or } \frac{n_{\mathrm{e0,P}} N_{0,\mathrm{P}} + n_{\mathrm{e0,M}} N_{0,\mathrm{M}}}{M_{\mathrm{MP}}} \tag{2-A7}$$

$$\bar{\upsilon}_i = \frac{\bar{\upsilon}_{\mathrm{P}} M_{\mathrm{P}} + \bar{\upsilon}_{\mathrm{A}} M_{\mathrm{A}}}{M_{\mathrm{AP}}} \text{ or } \frac{\bar{\upsilon}_{\mathrm{P}} M_{\mathrm{P}} + \bar{\upsilon}_{\mathrm{M}} M_{\mathrm{M}}}{M_{\mathrm{MP}}} \tag{2-A8}$$

where $n_{\mathrm{e0},j}$ is the number of electrons in the monomer unit $j$ (= P, A, or M), $N_{0,j}$, $M_j$, and $\bar{\upsilon}_j$ are the degree of polymerization, molar mass, and partial specific volume of the block chain $j$ (= P, A, or M), and $M_i$ is the molar mass of the copolymer $i$ ($i$ = AP and MP). While the

literature value[5] was used for $\bar{v}_A$, partial specific volumes $\bar{v}_P$ and $\bar{v}_M$ were determined by densitometry (see below). The weight fractions of MP ($w_{MP}$) and of AP ($w_{AP}$) can be calculated from $x_+$ (the mole fraction of cations borne by MP in the total charges borne by AP and MP) by

$$w_{MP} = 1 - w_{AP} = \frac{x_+ N_{0,A} M_{MP}}{(1 - x_+) N_{0,M} M_{AP} + x_+ N_{0,A} M_{MP}} \tag{2-A9}$$

**Composition in the Neutral Complex Solution.** Let us assume that a part of MP and AP in the mixture form the neutral complex. If $x_+ > 0.5$ and the mole fraction of free AP in the total AP is denoted as $x_{AP}^E$, the weight fractions of the free MP, the free AP, and the neutral complex are given respectively by

$$\begin{aligned} w_{AP}^E &= \frac{(1 - x_+) N_{0,M} x_{AP}^E M_{AP}}{(1 - x_+) N_{0,M} M_{AP} + x_+ N_{0,A} M_{MP}} \\ w_{MP}^E &= \frac{\left[2x_+ - 1 + (1 - x_+) x_{AP}^E\right] N_{0,A} M_{MP}}{(1 - x_+) N_{0,M} M_{AP} + x_+ N_{0,A} M_{MP}} \\ w_{NC} &= (1 - x_+) \frac{N_{0+} (1 - x_{AP}^E) M'_{AP} + N_{0,A} (1 - x_{AM}^E) M'_{MP}}{(1 - x_+) N_{0,M} M_{AP} + x_+ N_{0,A} M_{MP}} \end{aligned} \tag{2-A10}$$

In the neutral complex, $Na^+$ and $Cl^-$ are no more the counterions of AP and MP, respectively. As the result, $M'_{AP}$ and $M'_{MP}$ in the numerator of the equation of $w_{NC}$ in eq 2-A10 represent the molar masses of AP and MP without the counterions. When $x_{AP}^E = 0$, all AP forms the neutral complex, and when $x_{AP}^E = 1$, no neutral complex is formed.

If the neutral complex forms a micelle with a core-shell structure in water, the weight fractions of the core and shell parts in the neutral complex are given by

$$W_{core} = \frac{M'_{0,M} + M'_{0,A}}{(M'_{AP}/N_{0,A}) + (M'_{MP}/N_{0,M})}, \quad W_{shell} = \frac{M_{0,P} N_{0,P} (1/N_{0,A} + 1/N_{0,M})}{(M'_{AP}/N_{0,A}) + (M'_{MP}/N_{0,M})} \tag{2-A11}$$

**Scattering Functions.** For the block copolymer consisting of Gaussian a and b block chains and dispersed molecularly in the solution, the molar mass multiplied by the intramolecular interference factor $MP(k)$ is calculated by

$$\gamma_{av}{}^2 MP(k) = \frac{\gamma_a{}^2 M_a{}^2 P_a(k) + \gamma_b{}^2 M_b{}^2 P_b(k) + 2\gamma_a \gamma_b M_a M_b Q_{ab}(k)}{M_a + M_b} \tag{2-A12}$$

where $P_i(k)$ is the intramolecular interference factor for the block chain $i$ (= a, b) and $Q_{ab}(k)$ is the cross term of the ab block copolymer chain, both being given by

$$P_i(k) = \frac{2}{x_i^2}\left(\mathrm{e}^{-x_i} + x_i - 1\right)\mathrm{e}^{-d_i^2 k^2/16}, \quad x_i \equiv k^2\langle S^2\rangle_i \tag{2-A13}$$

and

$$Q_{\mathrm{ab}}(k) = \frac{N_{0\mathrm{ab}}{}^2 P_{\mathrm{ab}}(k) - N_{0\mathrm{a}}^2 P_{\mathrm{a}}(k) - N_{0\mathrm{b}}^2 P_{\mathrm{b}}(k)}{2N_{0\mathrm{a}}N_{0\mathrm{b}}} \tag{2-A14}$$

with the square radius of gyration $\langle S^2\rangle_i$, degree of polymerization $N_{0i}$, and diameter $d_i$ of the chain $i$ (= a, b, or ab chains) ($\langle S^2\rangle_{\mathrm{ab}} = \langle S^2\rangle_{\mathrm{a}} + \langle S^2\rangle_{\mathrm{b}}$; $N_{0\mathrm{ab}} = N_{0\mathrm{a}} + N_{0\mathrm{b}}$; $d_{\mathrm{ab}}{}^2 = (d_{\mathrm{a}}{}^2 + d_{\mathrm{b}}{}^2)/2$). In eq 2-A12, $\gamma_i$ is the contrast factor of the block chain $i$ (= a and b) calculated by

$$\gamma_i = \frac{n_{\mathrm{e}0i}}{M_{0i}} - \left(\frac{\bar{v}\rho_{\mathrm{e}}}{N_{\mathrm{A}}}\right)_{\mathrm{solv}} \tag{2-A15}$$

with the monomer unit molar mass $M_{0i}$ of the block chain $i$, and $(\bar{v}\,\rho_{\mathrm{e}}/N_{\mathrm{A}})_{\mathrm{solv}}$ given by eq 2-A6. We have neglected the salt exclusion effect for the polyelectrolyte. As seen from eq 2-A12, $M$ and $P(k)$ are not the true molar mass and intramolecular interference factor, strictly speaking, but include the effect of the difference in the scattering power between the blocks through $\gamma_i$.

When the neutral complex of AP and MP forms a spherical particle of the uniform density with the molar mass $M$, the scattering function (or the intra-particle interference factor) $P_M(k)$ of the particle is given by

$$\gamma_{\mathrm{av}}{}^2 P_M(k) = \gamma_{\mathrm{NC}}{}^2 \Phi^2(kR_M) \tag{2-A16}$$

where

$$\Phi(x) \equiv \frac{3(\sin x - x\cos x)}{x^3}, \quad R_M = \left(\frac{3M}{4\pi N_{\mathrm{A}} c_{\mathrm{c}}}\right)^{1/3} \tag{2-A17}$$

and the contrast factor $\gamma_{\mathrm{NC}}$ of the neutral complex is calculated by

$$\gamma_{\mathrm{NC}} = \frac{n'_{\mathrm{e}0+} + n'_{\mathrm{e}0,\mathrm{A}} + n_{\mathrm{e}0,\mathrm{P}}N_{0,\mathrm{P}}\left(1/N_{0,\mathrm{A}} + 1/N_{0,\mathrm{M}}\right)}{\left(M'_{\mathrm{AP}}/N_{0,\mathrm{A}}\right) + \left(M'_{\mathrm{MP}}/N_{0,\mathrm{M}}\right)} - \left(\frac{\bar{v}\rho_{\mathrm{e}}}{N_{\mathrm{A}}}\right)_{\mathrm{solv}} \tag{2-A18}$$

with $(\bar{v}\,\rho_{\mathrm{e}}/N_{\mathrm{A}})_{\mathrm{solv}}$ given by eq 2-A6.

If the neutral complex is a single bilayer vesicle, $P_M(k)$ is given by

$$\gamma_{\mathrm{av}}{}^2 P_M(k) = \left[ \begin{array}{l} \gamma_{\mathrm{core}} W_{\mathrm{core}} \dfrac{R_3{}^3 \Phi(kR_3) - R_2{}^3 \Phi(kR_2)}{R_3{}^3 - R_2{}^3} + \\ \gamma_{\mathrm{shell}} W_{\mathrm{shell}} \dfrac{R_2{}^3 \Phi(kR_2) - R_1{}^3 \Phi(kR_1) + R_4{}^3 \Phi(kR_4) - R_3{}^3 \Phi(kR_3)}{R_2{}^3 - R_1{}^3 + R_4{}^3 - R_3{}^3} \end{array} \right]^2 \tag{2-A19}$$

In this equation, the contrast factors of the core and shell parts are calculated by

$$\gamma_{\mathrm{core}} = \frac{n'_{0,\mathrm{A}} + n'_{0,\mathrm{M}}}{M'_{0,\mathrm{A}} + M'_{0,\mathrm{M}}} - \left( \frac{\bar{v}\rho_{\mathrm{e}}}{N_{\mathrm{A}}} \right)_{\mathrm{solv}}, \quad \gamma_{\mathrm{shell}} = \frac{n_{0,\mathrm{P}}}{M_{0,\mathrm{P}}} - \left( \frac{\bar{v}\rho_{\mathrm{e}}}{N_{\mathrm{A}}} \right)_{\mathrm{solv}} \tag{2-A20}$$

respectively, the weight fractions $W_{\mathrm{core}}$ and $W_{\mathrm{shell}}$ are given by eqs 2-A11, and the structure parameters $R_1$, $R_2$, $R_3$, and $R_4$ of the vesicle defined in Figure 2-4a in the text are related each other by

$$R_2 = R_1 + H, \quad R_3 = R_2 + D, \quad R_4 = R_3 + H \tag{2-A21}$$

where $D$ is the thickness of the hydrophobic layer and $H$ is the height of the outer and inner hydrophilic layer regions. Furthermore, when the concentration of the hydrophobic layer region is denoted as $c_{\mathrm{core}}$, we have the following relations

$$c_{\mathrm{core}} = \frac{3MW_{\mathrm{core}}}{4\pi N_{\mathrm{A}} \left( R_3{}^3 - R_2{}^3 \right)} \tag{2-A22}$$

Thus, if $D$ and $c_{\mathrm{core}}$ are given, $R_2$ can calculated from $M$ by

$$R_2 = \frac{D}{2} \left( \sqrt{\frac{MW_{\mathrm{core}}}{\pi N_{\mathrm{A}} c_{\mathrm{core}} D^3} - \frac{1}{3}} - 1 \right) \tag{2-A23}$$

Using eqs 2-A21, we can calculate the remaining $R_1$, $R_3$, and $R_4$ for suitably chosen value of $H$, then $\gamma_{\mathrm{av}}{}^2 P_M(k)$ from eq 2-A19 as a function of $M$.

The scattering function $P_M(k)$ for the single bilayer vesicle calculated by eq 2-A19 has a peak, and the peak width is very sensitive to the value of $D$. When $N_{0,\mathrm{A}}$ and $N_{0,\mathrm{M}}$ of the ionic block chains have some dispersities, $D$ has also a dispersity, which makes the peak broader. To take this dispersity effect into account, we average $P_M(k)$ with respect to the dispersity in $D$, using a Gaussian distribution function:

$$\langle MP_M(k) \rangle_D = \frac{1}{\sqrt{2\pi}\sigma_D} \int MP_M(k) \exp\left[ -\frac{\left( D - \langle D \rangle \right)^2}{2\sigma_D{}^2} \right] \mathrm{d}D \tag{2-A24}$$

where $\langle D \rangle$ and $\sigma_D{}^2$ are the mean value and variance of $D$, respectively. The adjustable

parameters to calculate $P_M(k)$ for polydisperse vesicles are $M_{NC}$, $Đ_{NC}$, $c_{core}$, $H$, $\langle D\rangle$, and $\sigma_D^2$. While the value of $H$ is roughly estimated from the mean end-to-end distance of the neutral block chain, the last $\langle D\rangle$ and $\sigma_D^2$ are determined almost uniquely from the small peak of the SAXS profile.

At last, if the neutral complex is a cylinder with the core-shell structure, $P_M(k)$ is calculated by

$$\gamma_{av}{}^2 P_M(k) = \left\langle \left[ \gamma_{core} W_{core} \Psi_\alpha(kR_c) + \gamma_{shell} W_{shell} \frac{R^2 \Psi_\alpha(kR) - R_c{}^2 \Psi_\alpha(kR_c)}{R^2 - R_c{}^2} \right]^2 \Omega_\alpha^2(kL) \right\rangle_\alpha \quad \text{(2-A25)}$$

where $R_c$ and $R$ are the radii of the core and shell of the cylindrical micelle (cf. Figure 2-4b),

$$\Psi_\alpha(x) \equiv \frac{2J_1(x\sin\alpha)}{x\sin\alpha}, \quad \Omega_\alpha(x) \equiv \frac{\sin\left(\frac{1}{2}x\cos\alpha\right)}{\frac{1}{2}x\cos\alpha} \quad \text{(2-A26)}$$

and $\langle\cdots\rangle_\alpha$ represents the isotropic average with respect to the angle a between the scattering vector **k** and the cylindrical axis of the micelle. If $M_{NC}$, $c_{core}$, $R_c$, and $H$ are given, we can calculate $L$ and $R$ by

$$L = \frac{MW_{core}}{\pi N_A R_c{}^2 c_{core}}, \quad R = R_c + H \quad \text{(2-A27)}$$

The $H$ value is roughly estimated from the mean end-to-end distance of the neutral block chain.

As in the case of the single bilayer vesicle, eq 2-A25 for the cylinder has a peak, and the peak width is very sensitive to the value of $R_c$. We average $P_M(k)$ for the cylindrical micelle with respect to the dispersity in $R_c$, using a Gaussian distribution function:

$$\langle MP_M(k)\rangle_{R_c} = \frac{1}{\sqrt{2\pi}\sigma_{R_c}} \int MP_M(k) \exp\left[ -\frac{\left(R_c - \langle R_c\rangle\right)^2}{2\sigma_{R_c}{}^2} \right] dR_c \quad \text{(2-A28)}$$

where $\langle R_c\rangle$ and $\sigma_{Rc}{}^2$ are the mean value and variance of $R_c$, respectively.

Pedersen and Gerstenberg [1,2] formulated scattering functions of various micelles where the hydrophilic shell part is represented as an assembly of Gaussian chains. Their scattering functions are almost identical with the above functions for the uniform density models for the vesicle and cylinder. In a high $k$ region, however, the scattering from individual chains in the hydrophilic shell part is not negligible. This contribution is given by

$$\gamma_{av}{}^2 P_{M,chain}(k) = \frac{2\gamma_{shell}{}^2 W_{shell}}{m_{AP} + m_{MP}} \frac{\exp(-k^2\langle S^2\rangle_P) - 1 + k^2\langle S^2\rangle_P}{\left(k^2\langle S^2\rangle_P\right)^2} \quad \text{(2-A29)}$$

where $m_{AP}$ and $m_{MP}$ are aggregation numbers of AP and MP of the micelle, and $\langle S^2 \rangle_P$ is the square radius of gyration of the coronal P chain.

**Scattering Functions of the AP and MP Block Copolymers.** SAXS profiles for aqueous solutions of the individual AP and MP block copolymer samples at $c$ = 0.005 g/cm$^3$ and at $C_S$ = 1 M and 0.1 M are shown in Figure 2-A1. According to Zimm [3], $K_e c/R_\theta$ is calculated by

$$\frac{K_e c}{R_\theta} = \frac{1}{MP(k)} + 2A_2 c \tag{2-A30}$$

For the block copolymer consisting of Gaussian a and b block chains, $MP(k)$ is calculated by eq 2-A12. Here we have neglected the salt exclusion effect for the polyelectrolyte. As seen from eq 2-A12, $M$ and $P(k)$ are not the true molar mass and the true intramolecular interference factor, strictly speaking, but include the effect of the difference in the scattering power between the blocks through $\gamma_i$.

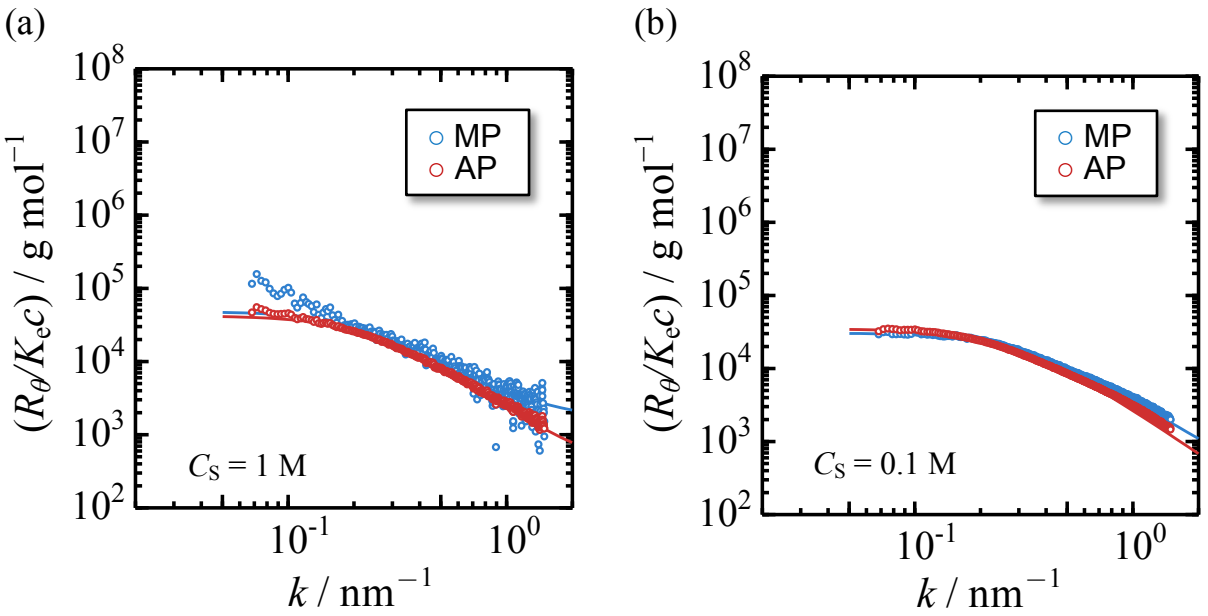


**Figure 2-A1**. SAXS profiles of the AP and MP block copolymer samples in aqueous NaCl at $C_S$ = 1 M (a) and 0.1 M (b). The polymer concentration of the all solutions is 0.005 g/cm$^3$. The red and blue solid curves indicate fitting results by eq 2-A12 using parameters listed in Table 2-A1.

The blue and red solid curves in Figure 2-A1 show fitting results by using the fitting parameters of block chains and copolymer chains of AP and MP listed in Table 2-A1. Data points for MP at $C_S$ = 1 M at low $k$ deviate from the fitting blue curve in Figure 2-A1, maybe

due to some non-ideal aggregates of MP chains. The radius of gyration of every block chain in Table 2-A1 is almost independent of $C_S$, because the chain is so short that the intramolecular excluded volume effect is not important. Second virial coefficients $A_2$ of AP and MP at 0.1 M are slightly larger than those at 1 M due to the contribution of the *inter*molecular excluded volume effect. If the radial electron density of the block chain along the chain thickness is not uniform, the scattering function at high $k$ increases and a negative value of $d^2$ may be provided [4]. This may be the reason why $d^2$ of every block chain at $C_S$ = 1 M is negative.

**Table 2-A1. Molecular Characteristics of the AP and MP samples at $C_S$ = 1 M and 0.1 M**

| sample | $C_S$ = 1 M | | | $C_S$ = 0.1 M | | |
|---|---|---|---|---|---|---|
| | $\langle S^2\rangle^{1/2}$/nm | $d^2$/nm$^2$ | $A_2$ [a] | $\langle S^2\rangle^{1/2}$/nm | $d^2$/nm$^2$ | $A_2$ [a] |
| PAMPS block | 8.0 | −1.5 | | 7.0 | −0.2 | |
| PMAPTAC block | 6.5 | −1.0 | | 5.7 | 1.0 | |
| PMPC block | 0.5 | −1.0 | | 0.5 | 1.0 | |
| AP | | | 1.0 | | | 1.5 |
| MP | | | 0.2 | | | 1.4 |

[a] In units of $10^{-3}$ cm$^3$mol g$^{-2}$.

**SAXS Profiles for Aqueous Solutions of the AP−MP Mixture at All $C_S$.** Figures 2-A2a−c show SAXS profiles for aqueous solutions of the AP−MP mixture ($c$ = 0.005 g/cm$^3$ and $x_+$ = 0.6) at all $C_S$ investigated in the present study.

**Partial Specific Volumes.** Density measurements were made on dilute aqueous NaCl solutions of three homopolymers of MAPTAC and MPC, the constituents of the MP copolymer at different $c$ and $C_S$, using an Anton Paar DMA 5000 densitometer, to determine partial specific volumes $\bar{v}_M$ and $\bar{v}_P$. Figure 2-A3 shows the $C_S$ dependences of $\bar{v}_M$ and $\bar{v}_P$ with literature data of $\bar{v}_A$ [5]. Contrast factors of the copolymers and copolymer block chains at each $C_S$ were calculated by eq 2-A6 with eq 2-A8 using these partial specific volume.

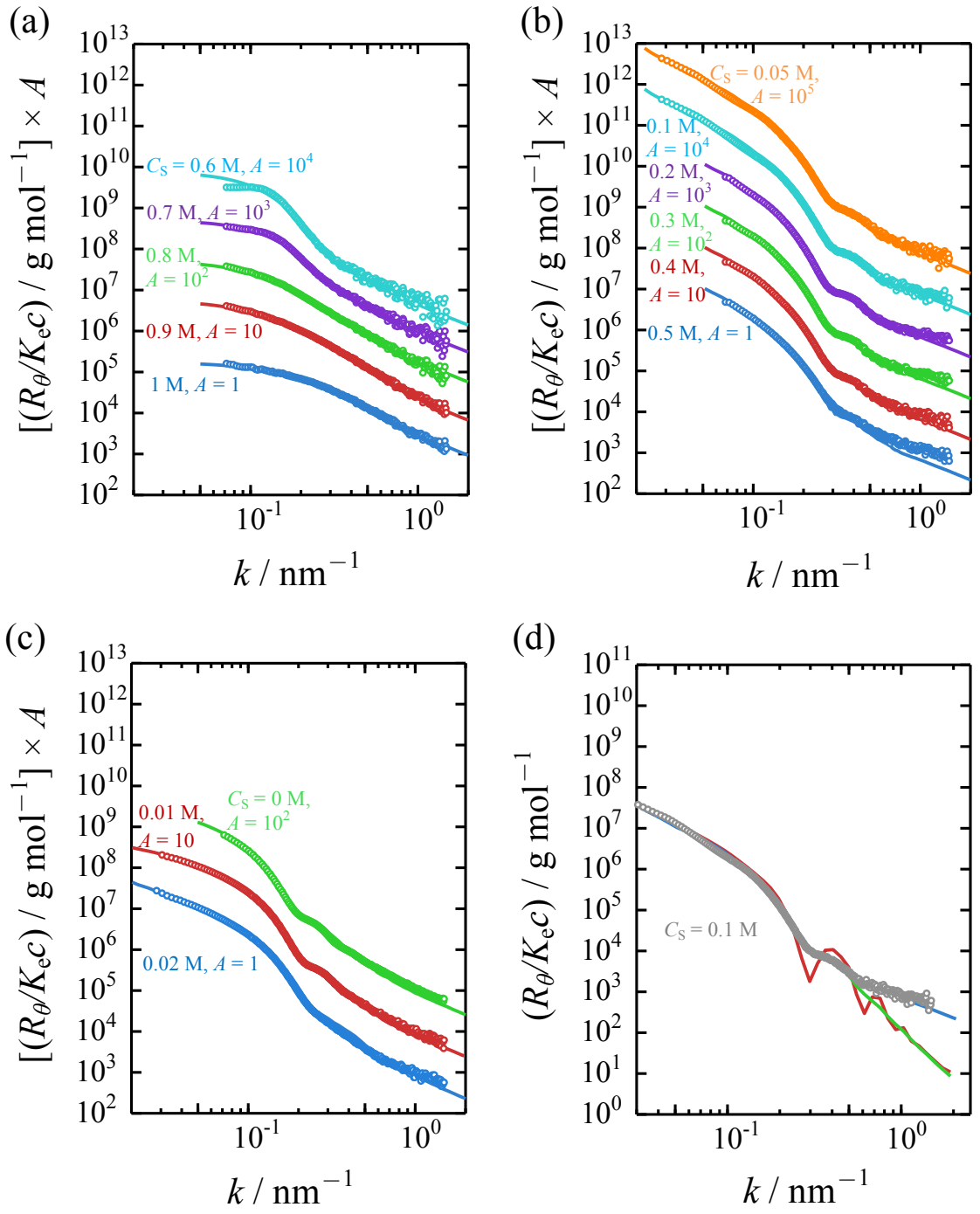


**Figure 2-A2.** SAXS profiles for aqueous solutions of the AP−MP mixture ($c$ = 0.005 g/cm$^3$ and $x_+$ = 0.6) at 1 M ≥ $C_S$ ≥ 0.6 M (a), 0.5 M ≥ $C_S$ ≥ 0.05 M (b), and at 0.02 M ≥ $C_S$ ≥ 0 M (c). The data points are shifted vertically by the factor $A$ for viewing clarity. Solid curves, fitting results calculated by eqs 2-3 and 2-4 in the text as well as eqs 2-A16−18 (a), by eqs 2-3' and 2-4 in the text as well as eqs 2-A19−24 and eq 2-A29 (b), and by eqs 2-3' and 2-4 in the text as well as eqs 2-A25−28 and eq A29 (c). Panel d compares the theoretical curve (blue curve) for $C_S$ = 0.1 M calculated by eqs 2-3', 2-4, 2-A19−24 and 2-A29, shown in Panel b, with theoretical curves without considering the dispersity of $D$ (red curve) and the

contribution of individual chains in the hydrophilic layer part (green curve).

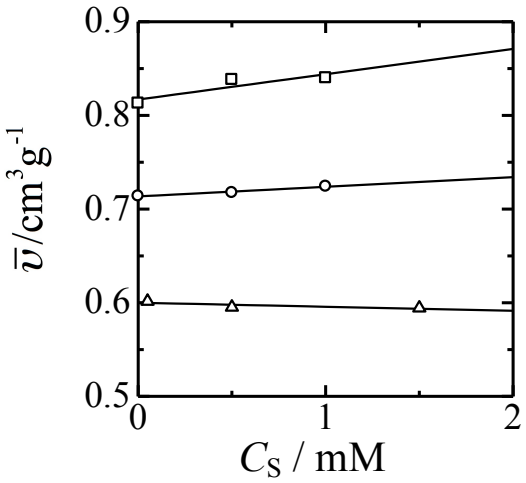


**Figure 2-A3.** $\bar{v}$ of PMPC (circle), PMAPTAC (square), and PAMPS (triangle; Ref. A5) in aqueous NaCl as a fuction of NaCl concentration at 25 °C.

**Electrophoretic Light Scattering.** The Electrophoretic mobility $U$ of the complex formed by AP and MP in a solution with $C_S$ = 0.1 M and $c$ = 0.005 g/cm$^3$ was acquired by a ELS-Z zeta potential analyzer, Otsuka Electronics Co., Ltd., Osaka. The zeta potential $\zeta$ of the complex was calculated to be +2.25 mV from $U$ by

$$\zeta = (\eta_0/\varepsilon)U \tag{2-A31}$$

where $\eta_0$ and $\varepsilon$ denotes the viscosity coefficient and the permittivity of the solvent, respectively. By assuming that the complex is a charged sphere [6], we have estimated the number of excess charges to be fewer than 1000 per the complex from the $\zeta$ value obtained. From the SAXS result, the total charge number of the complex (i.e., the vesicle) is in the order of $10^7$, so that the excess charge number is much fewer than the total charge number. Therefore, the complex is almost neutral, and adsorbs a tiny amount of the excess MP in the solution.

**More TEM Images of the AP−MP Polyion Complex Micelle.** Figure 2-5a showed a TEM image of threadlike particles dried from an aqueous solution of the AP−MP mixture ($x_+$ = 0.6) at $C_S$ = 0 M. Figure 2-A4a displays a TEM image taken in the same experimental condition, where a spherical particle coexists with threadlike particles. However, this was a very rare case, and mostly threadlike particles were observed as shown in Panel b of Figure 2-A4. On the other hand, only spherical particles were observed in all TEM images of samples prepared from aqueous AP−MP mixture solutions at $C_S$ = 0.1 M.

Figure 2-A4c shows another TEM image taken in the same experimental condition as in Figure 2-5b.

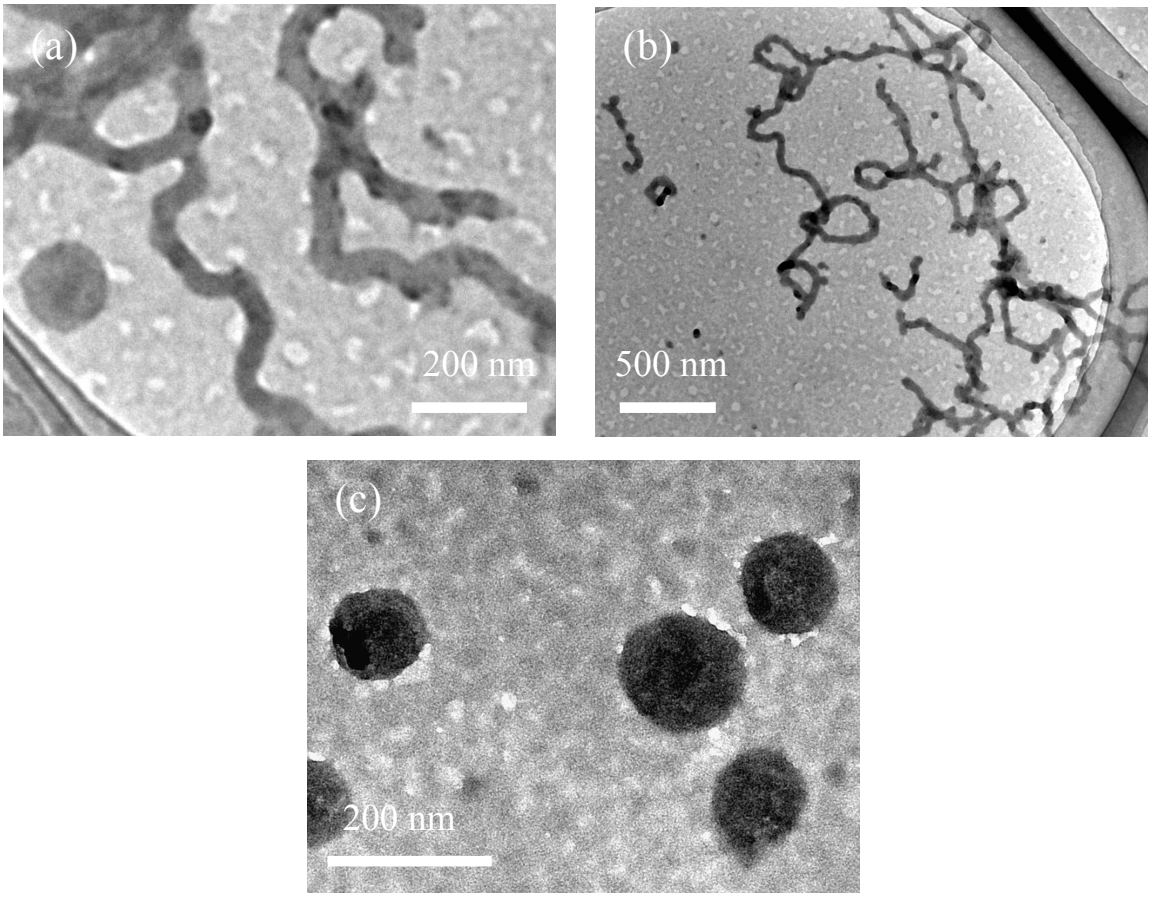


**Figure 2-A4.** TEM images of MP-AP mixtures with $x_+ = 0.6$ at $C_S = 0$ M (a, b) and 0.1 M (c).

**References**

1. J. S. Pedersen, M. C. Gerstenberg, Macromolecules **29,** 1363 (1996).
2. J. S. Pedersen, Adv. Colloid Int. Sci. **70,** 171 (1997).
3. B. H. Zimm, J. Chem. Phys. **16,** 1093 (1948).
4. S. Arakawa, K. Terao, S. Kitamura, T. Sato, Polym. Chem. **3,** 472 (2012).
5. R. Hagino, J. Yashiro, M. Sakata, T. Norisuye, Polym J. **38,** 861 (2006).
6. D. C. Henry, Proc. Roy. Soc. London A **133,** 106 (1931).

# Chapter 3. Reversible Morphology Transition of Polyion Complex Micelles Induced by Changing the Mixing Ratio of Copolymer Components

## 3.1. Introduction

Anionic−neutral and cationic−neutral block copolymers in aqueous solution form micelles with the polyion complex core (polyion complex micelle) via electrostatic interaction between cationic and anionic block chains. These polyion complex micelles have recently attracted extensive attention as nano-carriers or nano-containers for protection and controlled delivery of drugs or bio-active molecules. It is important to control the morphology and size of the polyion complex micelle at utilizing it as nano-carriers or nano-containers. Thus, extensive studies have been made [1–24], and several reviews [25−31] have been published on various aspects of the polyion complex micelle formation so far.

As shown in Figure 3-1, there are many parameters determining the morphology and size of the polyion complex micelle; the degrees of polymerization of the cationic block ($N_{0+}$), the anionic block ($N_{0-}$), and the neutral blocks ($N_{0n}^{(+)}$, $N_{0n}^{(-)}$), the molar concentrations of the cationic monomer unit ($C_{0+}$) and the anionic monomer unit ($C_{0-}$), as well as the molar concentration of the added salt ($C_S$) in the aqueous solution. Therefore, we have to study systematically dependences of the polyion complex micelle formation on each of all the above experimental parameters. Although many studies have been already performed on various polyion complex micelles, the morphology of the polyion complex micelle has not been thoroughly understood yet.

In this study, we have investigated the dependence of the morphology of the polyion complex micelle on the mixing ratio of the oppositely charged block copolymers at fixed $N_{0+}$, $N_{0-}$, $N_{0n}^{(+)}$, $N_{0n}^{(-)}$, $C_S$, and the total copolymer mass concentration $c$, by using ELS, isothermal titration calorimetry (ITC), and SAXS. In what follows, the mixing ratio is expressed in terms of the mole fraction $x_+$ of the cationic monomer unit in the total charged monomer units in the solution, defined as

$$x_+ \equiv C_{0+}/(C_{0+} + C_{0-}) \tag{3-1}$$

The effect of $x_+$ on the formation of the polyion complex micelle has been already investigated by many researchers [11–24]. In most cases, as $x_+$ approaches to ca. 0.5, $\zeta$-potential becomes 0, and both hydrodynamic radius and light scattering intensity increase. Lindhoud et al.[20] reported on the reversibility of the light scattering behavior with changing $x_+$. However, the detailed morphology of those polyion complex micelles has been investigated only at $x_+ \sim 0.5$ so far. In this paper, we report a reversible morphology

transition of a polyion complex micelle by changing $x_+$. To the best of our knowledge, this is the first report on the mixing-ratio-induced morphology transition of the polyion complex micelle.

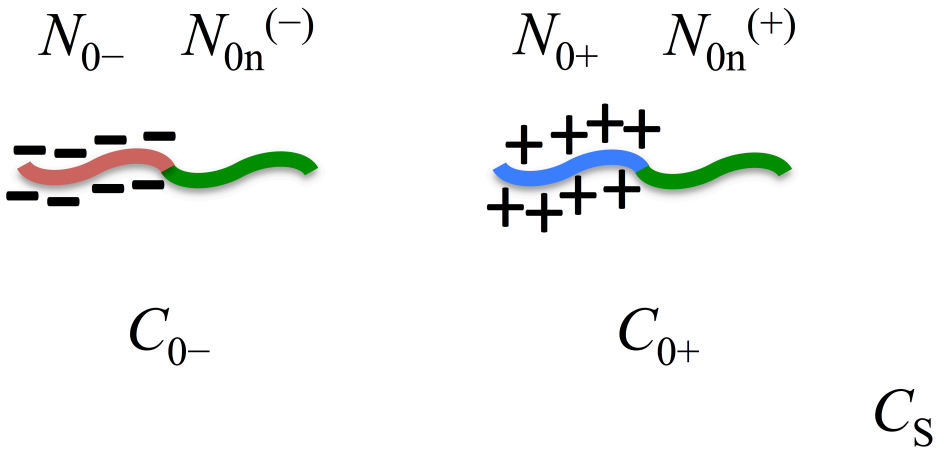


**Figure 3-1.** Various parameters determining the morphology and size of the polyion complex micelle.

We have chosen the same anionic–neutral block copolymer (AP) and cationic-neutral block copolymer (MP) used in Chapter 2 (cf. Chart 1-1). Although PMPC is not nonionic but zwitter ionic, it has been demonstrated that the inter-chain interaction of PMPC in aqueous solution is independent of the ionic strength [32,33], so that PMPC can be regarded as a neutral block chain. It is well known that PMPC is highly biocompatible, because its chemical structure resembles the lipid of biomembranes [34]. In the present study, we have used AP and MP samples with the degrees of polymerization $N_{0-} \sim N_{0+} >> N_{0n}^{(+)} \sim N_{0n}^{(-)}$, and fixed the added NaCl concentration $C_S$ to be 0.1 M. From the result of the previous Chapter 2, these AP and MP samples form a vesicle at $C_S = 0.1$ M and $x_+ \sim 0.5$.

The anionic monomer unit $A^-$ in the anionic block chain and the cationic monomer unit $M^+$ in the cationic block chain bear uni-valent negative and positive charges, respectively, and can form the neutral complex MA by the strong electrostatic attraction. If $A^-$ and the counterion, $M^+$ and the counterion, and MA are regarded as thermodynamically independent components, we view the block copolymer mixture solution as a quaternary system of $A^-$, $M^+$, MA, and the solvent. (Although the solution contains also NaCl and the neutral block chains of AP and MP, we do not consider them in discussion of the solution composition.)

Since the neutral complex MA has no net charges, its solubility to the aqueous medium should be much lower than $A^-$ or $M^+$, and a liquid-liquid phase separation may take place in the quaternary solution. If we regard the micellization as a kind of the phase

separation and the hydrophobic core of the micelle formed by AP and MP as the coexisting concentrated phase, we can specify the composition of the solution in terms of the molar concentrations of $A^-$ ($C_{0-}^{(d)}$), $M^+$ ($C_{0+}^{(d)}$), and MA ($C_{0\pm}^{(d)}$) in the coexisting dilute phase, and of $A^-$ ($C_{0-}^{(c)}$), $M^+$ ($C_{0+}^{(c)}$), and MA ($C_{0\pm}^{(c)}$) in the coexisting concentrated phase (or the hydrophobic core), as shown in Figure 3-2. In what follows, the hydrophobicity of MA is assumed to be so strong that $C_{0\pm}^{(d)} = 0$ [35,36]. Thus, we can specify the composition of the aqueous solution of the AP–MP mixture in terms of the six variables, $C_{0-}^{(d)}$, $C_{0+}^{(d)}$, $C_{0-}^{(c)}$, $C_{0+}^{(c)}$, $C_{0\pm}^{(c)}$, and the volume fraction of the concentrated phase (the hydrophobic cores) $\Phi^{(c)}$ in the solution.

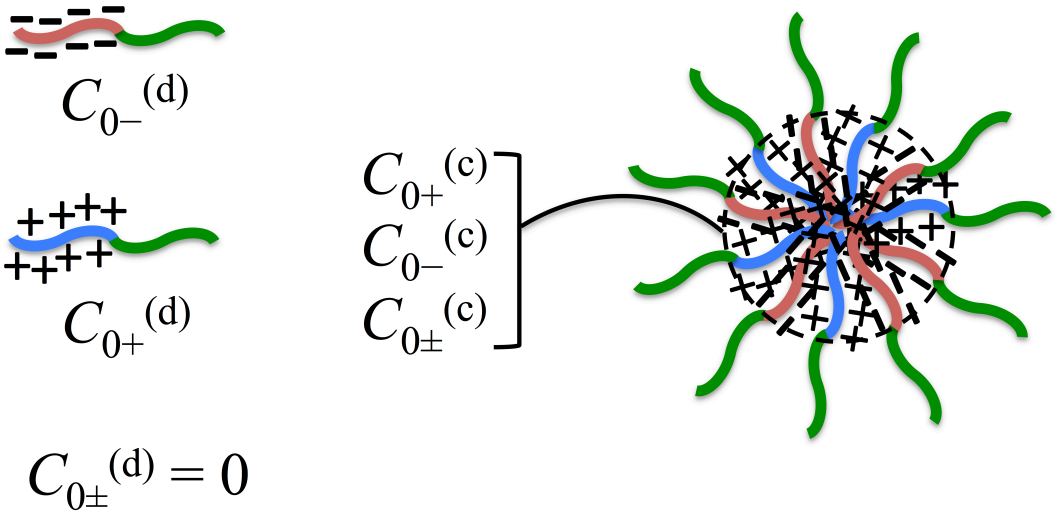


**Figure 3-2.** Composition variables in the aqueous solution containing the anionic−neutral and cationic−neutral block copolymers.

These composition variables change with the mixing ratio $x_+$ at constant total copolymer concentration $c$. With increasing $x_+$, $C_{0+}^{(c)}$ and $C_{0-}^{(c)}$ should increase and decrease, respectively, according to the phase equilibrium condition (cf. Appendix 3). When $C_{0+}^{(c)} > C_{0-}^{(c)}$ ($C_{0+}^{(c)} < C_{0-}^{(c)}$), the micelle is positively (negatively) charged, and the electrostatic interaction of the micelle changes along with $x_+$, which may induce the morphology transition of the micelle.

## 3. 2. Experimental Section

**Materials.** The same AP and MP as used in the previous Chapter focusing on the

effect of salt addition were also used in this chapter. Procedure for the synthesis of AP and MP was described previously [24]. Table 3-1 lists molecular characteristics of the AP and MP samples. Water was purified by using a Millipore Milli-Q system. Sodium chloride NaCl (> 99.5%) was purchased from Wako Pure Chemical Industries, Ltd., Osaka and used as received.

**Table 3-1. Molecular Characteristics of AP and MP Samples [10]**

| sample | $M_{n,1}$ [a] | $M_{w,1}/M_{n,1}$ [b] | $M_{w,1}$ [c] | $M_{wn,1}$ [d] | $M_{w-,1}$ [d] | $M_{w+,1}$ [d] | $N_{0n}$ [e] | $N_{0-}$ [e] | $N_{0+}$ [e] |
|---|---|---|---|---|---|---|---|---|---|
| PMPC | 6,210 | 1.03 | 6,400 | | | | | | |
| AP | 47,200 | 1.56 | 73,600 | 6,400 | 67,200 | | 21.7 | 293 | |
| MP | 49,300 | 1.09 | 53,700 | 6,400 | | 47,300 | 21.7 | | 215 |

[a]Number-average molecular weight determined by $^1$H NMR. [b]Dispersity index determined by SEC. [c]Weight-average molecular weight calculated from $M_{w,1}/M_{n,1}$ and $M_{n,1}$. [d]Weight-average molecular weight of the neutral block chain $M_{w\pm,1}$, the anionic block chain $M_{w-,1}$, or the cationic block chain $M_{w+,1}$ calculated from $M_{w,1}$ of the PMPC, AP, or MP samples. [e]Weight-average degree of polymerization of each block chain using the monomer-unit molar mass $M_{0n} = 295$, $M_{0-} = 229$, or $M_{0+} = 220.5$.

**Preparation of Test Solutions.** Test solutions were prepared by two different procedures. Firstly, the MP and AP samples were dissolved separately in pure water or in 0.1 M aqueous NaCl. In the one procedure, the aqueous MP solution was added into the aqueous AP solution dropwise with gentle stirring by hand and then the mixture solution was shaken by a vortex mixer. The solution prepared in this procedure is denoted as the solution MP→AP. In the other procedure, the aqueous AP solution was added into the aqueous MP solution in the same manner. The solution prepared in this procedure is denoted as the solution AP→MP. For the salt free solutions, solid NaCl was added after mixing MP and AP to adjust $C_S$ to be 0.1 M.

The solutions were prepared at room temperature without sonication or thermal treatment. The X-ray scattering intensity of the mixture solution did not change with time from 1 to 50 h after the preparation. The total polymer concentration $c$ and NaCl concentration $C_S$ were fixed at 0.005 g/cm$^3$ and 0.1 M, respectively.

**Electrophoretic Light Scattering.** Electrophoretic mobility $U_m$ of the complex formed of AP and MP in aqueous NaCl solution was obtained at 25 °C using a ELS-Z $\zeta$-potential analyzer (Otsuka Electronics Co., Ltd., Osaka). Test solutions for ELS were

prepared by mixing salt free solutions of MP and PA and then by adding NaCl to the mixture solution. The electro-osmotic effect was corrected. The zeta potential $\zeta$ of the complex was calculated from $U_m$ by

$$\zeta = \frac{\eta_0}{\varepsilon} U_m \tag{3-2}$$

where $\eta_0$ and $\varepsilon$ denotes the viscosity coefficient and the permittivity of the solvent, respectively.

**Isothermal Titration Calorimetry.** ITC were performed at 25 °C with MicroCal VP-ITC (Malvern Instruments Ltd, Worcestershire) in two procedures. In the first procedure, an aqueous solution of AP ($c = 5.0 \times 10^{-3}$ g/cm$^3$) containing 0.1 M NaCl was titrated from a syringe into the cell of volume 1.417 mL, filled with an aqueous solution of MP ($c = 2.5 \times 10^{-4}$ g/cm$^3$) containing 0.1 M NaCl. In the second procedure, an aqueous solution of MP ($c = 5.0 \times 10^{-3}$ g/cm$^3$) containing 0.1 M NaCl was titrated from a syringe into the cell filled with an aqueous solution of MP ($c = 2.5 \times 10^{-4}$ g/cm$^3$) containing 0.1 M NaCl. In both cases, 0.1 $\mu$L of the titrant was first added to the solution, and then 5 $\mu$L of the titrant was titrated 27 times by the intervals of 1000 s with stirring at 502 rpm. A reference cell was filled with an aqueous solution of 0.1 M NaCl. The heat of dilution (much smaller contribution) was subtracted from the data.

**Small-Angle X-Ray Scattering.** Synchrotron radiation SAXS experiments were carried out as described in Chapter 2.

## 3. 3. Results and Discussion

**Electrophoretic Light Scattering.** The net charge of the micelle formed by AP and MP was investigated using ELS. Figure 3-3 shows the $\zeta$-potential ($\zeta$) of the polyion complex micelles plotted against $x_+$. The results are almost identical for the solutions of MP→AP and AP→MP. It can be seen from the results that $\zeta$ becomes 0 or $C_{0+}^{(c)} = C_{0-}^{(c)}$ at $x_+ = 0.55$. In what follows, we denote this value of $x_+$ where $\zeta = 0$ as $x_+^{(c)}$ (= 0.55). The hydrophobic core contains an excess amount of anionic monomer unit $A^-$ at $x_+ < x_+^{(c)}$, and an excess amount of the cationic monomer unit at $x_+ > x_+^{(c)}$.

If the interaction between the neutral complex MA and the anionic monomer unit $A^-$ in the hydrophobic core is identical with that between MA and $M^+$, as well as $N_{0+} = N_{0-}$ and $N_{0n}^{(+)} = N_{0n}^{(-)}$ (cf. Figure 3-1), $x_+^{(c)}$ must be equal to 0.5 by symmetry. However, unless the above conditions are not fulfilled, $x_+^{(c)}$ is not necessarily be 0.5. If the *non-electrostatic*

attractive interaction between MA and $A^-$ is stronger than that between MA and $M^+$ under the conditions of $N_{0+} = N_{0-}$ and $N_{0n}^{(+)} = N_{0n}^{(-)}$, $x_+^{(c)}$ should be larger 0.5.

**Isothermal Titration Calorimetry.** Figure 3-4 shows the time course of heat flow at ITC measurements and the molar enthalpy $\Delta H$ of mixing obtained by integrating the heat flow peaks, plotted against $x_+$. When the aqueous MP solution is titrated into the aqueous AP solution (the solution MP →AP), $\Delta H$ is positive at $x_+ < 0.5$, but changes sign and takes a minimum at $x_+ \sim 0.55$, and finally tends to zero at $x_+ > 0.6$. On the other hand, when the aqueous AP solution is titrated into the aqueous MP solution (the solution AP →MP), $\Delta H$ is positive at $x_+ > 0.5$, takes a maximum at $x_+ \sim 0.55$, and tends to zero at $x_+ < 0.45$. Similar minimum and maximum of $\Delta H$ were reported in other polyion complex systems [14,37,38].

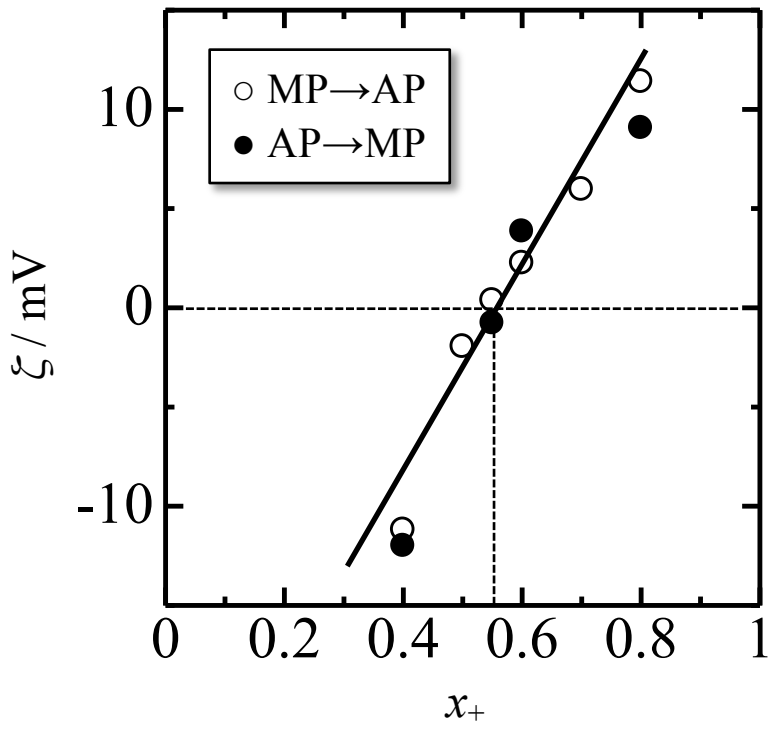


**Figure 3-3.** $\zeta$-potential for the polyion complex micelle formed of AM and MP, plotted against $x_+$. Unfilled symbol and filled symbol indicate that the solutions are prepared by the procedures MP→AP and AP→MP, respectively.

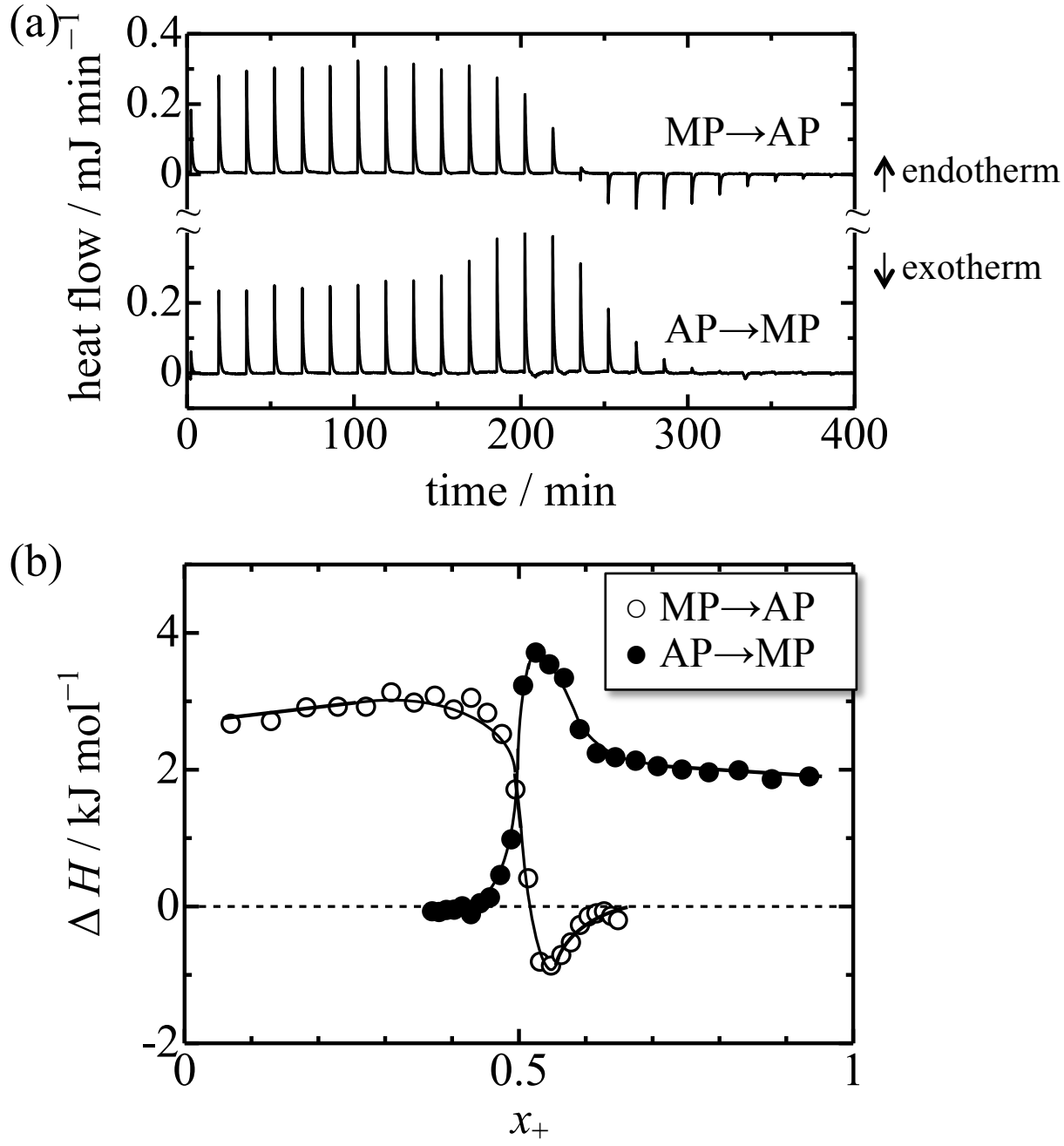


**Figure 3-4.** ITC thermograms (a) and the molar enthalpy of mixing Δ$H$ as a function of $x_+$ (b) in AP−MP complexation.

When MP and AP is mixed in aqueous solution, the cationic and anionic monomer units ($M^+$ and $A^-$) form the neutral complex MA, and MA forms the hydrophobic core. As shown in Figure 3-3, an excess amount of $A^-$ is included in the hydrophobic core at $x_+ < 0.55$, and the excess component in the hydrophobic core changes from $A^-$ to $M^+$ when $x_+$ exceeds 0.55. The positive Δ$H$ (endotherm) at small $x_+$ for the solution MP→AP and at large $x_+$ for

the solution AP→MP is mainly due to the increase in the electrostatic energy by the separation of counterions from the polyion chains at the complex formation. The minimum and maximum of $\Delta H$ may reflect the conversion of the excess component in the hydrophobic core between $M^+$ and $A^-$, indicating that the insertion of the MP chain into the hydrophobic core is exothermic, while the insertion of the AP chain into the hydrophobic core is endothermic. The endotherm in the latter case may be due to the dehydration of the AP chain at the insertion. After the minimum and maximum, $\Delta H$ becomes almost 0, demonstrating that the MP or AP chains added further do not interact with the polyion complex in the solution, but exist as dispersed single chains.

**SAXS profiles.** Figure 3-5a shows SAXS profiles for the mixtures in MP→AP solutions with $x_+ = 0.4$, 0.55, and 0.8 at $c = 0.005$ g/cm$^3$ and at $C_S = 0.1$ M; NaCl was added to the solution after mixing MP and AP. In the figure, $R_\theta$ is the excess Rayleigh ratio, $K_e$ is the optical constant (cf., eq 3-A1 in Appendix 3), and $k$ is the magnitude of the scattering vector. The profile at $x_+ = 0.55$ ($\equiv x_+^{(c)}$), where $\zeta \sim 0$, exhibits the power low, $R_\theta/K_e c \propto k^{-2}$, in the low $k$ region, and also has a small peak around $k \sim 0.3$ nm$^{-1}$, indicating vesicle formation as shown in Chapter 2. By changing $x_+$ to be 0.4 and 0.8, the profiles in the low $k$ region have slopes much weaker than $k^{-2}$, and the small peaks slightly shift toward lower $k$ and the peak heights diminish. The apparent radius of gyration was estimated to be 20 nm at both $x_+ = 0.4$ and 0.8 from the Guinier plot (not shown). However, values of $R_\theta/K_e c$ in the low $k$ region at $x_+ = 0.4$ and 0.8 are much higher than those of AP and MP individual solutions ($x_+ = 0$: dark red circle and $x_+ = 1$: dark blue circle, respectively) and the apparent molar mass obtained from $R_\theta/K_e c$ at $k = 0$ is ca. $10^7$, being much higher than $M_{w,1}$ of AP and MP samples (cf. Table 3-1). These results demonstrate that AP and MP form micelles also at $x_+ = 0.4$ and 0.8, but the micelles formed are much smaller than the vesicle at $x_+ = x_+^{(c)}$.

Figure 3-5b collects more SAXS profiles for MP→AP solutions with different $x_+$ (circles with downward bar). When $x_+$ departs from $x_+^{(c)} = 0.55$, the slope of the profile in the low $k$ region becomes smaller. Figure 3-5b also contains MP→AP solutions at $x_+ = 0.4$ and 0.8 where NaCl was added to the solutions before mixing MP and AP (blue and orange circles with upward bar). The scattering functions are almost identical with those for MP→AP solutions at the same $x_+$. Here, NaCl was added after mixing AP and MP. The micelle morphology at $x_+ = 0.4$ and 0.8 does not depend on the order of mixing of AP, MP, and NaCl.

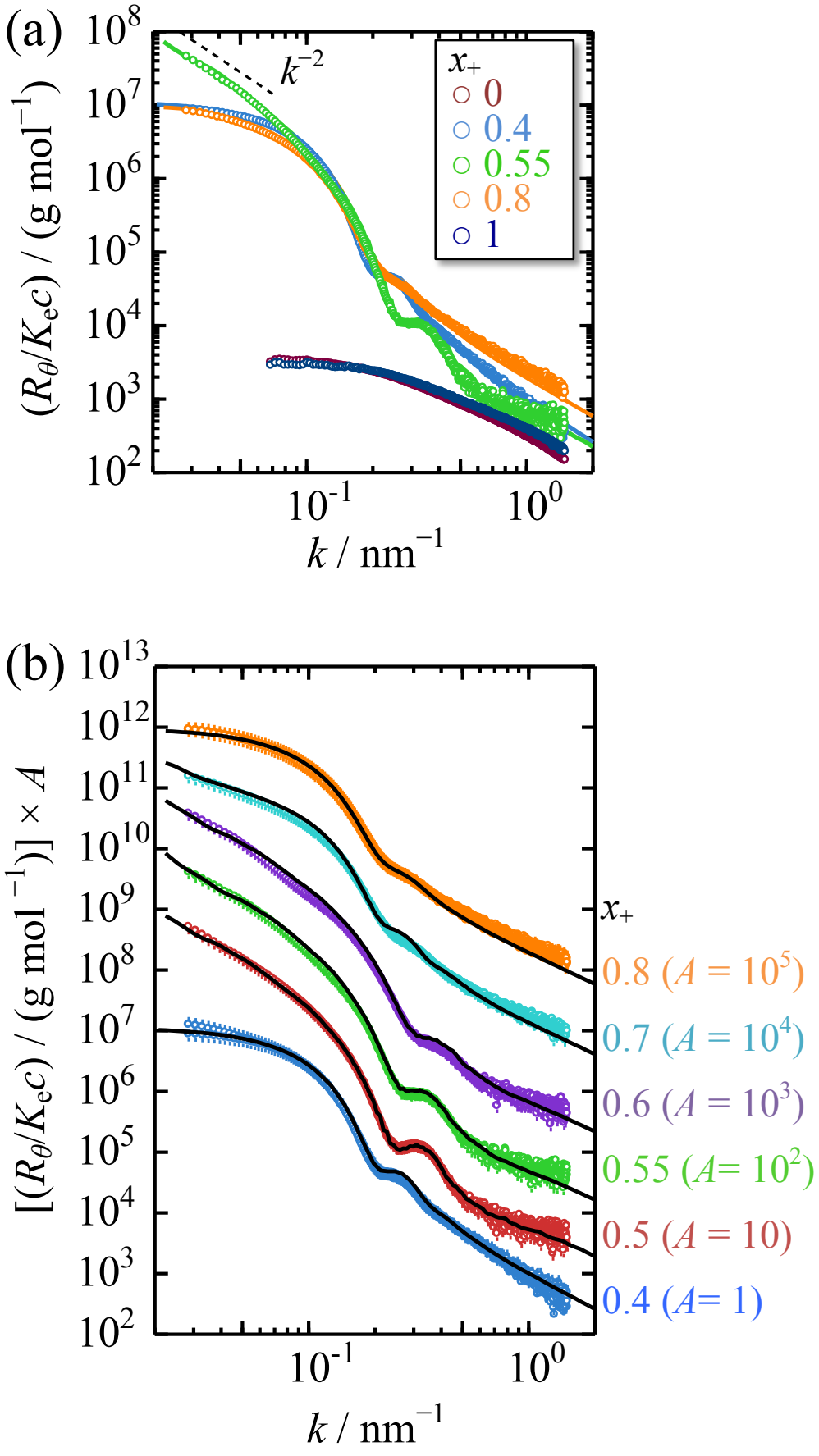


**Figure 3-5.** SAXS profiles of AP−MP mixtures with different $x_+$ in aqueous solution

containing 0.1 M NaCl. (a) Comparison with $x_+$ = 0, 0.4, 0.55, 0.8, and 1 in absolute intensity. The solutions were prepared by MP→AP, and NaCl is added after mixing AP and MP solution. (b) The data at $x_+$ = 0.4, 0.5, 0.55, 0.6, 0.7, and 0.8, shifted vertically multiplied by $A$ for clarity. Circles with downward bar indicate scattering functions for MP→AP solutions. Here, NaCl was added after mixing AP and MP. Circles with upward bar for $x_+$ = 0.4 and 0.8 indicate scattering functions for MP→AP solutions. Here, NaCl was also added before mixing AP and MP. The solid lines indicate theoretical curves calculated by eqs 3-8, 3-13, and equations in Appendix 3.

**Fitting the SAXS Profiles.** In the aqueous solution of AP−MP mixtures, the polyion complex micelle and the excess free AP or MP component coexist as binary scattering components. In what follows, the free AP or MP and the polyion complex micelle are referred to as component 1 and 2, respectively. When the molar mass distribution of the component obeys the log-normal distribution, the scattering function of the solution may be given by [10,39,40]

$$\frac{R_\theta}{K_e c} = \frac{1}{{\gamma_{av}}^2}\left\{\frac{{\gamma_1}^2 w_1 M_1 P_1(k)}{1+2A_{2,11}M_1P_1(k)cw_1} + \frac{{\gamma_2}^2 w_2}{\sqrt{2\pi \ln Đ_2}}\int P_M(k)\exp\left[-\frac{\ln^2\left(\sqrt{Đ_2}\,M/M_2\right)}{2\ln Đ_2}\right]\mathrm{d}M\right\} \quad (3\text{-}3)$$

Here, $\gamma_i$, $M_i$,, and $w_i$ are the contrast factor, the weight-average molar mass, and the weight fraction of the component $i$ (= 1, 2), respectively, $A_{2,11}$ and $P_1(k)$ are the second virial coefficient and the particle scattering function of the component 1, respectively, $P_M(k)$ is the particle scattering function of the component 2 with the molar mass $M$, and $Đ$ is the molar mass dispersity (i.e., the weight- to number-average molar mass ratio) of the component 2. We have ignored the interparticle interference between polyion complex micelles as well as between the polyion complex micelle and free AP or MP chain in eq 3-3. Second virial coefficients $A_{2,11}$ for AP and MP at $C_S$ = 0.1 M are 1.5 × $10^{-3}$ cm$^3$ g$^{-2}$mol and 1.4 × $10^{-3}$ cm$^3$ g$^{-2}$mol, respectively (cf. Chapter 2).

As explained in Appendix 3, $w_i$ is given by

$$w_1 = 1 - w_2 = \begin{cases} = \dfrac{x_+ - \rho(1-x_+)}{x_+ + (M_{AP}/M_{MP})(N_{0+}/N_{0-})(1-x_+)} & \left(x_+ \geq x_+^{(d)}\right) \\ = \dfrac{1-\left(1+\rho^{-1}\right)x_+}{x_+ + (M_{MP}/M_{AP})(N_{0-}/N_{0+})(1-x_+)} & \left(x_+ < x_+^{(d)}\right) \end{cases} \quad (3\text{-}4)$$

where $x_+^{(d)}$ is the mixing ratio at which the excess component in the dilute phase converts from AP to MP calculated by eq 3-A13, and $\rho$ is defined as

$$\rho \equiv \frac{C_{0\pm}^{(c)} + C_{0+}^{(c)}}{C_{0\pm}^{(c)} + C_{0-}^{(c)}} \tag{3-5}$$

with the molar concentrations of the cationic monomer unit ($C_{0+}^{(c)}$), of the anionic monomer unit ($C_{0-}^{(c)}$), and of the neutral complex ($C_{0\pm}^{(c)}$) in the hydrophobic core, which are formulated in Appendix 3 (eqs 3-A11 and 3-A12). The parameter $\rho$ corresponds to $1 + x_{AP}^{E}$ in the previous paper. While $x_{AP}^{E}$ was an adjustable parameter, $\rho$ can be calculated by eqs 3-5, 3-A11, and 3-A12.

At $x_+ = 0.55 = x_+^{(c)}$, we have $\rho = 1$ because $C_{0+}^{(c)} = C_{0-}^{(c)} = 0$ from eqs 3-A12. Thus, eq 3-4 gives us $w_1 = 0.10$ and $w_2 = 0.90$ at $x_+ = 0.55$ ($> x_+^{(d)}$). As demonstrated previously, the mixture of the MP and AP samples forms a vesicle in the aqueous solution with $C_S = 0.1$ M and $x_+ = 0.6$. The feature of the SAXS profile indicates the formation of the vesicle also at $x_+ = 0.55$, as mentioned above. The scattering function $P_M(k)$ for the vesicle is calculated by eqs 3-A21−28 in Appendix 3 [41−43]; $\gamma_{core}$ in eq 3-A22 is equal to $\gamma_\pm$ from eq 3-A19 at $C_{0+}^{(c)} = C_{0-}^{(c)} = 0$. The component 1 at $x_+ = 0.55$ is the free MP, of which scattering function is calculated from the thin solid curve in Figure 3-5b. However, it turns out that the contribution of the component 1 to $R_\theta/K_e c$ is negligibly small, as mentioned in Chapter 2.

The fitting of the scattering function for the vesicle to the experimental result at $x_+ = 0.55$ was made as follows. The radius of gyration $\langle S^2 \rangle_n^{1/2}$ of the coronal chain must be in the range of 1.1 nm (the coil limit) and 1.6 nm (the rod limit) from the degree of polymerization $N_{0\pm}$ (= 21.7) of the PMPC chain, and we have chosen $\langle S^2 \rangle_n^{1/2}$ to be 1.5 nm; the other choice within the above range does not affect the fitting. Thus, fitting parameters are the weight-average molar mass $M_2$ and the molar mass dispersity $Đ$ of the vesicle, the mass concentration $c_{core}$ of the hydrophobic core, and the mean value $\langle D \rangle$ and the variance $\sigma_D$ of the hydrophobic core thickness. Among them, $\langle D \rangle$ and $\sigma_D$ are almost uniquely determined from the small peak position ($k \sim 0.35$ nm$^{-1}$) and the sharpness of the scattering function, $M_2$ and $c_{core}$ are mainly determined from the absolute value and the $k$ dependence of $R_\theta/K_e c$ at low $k$, and $Đ$ slightly modifies the $k$ dependence of $R_\theta/K_e c$ at low $k$. Therefore, we can almost uniquely determine the five adjustable parameters by fitting the theoretical $R_\theta/K_e c$ to the experimental. The fitting result is shown by the green solid curve in Figure 3-5a, and the fitting parameters selected are listed in Table 3-2. Further details of the vesicle fitting are given in the Chapter 2.

**Table 3-2. Characteristics of the Micelles formed of AP and MP**

| $x_+$ | morphology | $M_2$ ($10^7$ g/mol) | $m_2$ | $Đ$ | $c_{core}$ (g cm$^{-3}$)[a] | $2R_{core}$ (nm) | $R_{in}$, $R_{out}$ (nm) | $\langle D \rangle$ (nm) | $s_D$ (nm) | $\langle S^2 \rangle_n^{1/2}$ (nm)[a] | $c_{corona}$ (g cm$^{-3}$) | $n_c$ [b] |
|---|---|---|---|---|---|---|---|---|---|---|---|---|
| 0.4 | sphere | 1.4 ± 1 | 250 | 1.2 ± 0.05 | | 46 | | | | | 0.13 | 3700 |
| 0.5 | vesicle | 80 ± 40 | 14000 | 2[c] | | | 97, 120 | 22.5 ± 0.5 | 2.5 | | 0.17 | |
| 0.55 | vesicle | 80 ± 40 | 14000 | 2[c] | 0.4 | | 100, 120 | 21.5 ± 0.5 | 3 | | 0.16 | |
| 0.6 | vesicle | 80 ± 40 | 14000 | 2[c] | ± 0.03 | | 110, 130 | 19 ± 0.5 | 3.5 | 1.5 | 0.15 | |
| 0.7 | sphere | +1.2 ± 1,[d] | 220,[d] | 1.3 ± 0.05,[d] | | 44[d] | 98, 120[e] | 22[c,e] | 3.5[c,e] | | 0.13,[d] 0.17[e] | |
| | vesicle | 80[c,e] | 14000[e] | 2[c,e] | | | | | | | | |
| 0.8 | sphere | 1.2 ± 1 | 220 | 1.3 ± 0.05 | | 44 | | | | | 0.13 | 3000 |

[a] The common value for all $x_+$. [b] Average values of the results in AP→MP and MP→AP. [c] Assumed values. [d] Values for the spherical micelle with the weight fraction $w_{sph} = 0.48$. [e] Values for the vesicle with the weight fraction $w_{ves} = 0.15$.

We can expect that the smaller micelles in the solutions at $x_+$ = 0.4 and 0.8 are spherical one, because the apparent radii of gyration of the micelles (see above) were consistent with those expected for the spherical micelle formed by the AP and MP samples [44]. In the first approximation, we take $\rho$ to be unity also at $x_+$ = 0.4 and 0.8, assuming that $C_{0+}^{(c)}$, $C_{0-}^{(c)} << C_{0\pm}^{(c)}$. Then, we can calculate $w_1$ by eq 3-4 to be 0.20 (0.60), and the component 1 is AP (MP) at $x_+$ = 0.40 (0.8). The scattering function for the component 1 can be calculated from the thin solid and dashed curves in Figure 3-5a as well as $A_{2,11}$ values determined experimentally (see above).

The scattering function $P_M(k)$ for the spherical micelle is calculated by eqs 3-A29−31 in Appendix 3 [41−43], and we can use the same values for the radius of gyration $\langle S^2\rangle_n^{1/2}$ of the coronal chain and the mass concentration $c_{core}$ of the hydrophobic core as in the case of the vesicle at $x_+$ = 0.55. Thus, the adjustable parameters are only $M_2$ and $Đ$ in eq 3-3. As shown by the blue and orange curves in Figure 3-5b, the fittings are very good, so that we can conclude the smaller micelles at $x_+$ = 0.4 and 0.8 are spherical one. TEM Images for the spherical micelles are given in Appendix 3. The thickness of the hydrophobic core is $2R_{core}$ for the spherical micelle, which can be calculated by eq 3-A31 in Appendix 3.

Table 3-2 also lists the aggregation number $m_2$ (i.e., the number of block copolymer chains per micelle) calculated by eq 3-A26 in Appendix 3, the radius $R_{core}$ of the hydrophobic core of the spherical micelle by eq 3-A31, the inner and outer radii $R_{in}$ and $R_{out}$ of the hydrophobic shell of the vesicle by eqs 3-A28, and the polymer mass concentration $c_{corona}$ in the coronal region by eq 3-A32. Although we do not consider the interfacial thickness between the core (or shell) and coronal regions, the SAXS profiles are well fitted, indicating that the hydrophobic core and shell have sharp interface.

As mentioned in Chapter 2, the thickness of the hydrophobic region must be larger in the order of vesicle, cylinder, and sphere, due to the interfacial energy of the micelles. As seen in Table 3-2, the thickness of the hydrophobic core $2R_{core}$ for the spherical micelle is larger than the corresponding thickness $\langle D\rangle$ for the vesicle. This is consistent with the interfacial energy prediction (c.f. Chapter 2) and also with the literature data [43,45−48].

For the spherical particle of the radius $R$, the total net charge number $n_c$ can be calculated from the $\zeta$ by [49,50]

$$\zeta = \frac{n_c e(1+\kappa a)}{6\pi\varepsilon[1+\kappa(R+a)]} F(\kappa R) \tag{3-6}$$

with

$$F(x) \equiv 1 + \frac{1}{16}x^2 - \frac{5}{48}x^3 - \frac{1}{96}x^4 + \frac{1}{96}x^5 - \exp(x)\left(\frac{1}{8}x^4 - \frac{1}{96}x^6\right)\int_\infty^x \frac{\exp(-t)}{t}dt \tag{3-7}$$

where $e$ is the elementary charge, $\kappa$ is the reciprocal of the Debye length, $a$ is the effective radius of the ion, approximately equal to be 0.1 nm, and $\varepsilon$ is the permittivity of the solvent. Because $\langle S^2 \rangle_n^{1/2} << R_{core}$ for the spherical micelle at $x_+ = 0.4$ and 0.8, we can approximate $R$ to $R_{core}$. Table 3-2 lists the values of $n_c$ calculated by the above equations using the results shown in Figure 3-3. The total charge of the spherical micelle calculated by $(N_{0+} + N_{0-})m_2$ ($m_2$: the aggregation number of the micelle, calculated by eq 3-A26 in Appendix 3) is in order of $10^5$, so that the net charge is much smaller than the total charge in the spherical micelle. As explained in Appendix 3, the molar concentrations $C_{0+}^{(c)}$, $C_{0-}^{(c)}$, and $C_{0\pm}^{(c)}$ in the hydrophobic core, and thus $\rho$ in eq 3-10, can be calculated from $n_c$ by eqs 3-A8, 3-A11 and 3-A12 where $c^{(c)} = c_{core}$ and $M^{(c)} = M_2$. The result of $\rho$ for the spherical micelle is 1.1 at $x_+ = 0.4$ and 0.9 at $x_+ = 0.8$, and the above fittings for the spherical micelles at $x_+ = 0.4$ and 0.8 (approximating $\rho = 1$) are little affected by the correction of the $\rho$ value.

The scattering functions at $x_+ = 0.5$ and 0.6 in Figure 3-5b are also fitted by the vesicle model, but that at $x_+ = 0.7$ had to be fitted by the mixture of the vesicle and the spherical micelle. The scattering function for the mixture is calculated by

$$\sum_{i=\text{sph, ves}} \frac{w_i}{\sqrt{2\pi \ln Đ_i}} \int \left[ {\gamma_2}^2 P_M(k) \right]_i \exp\left[ -\frac{\ln^2\left(\sqrt{Đ_i}\, M/M_i\right)}{2 \ln Đ_i} \right] \mathrm{d}M \tag{3-8}$$

instead of the second term in the parentheses on the right-hand side of eq 3-3. The fitting results are shown by solid curves in Figure 3-5b, and fitting parameters chosen at $x_+ = 0.5$, 0.6, and 0.7 are listed in Table 3-2.

**Reversibility of the Morphology Transition.** When the MP→AP solution of $x_+ = 0.55$ with $C_S = 0.1$ M was mixed with AP and MP solutions including 0.1 M NaCl to prepare solutions of $x_+ = 0.4$ and 0.8, respectively, the scattering intensity in the low $k$ region decrease and small peaks shift toward lower $k$, as shown in Figure 3-6 (from green circles to blue and orange circles). The scattering functions are almost identical with those for MP→AP solutions at $x_+ = 0.4$ and 0.8 in Figure 3-5. Moreover, the solutions of $x_+ = 0.4$ and 0.8 such prepared were mixed with MP and AP solutions including 0.1 M NaCl, respectively, to recover $x_+$ to be 0.55, the SAXS profiles (brown and purple circles) return to that for the original MP→AP solution at $x_+ = 0.55$ (green circles). These results demonstrate that the morphology transition between the spherical micelle and the vesicle induced by changing $x_+$ is reversible. Furthermore, the vesicle size is independent of the mixing pathway and reproducible without a sonication or thermal treatment, although in usual cases of block copolymer vesicles the size depends on the preparation procedure and is hard to be reproduced [51−53]. The reversibility and reproducibility in the size are additionally

evidenced by dynamic light scattering (DLS) given in Appendix 3. The independence of the SAXS profile of the order of mixing of AP, MP, and NaCl shown in Figure 3-5b also supports the reversibility of the morphology transition.

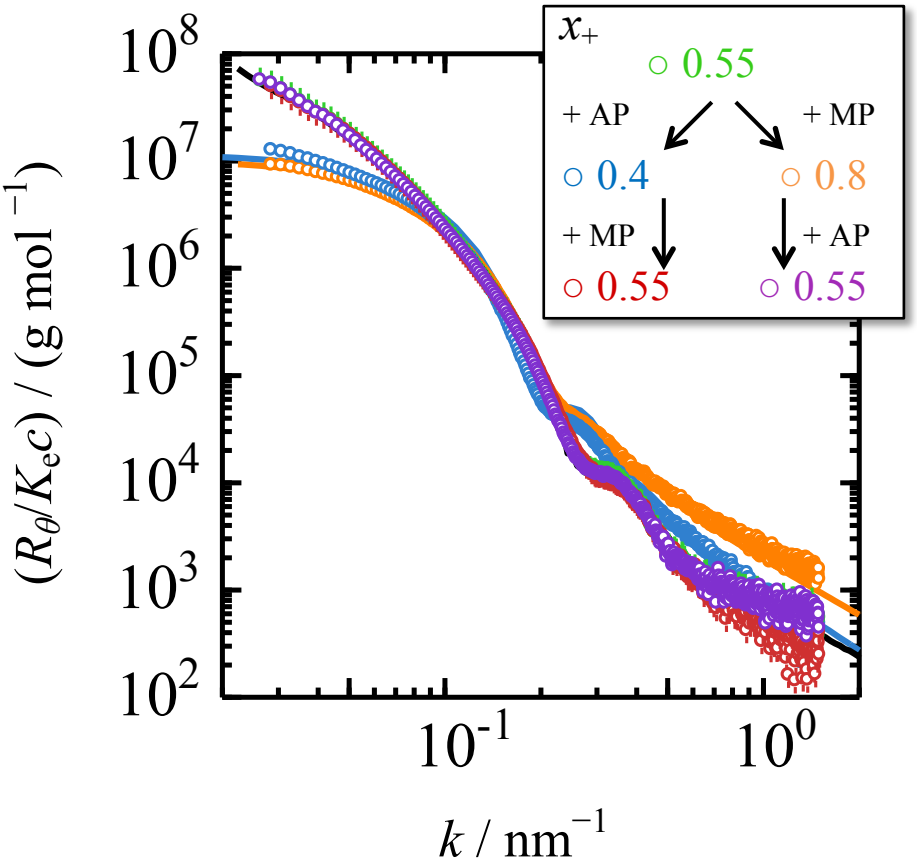


**Figure 3-6.** Reversibility of the SAXS profiles of AP–MP mixtures with in aqueous solution containing 0.1 M NaCl. Green circle with upward bar: $x$ = 0.55 prepared by MP→AP, blue circle: $x$ = 0.4 prepared by adding AP solution into the solution of $x$ = 0.55, red circle with downward bar: $x$ = 0.55 prepared by adding MP solution into the solution of $x$ = 0.4, orange circle: $x$ = 0.8 prepared by adding MP solution into the solution of $x$ = 0.55, purple circle: $x$ = 0.55 prepared by adding AP solution into the solution of $x$ = 0.8. The three scattering functions of $x_+$ 0.55 (green, red, and purple circles) are overlapped. The solid curves indicate theoretical values (eq 3-3 and equations in Appendix 3).

**Electrostatic Energy of the Micelles.** As mentioned in Chapter 2, we explained the morphology change of the polyion complex micelle formed by the MP and AP samples at $x_+$ = 0.6 from the cylindrical micelle to the vesicle with increasing $C_S$ in terms of Israelachvili's packing parameter [54] defined as

$$\lambda = v/a_0 l_c \tag{3-9}$$

where $v$ is the effective volume of the hydrophobic chain, $a_0$ is the area per chain of the core-shell interface, and $l_c$ is the length of the hydrophobic chain in the core. From this explanation, $\lambda$ for our polyion complex micelle formed by the MP and AP samples should be ca. 1 [54] $x_+ = 0.55$ and $C_S = 0.1$ M, and decrease at $x_+ = 0.4$ and 0.8. However, there is no reason for the decreasing $\lambda$ at $x_+ = 0.4$ and 0.8. (If the hydrophobic core of the spherical micelle is swollen isotropically by the excess charged chains, $\lambda$ should even increase.) Because the hydrophobic core of the spherical micelle is negatively and positively charged at $x_+ = 0.4$ and 0.8, we have to take into account the electrostatic energy of the micelles at such $x_+$. The electrostatic energies of the spherical micelle $U_{sph}$ and of the vesicle $U_{ves}$ both with the charged hydrophobic cores in aqueous salt solution are given by (see Appendix 3)

$$U_{sph} = \frac{{Q_{sph}}^2}{40\pi\varepsilon R_{core}}\left[1 + J(\kappa R_{core})\right] \tag{3-10}$$

$$U_{ves} = \frac{{Q_{ves}}^2}{40\pi\varepsilon R_{out}}\left\{\frac{\left(R_{out}/R_{in}\right)^6 - 5\left(R_{out}/R_{in}\right)^3 + 9\left(R_{out}/R_{in}\right) - 5}{\left[\left(R_{out}/R_{in}\right)^3 - 1\right]^2} + J(\kappa R_{out})\right\} \tag{3-11}$$

where $Q_{sph}$ and $Q_{ves}$ are charges of the spherical micelle and the vesicle, $\varepsilon$ is the dielectric constant of the solvent water, and $J(x)$ is the function defined by

$$J(x) \equiv \frac{5\left(1 + \frac{1}{2}x\right)\exp(-x)}{\left(1 + x\right)^2} \tag{3-12}$$

Because of the geometrical reason, the aggregation number of the vesicle must be much larger than that of the spherical micelle. We therefore consider the split of one charged vesicle of the outer and inner core radii $R_{out}$ and $R_{in}$ into $N$ charged spheres of the core radius $R_{core}$, under the condition $Q_{ves} = NQ_{sph}$. Assuming that the concentration $c_{core}$ within the hydrophobic core of the spherical micelle is equal to that of the vesicle as above, we have the following relation:

$$R_{core} = \left(\frac{{R_{out}}^3 - {R_{in}}^3}{N}\right)^{1/3} \tag{3-13}$$

The electrostatic energy difference $\Delta U$ at splitting the vesicle into $N$ spherical micelles is calculated by $\Delta U = NU_{sph} - U_{ves}$. When we choose the experimental values for $R_{out}$ (= 100 nm) and $R_{in}$ (= 80 nm) and the salt concentration $C_S = 0.1$ M, $(40\pi\varepsilon R_{out}/{Q_{ves}}^2)\Delta U$ is calculated

as the function of $N$, which is shown in Figure 3-7. Note that $\Delta U \sim 0$ at $x_+ \sim 0.55$ because the polyion complex micelle is neutral as seen from Figure 3-3. At $x_+ = 0.4$ and 0.8, $N$ is estimated to be ca. 50 from $M_2$ at $x_+ = 0.55$, 0.4, and 0.8 (cf. Table 3-2), and the sign of $\Delta U$ in Figure 3-7 is negative at $N = 50$. Thus, the transformation from the charged vesicle to $N$ charged spherical micelles is energetically favorable. This energetic favorability overcomes the geometrical un-favorability implied by the packing parameter at $x_+ = 0.4$ and 0.8. On the other hand, the electrostatic energy diminishes at $x_+ = 0.55$ by neutralization, so that the vesicle becomes more stable than the spherical micelle.

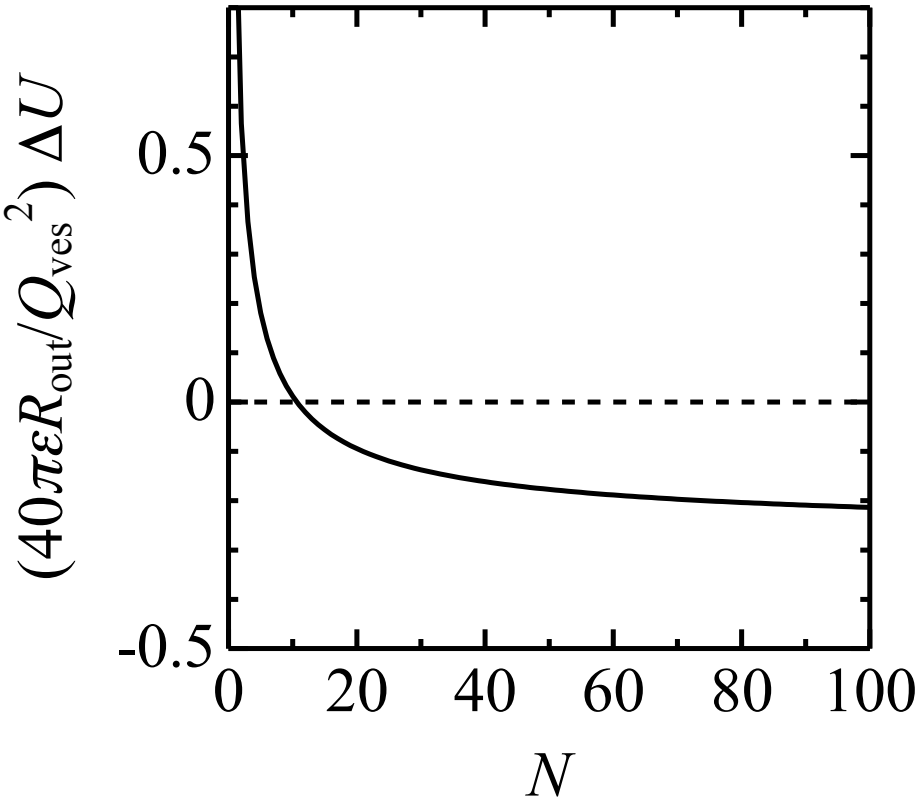


**Figure 3-7.** Energetic favorability of spherical micelles and a vesicle: $(40\pi\varepsilon R_{out}/Q_{ves}^2)\Delta U$ as a function of $N$ in $R_{out} = 120$ nm $R_{in} = 100$ nm.

## 3. 4. Conclusion

We have studied the polyion complex micelle formed by a cation−neutral block copolymer (MP) and an anion−neutral block copolymer (AP) in aqueous solution, focusing on the effect of the mixing ratio of MP and AP $x_+ = C_{0+}/(C_{0+} + C_{0-})$ on the micelle morphology and size, under the condition of $C_S = 0.1$ M and $N_{0+} \sim N_{0-}$ being ca. 10 times higher than

$N_{0n}^{(+)} \sim N_{0n}^{(-)}$. The vesicle formed at $x_+ \sim 0.55$, where $\zeta$ potential is 0, is transformed into smaller spherical micelles when $x_+$ increases or decreases from 0.55, or the micelle is positively and negatively charged, respectively. Furthermore, we have found that the morphology and size transitions reversibly take place by simply adding AP or MP solution to the micellar solutions to adjust $x_+$. The control and reproducibility of the vesicle size is crucial, when the vesicle is utilized as nanomedicines. Usually, strongly amphiphilic block copolymers form vesicles in solution irreversibly, and it is rather difficult to control their size [51−53]. Therefore, the polyion complex vesicle is of great advantage to use for nanomedicines. The split of the large vesicle into smaller spherical micelles for the polyion complex micelle may be induced by the electrostatic instability, which is controlled by the mixing ratio of AP and MP, and it is the novel type of the micellar morphology transition.

**References**


[1] A. Harada, K. Kataoka, Macromolecules **28,** 5294 (1995).

[2] A. Harada, K. Kataoka, Science **283,** 65 (1999).

[3] S. Schrage, R. Sigel, H. Schlaad, Macromolecules **36,** 1417 (2003).

[4] A. Koide, A. Kishimura, K. Osada, W.-D. Jang, Y. Yamasaki, K. Kataoka, J. Am. Chem. Soc. **128,** 5988 (2006).

[5] M. Burkhardt, N. Martinez-Castro, S. Tea, M. Drechsler, I. Babin, I. Grishagin, R. Schweins, D. V. Pergushov, M. Gradzielski, A. B. Zezin, A. H. E. Müller, Langmuir **23,** 12864 (2007).

[6] W.-F. Dong, A. Kishimura, Y. Anraku, S. Chuanoi, K. Kataoka, J. Am. Chem. Soc. **131,** 3804 (2009).

[7] Y. Anraku, A. Kishimura, M. Oba, Y. Yamasaki, K. Kataoka, J. Am. Chem. Soc. **132,** 1631 (2010).

[8] D. V. Krogstad, S.-H. Choi, N. A. Lynd, D. Audus, S. L. Perry, J. D. Gopez, C. J. Hawker, E. J. Kramer, M. V. Tirrell, J. Phys. Chem. B **118,** 13011 (2014).

[9] S. Sakamoto, Y. Sanada, M. Sakashita, K. Nishina1, K. Nakai, S. Yusa, K. Sakurai, Polym J **46,** 617 (2014).

[10] R. Takahashi, T. Sato, K. Terao, S. Yusa, Macromolecules **48,** 7222 (2015).

[11] A. Harada, K. Kataoka, Macromolecules **31,** 288 (1998).

[12] A. Harada, K. Kataoka, Langmuir **15,** 4208 (1999).

[13] S. van der Burgh, A. de Keizer, M. A. Cohen Stuart, Langmuir **20,** 1073 (2004).

[14] B. Hofs, I. K. Voets, A. de Keizer, M. A. Cohen Stuart, Phys. Chem. Chem. Phys. **8,** 4242 (2006).

[15] J. F. Tan, H. P. Too, T. A. Hatton, K. C. Tam, Langmuir **22,** 3744 (2006).
[16] I. K. Voets, A. de Keizer, M. A. Cohen Stuart, Macromolecules **40,** 2158 (2007).
[17] I. K. Voets, S. van der Burgh, B. Farago, R. Fokkink, D. Kovacevic, T. Hellweg, A. de Keizer, M. A. Cohen Stuart, Macromolecules **40,** 8476 (2007).
[18] B. Hofs, A. de Keizer, M. A. Cohen Stuart, J. Phys. Chem. B **111,** 5621 (2007).
[19] A. Harada, K. Kataoka, Soft Matter **4,** 162 (2008).
[20] S. Lindhoud, W. Norde, M. A. Cohen Stuart, J. Phys. Chem. B **113,** 5431 (2009).
[21] I. K. Voets, A. de Keizer, F. A. M. Leermakers, A. Debuigne, R. Jérôme, C. Detrembleur, M. A. Cohen Stuart, Eur. Polym. J. **45,** 2913 (2009).
[22] I. K. Voets, R. Fokkink, T. Hellweg, S. M. King, P. de Waard, A. de Keizer, M. A. Cohen Stuart, Soft Matter **5,** 999 (2009).
[23] M. Lemmers, I. K. Voets, M. A. Cohen Stuart, J. van der Gucht, Soft Matter **7,** 1378 (2011).
[24] K. Nakai, M. Nishiuchi, M. Inoue, K. Ishihara, Y. Sanada, K. Sakurai, S. Yusa, Langmuir **29,** 9651 (2013).
[25] A. Harada, K. Kataoka, Prog. Polym. Sci. **31,** 949 (2006).
[26] I. K. Voets, A. de Keizer, M. A. Cohen Stuart, Adv. Colloid Interface Sci. **147−148,** 300 (2009).
[27] Y. Lee, K. Kataoka, Soft Matter **5,** 3810 (2009).
[28] N. Lefèvre, C.-A. Fustin, J.-F. Gohy, Macromol. Rapid Commun. **30,** 1871 (2009).
[29] J. van der Gucht, E. Spruijt, M. Lemmers, M. A. Cohen Stuart, J. Colloid Interface Sci. **361,** 407 (2011).
[30] D. V. Pergushov, A. H. E. Müller, F. H. Schacher, Chem. Soc. Rev. **41,** 6888 (2012).
[31] A. Kishimura, Polym. J. **45,** 892 (2013).
[32] Y. Matsuda, M. Kobayashi, M. Annaka, K. Ishihara, A. Takahara, Langmuir **24,** 8772 (2008).
[33] S. Morozova, G. Hu, T. Emrick, M. Muthukumar, ACS Macro Lett. **5,** 118 (2016).
[34] T. Goda, K. Ishihara, Y. Miyahara, J. Appl. Polym. Sci. 41766 (2015).
[35] K. Ueno, H. Ueno, T. Sato, Polym. J. **44,** 59 (2012).
[36] H.-D. Liu, T. Sato, Chin. J. Polym. Sci. **31,** 39 (2013).
[37] D. Prifitsis, N. Laugel, M. Tirrell, Langmuir **28,** 15947 (2012).
[38] L. Vitorazi, N. Ould-Moussa, S. Sekar, J. Fresnais, W. Loh, J.-P. Chapel, J.-F. Berret, Soft Matter **10,** 9496 (2014).
[39] B. H. Zimm, J. Chem. Phys. **16,** 1093 (1948).
[40] J.-F. Berret, Macromolecules **40,** 4260 (2007).

[41] J. S. Pedersen, M. C. Gerstenberg, Macromolecules **29,** 1363 (1996).
[42] J. S. Pedersen, Adv. Colloid Int. Sci. **70,** 171 (1997).
[43] J. Bang, S. Jain, Z. Li, T. P. Lodge, J. S. Pedersen, E. Kesselman, Y. Talmon, Macromolecules **39,** 1199 (2006).
[44] T. Sato, Y. Matsuda, Polym. J. **41,** 241 (2009).
[45] L. Zhang, A. Eisenberg, Macromolecules **32,** 2239 (1999).
[46] P. Bhargava, J. X. Zheng, P. Li, R. P. Quirk, F. W. Harris, S. Z. D. Cheng, Macromolecules **39,** 4880 (2006).
[47] Y.-Y. Won, A. K. Brannan, H. T. Davis, F. S. Bates, J. Phys. Chem. B **106,** 3354 (2002).
[48] S. Jain, F. S. Bates, Macromolecules **37,** 1511(2004).
[49] D. C. Henry, Proc. Roy. Soc. London A **133,** 106 (1931).
[50] T. Doane, C.-H. Chuang, R. Hill, C. Burda, Acc. Chem. Res. **45,** 317 (2012).
[51] M. Antonietti, S. Forster, Adv. Mater. **15,** 1323 (2003).
[52] J. Du, R. K. O'Reilly, Soft Matter **5,** 3544 (2009).
[53] R. Bleul, R. Thiermann, M. Maskos, Macromolecules **48,** 7396 (2015).
[54] J. N. Israelachvili, Intermolecular and Surface Forces. 3rd ed., Academic Press, MA, 2011.

**Appendix 3.**

**Compositions in the Polyion Complex Micelle Solution.** Let us consider a mixture of a polyanion and a polycation dissolved in aqueous solution. Here, the polyanion and polycation are assumed to consist of $A^-$ and $M^+$ segments with uni-valent negative and positive charges, respectively, and the molar concentrations of the $A^-$ and $M^+$ segments in the solution are denoted as $C_{0-}$ and $C_{0+}$, respectively. By the strong electrostatic attraction, $A^-$ and $M^+$ form a neutral complex AM (= P):

$$A^- + M^+ \underset{}{\overset{K_a}{\rightleftharpoons}} AM \tag{3-A1}$$

where $K_a$ is the association constant. Thus, we regard the polyion mixture solution as a quaternary system of $A^-$, $M^+$, AM, and the solvent. (Here, the aqueous salt is regarded as a single solvent component.)

Since the neutral complex AM has no net charges, its solubility to the aqueous medium should be much lower than $A^-$ or $M^+$, and a phase separation may take place in the solution. The compositions of the coexisting dilute and concentrated phases are specified in terms of the molar concentrations of $A^-$ ($C_{0-}^{(d)}$), $M^+$ ($C_{0+}^{(d)}$), and AM ($C_{0\pm}^{(d)}$) in the dilute phase, and of $A^-$ ($C_{0-}^{(c)}$), $M^+$ ($C_{0+}^{(c)}$), and AM ($C_{0\pm}^{(c)}$) in the concentrated phase. According

to the law of mass action, we have the following relations among the molar concentrations:

$$\begin{aligned} C_{0\pm}^{(\mathrm{d})} &= K_{\mathrm{a}} C_{0-}^{(\mathrm{d})} C_{0+}^{(\mathrm{d})} \\ C_{0\pm}^{(\mathrm{c})} &= K_{\mathrm{a}} C_{0-}^{(\mathrm{c})} C_{0+}^{(\mathrm{c})} \end{aligned} \tag{3-A2}$$

The mass conservation rule gives us the relations:

$$\begin{cases} C_{0+} = (C_{0+}^{(\mathrm{d})} + C_{0\pm}^{(\mathrm{d})})(1-\Phi^{(\mathrm{c})}) + (C_{0+}^{(\mathrm{c})} + C_{0\pm}^{(\mathrm{c})})\Phi^{(\mathrm{c})} \\ C_{0-} = (C_{0-}^{(\mathrm{d})} + C_{0\pm}^{(\mathrm{d})})(1-\Phi^{(\mathrm{c})}) + (C_{0-}^{(\mathrm{c})} + C_{0\pm}^{(\mathrm{c})})\Phi^{(\mathrm{c})} \end{cases} \tag{3-A3}$$

where $\Phi^{(\mathrm{c})}$ is the volume fraction of the concentrated phase in the solution. In addition to these equations, the phase equilibrium conditions with respect to the chemical potentials $\mu$ of the three components must be fulfilled

$$\mu_{-}^{(\mathrm{d})} = \mu_{-}^{(\mathrm{c})}, \quad \mu_{+}^{(\mathrm{d})} = \mu_{+}^{(\mathrm{c})}, \quad \mu_{\pm}^{(\mathrm{d})} = \mu_{\pm}^{(\mathrm{c})} \tag{3-A4}$$

In principle, the six molar concentrations plus $\Phi^{(\mathrm{c})}$ can be determined by the above seven simultaneous equations. However, due to the lack of precise expressions of the chemical potentials, it is practically impossible to determine the composition from the above equations.

We use the following phenomenological equations, instead of eqs 3-A4, to determine the six molar concentrations and $\Phi^{(\mathrm{c})}$. First, the neutral complex AM is assumed to be so hydrophobic that the dilute phase does not contain AM, i.e.,

$$C_{0\pm}^{(\mathrm{d})} = 0 \tag{3-A5}$$

If the concentrated phase is dispersed as colloidal particles in the solution, we can determine from the scattering experiment the polymer mass concentration $c^{(\mathrm{c})}$ in the concentrated phase, which is related to $C_{0-}^{(\mathrm{c})}$, $C_{0+}^{(\mathrm{c})}$, and $C_{0\pm}^{(\mathrm{c})}$ by

$$c^{(\mathrm{c})} = M_{0+} C_{0+}^{(\mathrm{c})} + M_{0-} C_{0-}^{(\mathrm{c})} + (M_{0+} + M_{0-}) C_{0\pm}^{(\mathrm{c})} \tag{3-A6}$$

where $M_{0+}$ and $M_{0-}$ are the molar masses of the polycation and polyanion repeating units, respectively (including the counter ions). Furthermore, from the ELS result, we can obtain the net charge $n_{\mathrm{c}}$ of the colloidal droplet of the concentrated phase (in the unit of the elementary charge), which can be related to $C_{0-}^{(\mathrm{c})}$ and $C_{0+}^{(\mathrm{c})}$ by

$$n_{\mathrm{c}} = \frac{M^{(\mathrm{c})}}{c^{(\mathrm{c})}} (c_{0+}^{(\mathrm{c})} - c_{0-}^{(\mathrm{c})}) \tag{3-A7}$$

where $M^{(\mathrm{c})}$ is the molar mass of the colloidal droplet of the concentrated phase, which can be determined from the scattering experiment. Equations 3-A5−A7, instead of eqs 3-4, are used to calculate the six molar concentrations.

The $x_+$ dependence of $n_{\mathrm{c}}$ may be written as

$$n_{\mathrm{c}} = \frac{2M^{(\mathrm{c})}}{c^{(\mathrm{c})}} \xi (x_{+} - x_{+}^{(\mathrm{c})}) \tag{3-A8}$$

where $\xi$ and $x_+^{(c)}$ are parameters determined experimentally.; the latter parameter $x_+^{(c)}$ is $x_+$ where the zeta potential of the concentrated-phase droplet becomes zero. From eqs 3-A2, 3-A3, and 3-A5−A8, we can obtain the relations

$$\begin{aligned} C_{0\pm}^{(c)} &= a + \tfrac{1}{2}K_a^{-1} \pm \sqrt{aK_a^{-1} + \tfrac{1}{4}K_a^{-2} + \xi^2(x_+ - x_+^{(c)})^2} \\ C_{0+}^{(c)} &= \sqrt{\xi^2(x_+ - x_+^{(c)})^2 + K_a^{-1}C_{0\pm}^{(c)}} + \xi(x_+ - x_+^{(c)}) \\ C_{0-}^{(c)} &= \sqrt{\xi^2(x_+ - x_+^{(c)})^2 + K_a^{-1}C_{0\pm}^{(c)}} - \xi(x_+ - x_+^{(c)}) \end{aligned} \tag{3-A9}$$

with parameter $a$ defined by

$$a \equiv \frac{c^{(c)} - \xi\left(M_{0+} - M_{0-}\right)(x_+ - x_+^{(c)})}{M_{0+} + M_{0-}} \tag{3-A10}$$

In the right-hand side of the equation for $C_{0\pm}^{(c)}$ in eq 3-A9, the double sign indicates plus at $x_+ > x_+^{(c)}$ and minus at $x_+ < x_+^{(c)}$.

Because the electrostatic attraction between $A^-$ and $M^+$ is strong, we can approximate $K_a$ to be infinity. Using this approximation, we obtain from eqs 3-A9

$$C_{0\pm}^{(c)} = \frac{c^{(c)} - 2\xi M_{0+}\left|x_+ - x_+^{(c)}\right|}{M_{0+} + M_{0-}} \tag{3-A11}$$

$$C_{0+}^{(c)} = \begin{cases} 2\xi(x_+ - x_+^{(c)}) & (x_+ \geq x_+^{(c)}) \\ 0 & (x_+ < x_+^{(c)}) \end{cases}, \quad C_{0-}^{(c)} = \begin{cases} 0 & (x_+ \geq x_+^{(c)}) \\ -2\xi(x_+ - x_+^{(c)}) & (x_+ < x_+^{(c)}) \end{cases} \tag{3-A12}$$

If $x_+^{(c)} = 1/2$, the major component in the dilute phase is $A^-$ at $x_+ < 1/2$ and $M^+$ at $x_+ > 1/2$. However, if $x_+^{(c)} > 1/2$, the conversion of the major component in the dilute phase occurs at $x_+ = x_+^{(d)} < 1/2$, and if $x_+^{(c)} < 1/2$, it occurs at $x_+ = x_+^{(d)} > 1/2$. The conversion mixing ratio $x_+^{(d)}$ in the dilute phase can be calculated by

$$x_+^{(d)} = \frac{1 + \Xi_M x_+^{(c)} - \sqrt{1 - 2\Xi_M\left(1 - x_+^{(c)}\right) + \left(\Xi_M x_+^{(c)}\right)^2}}{2\Xi_M}, \quad \Xi_M \equiv \frac{\xi}{C_{0\pm}^{(c)} + C_{0+}^{(c)}} \tag{3-A13}$$

As in the case of the concentrated phase, we neglect the minor component in the dilute phase, i.e., $C_{0-}^{(d)} = 0$ at $x_+ > x_+^{(d)}$ and $C_{0+}^{(d)} = 0$ $x_+ < x_+^{(d)}$. Using eqs 3-3, 3-5, and 3-12, we obtain the following equations.

$$\Phi_c = \frac{C_{0-}}{C_{0\pm}^{(c)} + C_{0-}^{(c)}}, \quad C_{0+}^{(d)} = \frac{C_{0+} - C_{0-} - \left(C_{0+}^{(c)} - C_{0-}^{(c)}\right)\Phi_c}{1 - \Phi_c} \quad \left(x_+ > x_+^{(d)}\right) \tag{3-A14}$$

$$\Phi_c = \frac{C_{0+}}{C_{0\pm}^{(c)} + C_{0+}^{(c)}}, \quad C_{0-}^{(d)} = \frac{C_{0-} - C_{0+} + \left(C_{0+}^{(c)} - C_{0-}^{(c)}\right)\Phi_c}{1 - \Phi_c} \quad \left(x_+ < x_+^{(d)}\right) \tag{3-A15}$$

**Contrast Factors.** The optical constant $K_e$ is defined by

$$K_e = N_A a_e^{\,2} \gamma_{av}^{\,2} \tag{3-A15}$$

with the Avogadro constant $N_A$, the classical radius of electron $a_e$, and the average contrast factor $\gamma_{av}$ of the polymers. For the mixture of the AP and MP copolymers in aqueous NaCl, $\gamma_{av}$ was calculated by

$$\gamma_{av} \equiv \gamma_{MP} w_{MP} + \gamma_{AP} w_{AP} \tag{3-A16}$$

where $w_{MP}$ and $w_{AP}$ are the weight fractions of the copolymers MP and AP in the solution, respectively, and $\gamma_{MP}$ and $\gamma_{AP}$ are their contrast factors, calculated by

$$\gamma_{MP} = \frac{\gamma_+ M_{0+} N_{0+} + \gamma_n M_{0n} N_{0n}^{(+)}}{M_{0+} N_{0+} + M_{0n} N_{0n}^{(+)}}, \quad \gamma_{AP} = \frac{\gamma_- M_{0-} N_{0-} + \gamma_n M_{0n} N_{0n}^{(-)}}{M_{0-} N_{0-} + M_{0n} N_{0n}^{(-)}} \tag{3-A17}$$

with $\gamma_i$ ($i$ = +, −, n) defined by

$$\gamma_i \equiv \frac{n_{e0i}}{M_{0i}} - \frac{\bar{\upsilon}_i}{\upsilon_{solv}} \left[ \frac{n_{e,H_2O}}{M_{H_2O}} \left(1 - w_{NaCl}\right) + \frac{n_{e,NaCl}}{M_{NaCl}} w_{NaCl} \right] \tag{3-A18}$$

Here $n_{e0i}$, $n_{e,H_2O}$, and $n_{e,NaCl}$ are numbers of electrons of the monomer unit $i$ (including the counterion), $H_2O$ molecule, and NaCl, respectively, $M_{0i}$, $M_{H_2O}$, and $M_{NaCl}$ are molar masses of the monomer unit $i$, $H_2O$, and NaCl, respectively, $\bar{\upsilon}_i$ is the partial specific volume of the monomer unit $i$, $\upsilon_{solv}$ is the specific volume of the solvent (aqueous NaCl), and $w_{NaCl}$ is the weight fraction of NaCl in aqueous NaCl.

The mixture of MP and AP forms the polyion complex micelle, of which hydrophobic core consists of the monomer units $M^+$ and $A^-$ as well as the neutral complex AM (see above). The molar concentrations of $M^+$, $A^-$, and AM in the hydrophobic core are $C_{0+}^{(c)}$, $C_{0-}^{(c)}$, and $C_{0\pm}^{(c)}$, respectively, as discussed above. The contrast factor $\gamma_{mic}$ of the micelle is given by

$$\gamma_{core} = \frac{\gamma_\pm \left(M'_{0+} + M'_{0-}\right) C_{0\pm}^{(c)} + \gamma_+ M_{0+} C_{0+}^{(c)} + \gamma_- M_{0-} C_{0-}^{(c)}}{\left(M'_{0+} + M'_{0-}\right) C_{0\pm}^{(c)} + M_{0+} C_{0+}^{(c)} + M_{0-} C_{0-}^{(c)}} \tag{3-A19}$$

where $M'_{0+}$ and $M'_{0-}$ are the molar masses of $M^+$ and $A^-$ ions, respectively (without the counterions), and $\gamma_\pm$ is the contrast factor of the neutral complex AM calculated by

$$\gamma_{\pm} \equiv \frac{n'_{e0+} + n'_{e0-}}{M'_{0+} + M'_{0-}} - \frac{M_{0+}\bar{\upsilon}_{+} + M_{0-}\bar{\upsilon}_{-} - M_{\mathrm{NaCl}}\bar{\upsilon}_{\mathrm{NaCl}}}{\left(M'_{0+} + M'_{0-}\right)\upsilon_{\mathrm{solv}}}\left[\frac{n_{\mathrm{e,H_2O}}}{M_{\mathrm{H_2O}}}\left(1 - w_{\mathrm{NaCl}}\right) + \frac{n_{\mathrm{e,NaCl}}}{M_{\mathrm{NaCl}}} w_{\mathrm{NaCl}}\right] \tag{3-A20}$$

with the numbers of electrons $n'_{e0+}$,and $n'_{e0-}$,of the monomer unit ions $i$ (without the counterion) and the specific volume $\bar{\upsilon}_{\mathrm{NaCl}}$ of NaCl.

**Scattering Functions for Micelles.** When the complex of AP and MP forms a single bilayer vesicle, the particle scattering function (or the intra-particle interference factor) $P_M(k)$ with the molar mass $M$ is given by [1,2]

$$P_M(k) = \frac{1}{\sqrt{2\pi}\sigma_D}\int {\gamma_2}^2 M P_{M,D}(k) \exp\left[-\frac{\left(D - \langle D\rangle\right)^2}{2{\sigma_D}^2}\right] \mathrm{d}D \tag{3-A21}$$

where $P_{M,D}(k)$ is the particle scattering function of the vesicle with the molar mass $M$ and the thickness of the hydrophobic core $D$, and $\langle D\rangle$ and ${\sigma_D}^2$ are the mean value and variance of the thickness of the hydrophobic core, respectively. If the shell part is represented as an assembly of Gaussian chains, the scattering function $P_{M,D}(k)$ is given by

$$\begin{aligned}\gamma_2^2 P_{M,D}(k) = &\left[\gamma_{\mathrm{core}} W_{\mathrm{core}} \frac{R_{\mathrm{out}}^3 \Phi(kR_{\mathrm{out}}) - R_{\mathrm{in}}^3 \Phi(kR_{\mathrm{in}})}{R_{\mathrm{out}}^3 - R_{\mathrm{in}}^3} + \gamma_{\mathrm{n}} W_{\mathrm{shell}} A_{\mathrm{corona,ves}}(k)\right]^2 \\ &+ \gamma_{\mathrm{n}}^2 \frac{W_{\mathrm{shell}}^2}{m_2}\left[\Omega(k^2\langle S^2\rangle_{\mathrm{n}}) - A_{\mathrm{corona,ves}}^2(k)\right]\end{aligned} \tag{3-A22}$$

with

$$\Phi(x) \equiv \frac{3(\sin x - x\cos x)}{x^3} \tag{3-A23}$$

$$A_{\mathrm{corona,ves}}(k) = \frac{1 - \mathrm{e}^{-k^2\langle S^2\rangle_{\mathrm{n}}}}{2k^2\langle S^2\rangle_{\mathrm{n}}}\left\{\frac{\sin\left[k\left(R_{\mathrm{out}} + \langle S^2\rangle_{\mathrm{n}}^{1/2}\right)\right]}{k\left(R_{\mathrm{out}} + \langle S^2\rangle_{\mathrm{n}}^{1/2}\right)} + \frac{\sin\left[k\left(R_{\mathrm{in}} - \langle S^2\rangle_{\mathrm{n}}^{1/2}\right)\right]}{k\left(R_{\mathrm{in}} - \langle S^2\rangle_{\mathrm{n}}^{1/2}\right)}\right\} \tag{3-A24}$$

$$\Omega(x) \equiv \frac{2\left[\exp(-x) - 1 + x\right]}{x^2} \tag{3-A25}$$

$$m_2 = M_2 \frac{\left(C_{0+}^{(\mathrm{c})} + C_{0\pm}^{(\mathrm{c})}\right)/N_{0+} + \left(C_{0-}^{(\mathrm{c})} + C_{0\pm}^{(\mathrm{c})}\right)/N_{0-}}{M_{0+}\left(C_{0+}^{(\mathrm{c})} + C_{0\pm}^{(\mathrm{c})}\right) + M_{0-}\left(C_{0-}^{(\mathrm{c})} + C_{0\pm}^{(\mathrm{c})}\right)} \tag{3-A26}$$

In those equations, $\langle S^2\rangle_{\mathrm{n}}$ denotes the square radius of gyration of the coronal chain, and $R_{\mathrm{in}}$ and $R_{\mathrm{out}}$ are the inner and outer radii of the hydrophobic core, respectively. The weight fractions of the core and shell parts in the micelle are given by

$$W_{\text{core}} = 1 - W_{\text{shell}} = \frac{M'_{0+}\left(C^{(c)}_{0+} + C^{(c)}_{0\pm}\right) + M'_{0-}\left(C^{(c)}_{0-} + C^{(c)}_{0\pm}\right)}{\left(M'_{\text{MP}}/N_{0+}\right)\left(C^{(c)}_{0+} + C^{(c)}_{0\pm}\right) + \left(M'_{\text{AP}}/N_{0-}\right)\left(C^{(c)}_{0-} + C^{(c)}_{0\pm}\right)} \tag{3-A27}$$

where $M'_{\text{MP}}$ and $M'_{\text{AP}}$ are the molar masses of the polycation and polyanion block chains without the counterions, respectively. $R_{\text{in}}$ and $R_{\text{out}}$ are given by

$$R_{\text{in}} = R - \frac{D}{2}, \quad R_{\text{out}} = R + \frac{D}{2}, \quad R \equiv \frac{D}{2}\sqrt{\frac{MW_{\text{core}}}{\pi N_{\text{A}} c_{\text{core}} D^3} - \frac{1}{3}} \tag{3-A28}$$

with the mass concentration $c_{\text{core}}$ of the hydrophobic core, the molar mass of the vesicle $M$, the hydrophobic core thickness $D$, and $W_{\text{core}}$. The adjustable parameters to calculate $P_M(k)$ for the vesicle are $c_{\text{core}}$, $\langle S^2\rangle_{\text{n}}$, $\langle D\rangle$, and $\sigma_D^2$.

In the case that neutral complex is a spherical micelle, $P_2(k)$ is given by [1,2]

$$\begin{aligned}\gamma_2^2 P_M(k) = &\left[\gamma_{\text{core}} W_{\text{core}} \Phi(kR_{\text{core}}) + \gamma_{\text{n}} W_{\text{shell}} A_{\text{corona,sph}}(k)\right]^2 \\ &+ \gamma_{\text{n}}{}^2 \frac{W_{\text{shell}}{}^2}{m_2}\left[\Omega(k^2\langle S^2\rangle_{\text{n}}) - A^2_{\text{corona,sph}}(k)\right]\end{aligned} \tag{3-A29}$$

$$A_{\text{corona,sph}}(q,R) = \frac{1 - \mathrm{e}^{-k^2\langle S^2\rangle_{\text{n}}}}{k^2\langle S^2\rangle_{\text{n}}} \frac{\sin\left[k\left(R_{\text{core}} + \langle S^2\rangle_{\text{n}}^{1/2}\right)\right]}{k\left(R_{\text{core}} + \langle S^2\rangle_{\text{n}}^{1/2}\right)} \tag{3-A30}$$

where $R_{\text{c}}$ is radius of the hydrophobic calculated from the mass concentration $c_{\text{core}}$ of the hydrophobic core by

$$R_{\text{core}} = \left(\frac{3MW_{\text{core}}}{4\pi N_{\text{A}} c_{\text{core}}}\right)^{1/3} \tag{3-A31}$$

The polymer mass concentration $c_{\text{corona}}$ in the coronal region calculated by

$$c_{\text{corona}} = \begin{cases} \dfrac{m_2 M_{\text{wn,1}}}{8\pi N_A R_{\text{core}}^2 \langle S^2\rangle_{\text{n}}^{1/2}} & \text{(spherical micelle)} \\ \dfrac{m_2 M_{\text{wn,1}}}{8\pi N_A (R_{\text{in}}^2 + R_{\text{out}}^2)\langle S^2\rangle_{\text{n}}^{1/2}} & \text{(vesicle)} \end{cases} \tag{3-A32}$$

where the thickness of the coronal region is approximated by $2\langle S^2\rangle_{\text{n}}^{1/2}$. We did not consider the interfacial thickness between the core (or shell) and coronal regions.

**Electrostatic Energy of Charged Micelles.** Let us consider the vesicle with the uniformly charged hydrophobic core of the outer and inner radius $R_{\text{out}}$ and $R_{\text{in}}$ and with the charge $Q_{\text{ves}}$, immersed in the aqueous solution with the Debye length $\kappa^{-1}$ (= $(8\pi N_{\text{A}} Q C_{\text{S}})^{-1/2}$, where $N_{\text{A}}$ is the Avogadro constant and $Q$ is the Bjerrum length). According to the Gauss

law, the electrostatic energies outside ($r > R_{out}$) and within ($R_{in} < r < R_{out}$) the charged hydrophobic core are given by

$$U_{out} = \frac{Q_{ves}{}^2 \left(1 + \frac{1}{2}\kappa R_{out}\right) e^{-\kappa R_{out}}}{8\pi\varepsilon R_{out}\left(1 + \kappa R_{out}\right)^2} \tag{3-A33}$$

$$U_{core} = \frac{Q_{ves}{}^2}{40\pi\varepsilon R_{out}} \frac{\left(R_{out}/R_{in}\right)^6 - 5\left(R_{out}/R_{in}\right)^3 + 9\left(R_{out}/R_{in}\right) - 5}{\left[\left(R_{out}/R_{in}\right)^3 - 1\right]^2} \tag{3-A34}$$

respectively, with the dielectric constant $\varepsilon$ of the solvent water. In eq 3-A32, we have approximated $\kappa^{-1}$ in the outside coronal region to be equal to that in the outside the coronal region. Furthermore, neglecting counterions of the charged core within the inner coronal and solvent region of the vesicle, we have the total electrostatic energy of the vesicle $U_{ves}$ by eq 3-16 in the text.

The electrostatic energy of the spherical micelle with the uniformly charged hydrophobic core of the radius $R_{core}$ and with the charge $Q_{sph}$, immersed in the aqueous solution can be calculated similarly. The electrostatic energies outside ($r > R_{core}$) and within ($0 < r < R_{core}$) the charged hydrophobic core are given by eqs 3-A32 and 3-A33 where $Q_{ves}$, $R_{out}$, and $R_{in}$ are replaced by $Q_{sph}$, $R_{core}$, and 0, respectively. The total electrostatic energy of the spherical micelle $U_{sph}$ by eq 3-15 in the text.

**Transmittance Electron Microscopy.** The test solutions for TEM were prepared by *MP→AP* procedure (cf. experimental section). A drop of each solution was placed on a copper grid coated with Formvar film. The sample was stained by an aqueous solution of sodium phosphotungstate (0.2wt%), dried in vacuo, and then observed using a JEM-2100 transmittance electron microscope (JEOL Ltd., Tokyo).

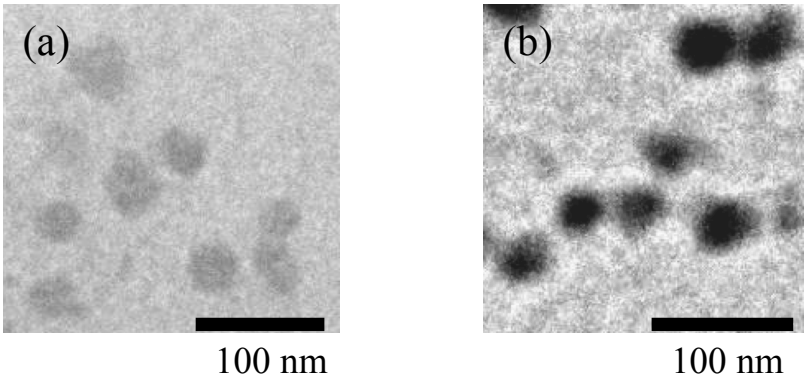


**Figure 3-A1.** TEM images of MP−AP mixtures at $x_+ = 0.4$ and 0.8.

Figure 3-A1 shows TEM images of particles formed by AP−MP mixtures at $x_+ = 0.4$. In both images, spherical objects are observed. The shape and radius (~ 20 nm) agree with the SAXS results, supporting the formation of the spherical micelle. A part of the spherical objects secondarily aggregate, which probably take place in drying for the sample preparation. In the case of $x_+ = 0.6$, larger spherical objects are observed, given elsewhere [3]. Note that such larger spherical objects observed at $x_+ = 0.6$ were never found at $x_+ = 0.4$ and 0.8.

**Dynamic Light Scattering.** Dynamic light scattering (DLS) measurements were performed using an ALV/DLS/SLS-5000 light scattering photometer at 25 °C. A vertically polarized YAG laser (wavelength: 532 nm) was used as incident light. Each test solutions, prepared in the same manner as reversibility investigation using SAXS, was diluted with 0.1 M aqueous NaCl solution to adjust the polymer concentration $c = 1 \times 10^{-4}$ g/cm$^3$ for transparency, and poured into a quartz cell.

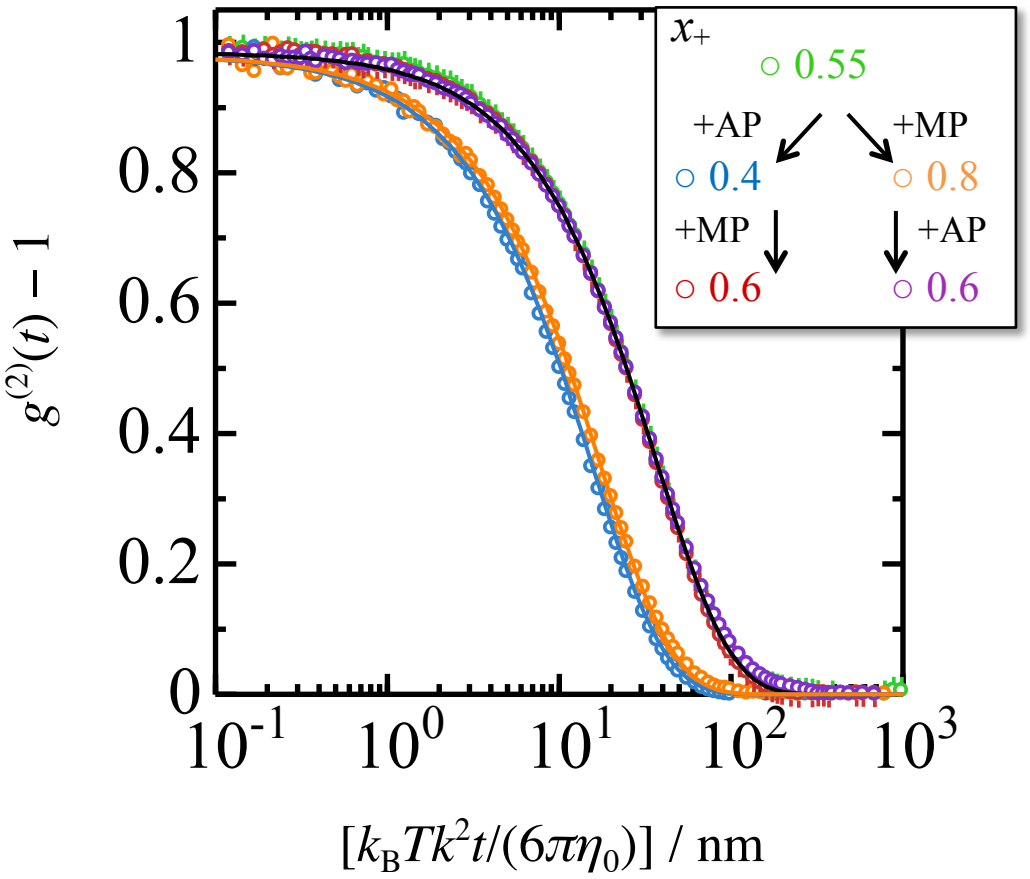


**Figure 3-A2.** Auto-correlation functions at the scattering angle of 90° for the polyion

complex micelle formed of AP and MP in aqueous NaCl solution, plotted against $k_B Tk^2 t/(6\pi\eta_0)$ ($k_B$ is the Boltzmann constant, $T$ is the absolute temperature, and $\eta_0$ is the viscosity coefficient of the solvent). Green circle with upward bar: $x$ = 0.6 prepared by MP→AP, blue circle: $x$ = 0.4 prepared by adding AP solution into the solution of $x$ = 0.6, red circle with downward bar: $x$ = 0.6 prepared by adding MP solution into the solution of $x$ = 0.4, orange circle: $x$ = 0.8 prepared by adding MP solution into the solution of $x$ = 0.6, purple circle: $x$ = 0.6 prepared by adding AP solution into the solution of $x$ = 0.8. The three scattering functions of $x_+$ 0.6 (green, red, and purple circles) are overlapped. Solid curves indicate results of the single exponential fitting.

Figure 3-A2 compares the auto-correlation functions $g^{(2)}(t) - 1$ plotted against $R_{H,app}$ at $x_+$ = 0.6, 0.4, and 0.8. Here, the test solutions of $x_+$ = 0.4 and 0.8 were prepared from the solution of $x_+$ = 0.6 by adding AP or MP solution. The scattering from the free single chain was so weak and not observed even at $x_+$ = 0.4 and 0.8. The scattering components at $x_+$ = 0.6 is therefore assigned to the vesicle, and those at $x_+$ = 0.4 and 0.8 are to the spherical micelle split from the vesicle. The $g^{(2)}(t)$ for the spherical micelle at $x_+$ = 0.4 and 0.8 is almost single exponential function, indicating narrow distribution and being consistent with the results of the SAXS profile fitting (cf. Table 3-2). When MP or AP solution was added into the solution of $x_+$ = 0.4 and 0.8 to recover $x_+$ to be 0.6 again, the spectra almost completely recover to the $g^{(2)}(t)$ of the original solution of $x_+$ = 0.6. Therefore, the size and size distribution of the vesicle are reproducible.

**References**


1. J. S. Pedersen, M. C. Gerstenberg, Macromolecules **29,** 1363 (1996).
2. J. S. Pedersen, J. S. Adv. Colloid Int. Sci. **70,** 171 (1997).
3. R. Takahashi, T. Sato. K. Terao, S. Yusa, Macromolecules **48,** 7222 (2015).

# Chapter 4. Self-Assembly of a Thermosensitive Block Copolymer in Water−Methanol Mixtures

## 4. 1. Introduction

The facile synthesis of libraries of diblock copolymers has been an impetus for the creation of new polymeric materials of technological importance. It has also rejuvenated colloid science ever since it was demonstrated that polymeric micelles readily form upon treatment of diblock copolymers with selective solvents [1]. Extensive studies have been carried out on various diblock copolymer micelles, in view of their potential applications as nanocarriers and nanoreactors. Recently, there has been increasing interest in the so-called stimulus-responsive polymeric micelles that form or disintegrate upon application of an external trigger, such as a change in solution temperature, pH, salinity, or light. In particular, diblock copolymers containing a thermosensitive block, such as poly(*N*-isopropylacrylamide) (PNIPAM) or poly(2-alkyl-2-oxazoline) (POZ), have been investigated extensively in view of their thermoresponsive self-association behavior [2−13]. Several reviews have been published on various aspects of the assembly/disassembly of stimulus-responsive polymeric micelles [14−17].

We reported previously an investigation of the thermoresponsive self-assembly in water of a doubly thermosensitive diblock copolymer (PIPOZ-*b*-PEOZ) consisting of a poly(2-isopropyl-2-oxazoline) (PIPOZ) block and a poly(2-ethyl-2-oxazoline) (PEOZ) block [18]. The dehydration temperatures of the PIPOZ and PEOZ blocks in PIPOZ-*b*-PEOZ were 43 and 54 °C, respectively, for a copolymer having PIPOZ and PEZ blocks of $M_n$ = 7600 and 3600, respectively. Upon heating past ~ 50 °C the PIPOZ-*b*-PEOZ copolymer in water underwent simultaneous micellization and liquid−liquid phase separation. The heat-induced amphiphilicity of the diblock copolymer facilitated the flocculation or coalescence of the polymer-rich liquid droplets and the formation of a macroscopically separated polymer-rich solution.

Subsequently, Sato et al. [19] reported an investigation of a singly thermosensitive diblock copolymer, PNIPAM-*b*-PNVP, consisting of a PNIPAM block and a poly(*N*-vinyl-2-pyrrolidone) (PNVP) block. While PNIPAM becomes hydrophobic in aqueous solutions heated above ca. 30 °C, PNVP is water−soluble over a wider temperature range, up to nearly the water boiling temperature. Aqueous solutions of this diblock copolymer also exhibit simultaneous micellization and liquid−liquid phase separation. However, the amphiphilicity of the copolymer at the phase separation temperature is such that

the polymer-rich droplets are colloidally stable in the phaseseparated dispersion with no tendency toward flocculation or droplet coalescence. It was suggested that the hydrophilic PNVP chains are located on the interface of the polymer-rich droplets, thus they slightly enhance the droplets colloidal stability in the continuous liquid phase. We present here an investigation of the solution properties of the thermosensitive diblock copolymer, poly(2-isopropyl-2-oxazoline)-*b*-poly(*N*-isopropylacrylamide) (PIPOZ-*b*-PNIPAM; Chart 4-1). The corresponding homopolymers, PIPOZ and PNIPAM, undergo heat-induced phase separation in water at nearly identical temperatures. Under these conditions, it is difficult, if not impossible, to change selectively the solvent quality of water for one of the two blocks using temperature as the sole trigger.

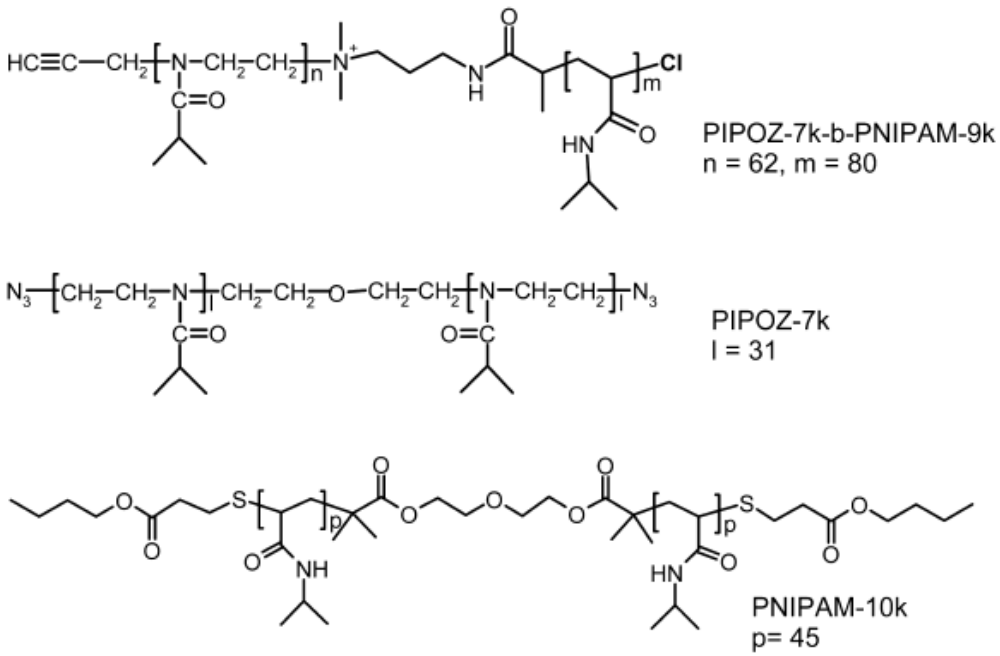


**Chart 4-1.** Chemical Structures of the Polymers Used in This Chapter.

On the basis of previous reports, we anticipated that, in water, this copolymer would not attain the amphiphilicity needed for micellization upon raising the solution temperature. We were aware that the cloud point temperature $T_{CP}$ of PNIPAM in water is often affected by the addition of a water-miscible liquid. Invariably, as long as it remains a minority component, the second component induces a decrease in the $T_{CP}$ of PNIPAM. Recent studies have shown that the $T_{CP}$ of PIPOZ in water increases upon addition of ethanol as a minority component [20]. These opposing trends offer the opportunity to tune the amphiphilicity of PIPOZ-*b*-PNIPAM in a binary solvent system by changing the composition of the mixed solvent. The objective of this chapter was to demonstrate that the dehydration

and self-association of PIPOZ-*b*-PNIPAM in water−methanol (MeOH) mixtures can be controlled by adjusting in concert the solution temperature and the MeOH content.

First, we describe the thermodynamic features of the heat/MeOH induced phase transition of PIPOZ-*b*-PNIPAM in water−MeOH using turbidimetry and high-sensitivity diff erential scanning calorimetry (DSC). Then, we use fluorescence depolarization and small-angle X-ray scattering (SAXS) to uncover the underlying molecular interactions at play. By comparing the results obtained here to those reported earlier for solutions of PIPOZ-*b*-PEOZ in water, we discuss how the self-association behavior of thermosensitive diblock copolymers is affected by the strength of their amphiphilicity.

## 4. 2. Experimental Section

**Materials.** Polymer sample of PIPOZ-7k-b-PNIPAM-9k, PIPOZ-7k, and PNIPAM-10k (Chart 4-1) were synthesized and provided by Professor Françoise M. Winnik and Dr. Xing-Ping Qiu at University of Montreal. The synthesis and characterization of the samples are described in ref. 4 of Chapter 2.

**Turbidimetry.** The cloud point of copolymer solutions with $c = 1.0 \times 10^{-3}$ g/cm$^3$ and different $\phi_{MeOH}$ was determined by spectrometric detection of the changes in transmittance at $\lambda = 550$ nm using an Agilent 8453 UV−visible spectrometer equipped with an HP 89090A Peltier temperature controller. The heating rate was 0.2 °C/min. The solution was not stirred during measurements. The inflection point of the transmittance vs temperature curve was taken as the cloud point temperature. In addition, the temperature of the onset of turbidity of PIPOZ-7k-*b*-PNIPAM-9k solutions (0.2 g/cm$^3$) in mixed $H_2O$/MeOH of various $\phi_{MeOH}$ was monitored visually upon heating solutions from room temperature to 40 °C.

**Differential Scanning Calorimetry.** DSC measurements for PIPOZ-7k-*b*-PNIPAM-9k, PIPOZ-7k, and PNIPAM-10k in water and water−MeOH mixtures were performed on a VP-DSC microcalorimeter (MicroCal Inc.) at an external pressure of ca. 250 kPa. The cell volume was 0.520 cm$^3$. The polymer mass concentration *c* was set to $1.0 \times 10^{-3}$ g/cm$^3$ for all polymers. Solutions were heated at a rate of 1.0 °C/min in the temperature range 10−70 °C. For each measurement, the reference solution was the same as the solvent (water or water/MeOH) of the polymer solution analyzed. The experimental data were analyzed using the Origin-based software supplied by the manufacturer. A cubic connect baseline was subtracted from the data prior to fitting.

**Small-Angle X-ray Scattering.** SAXS measurements were conducted on solutions of PIPOZ-7k-*b*-PNIPAM-9k ($c$ = 0.02 g/cm$^3$) of $\phi_{MeOH}$ = 0, 0.2, 0.3, and 0.4 kept at 25, 40, and 70 °C, using the beamline BL40B2 in SPring-8, Hyogo, Japan. The solutions were poured in capillary tubes and rapidly heated by setting the capillary tube in a heating block. The intensity of the scattered X-ray was detected using an imaging plate detector ca. 3 min after placing the capillary tube in the heating block. The scattering intensity remained approximately constant over time.

**Fluorescence Depolarization.** Steady-state fluorescence spectra were measured at 45 °C on water−MeOH mixed solutions of PIPOZ-7k-*b*-PNIPAM-9k including a small amount of 1-(4-trimethylammoniumphenyl)-6-phenyl-1,3,5-hexatriene (TMA-DPH) with an F-4500 fluorescence spectrometer (Hitachi Ltd., Japan) equipped with polarizers and analyzers on the excitation and emission sides. The excitation of TMA-DPH was done with a vertically polarized light ($\lambda$ = 360 nm). The intensities $I_{vv}$ and $I_{vh}$ of the emitted fluorescence at 450 nm of the solutions were measured with the analyzers set vertically and horizontally, respectively. The fluorescence anisotropy $r$ was calculated by using the following equation:

$$I = \frac{I_{vv} - GI_{vh}}{I_{vv} + 2GI_{vh}} \tag{4-1}$$

Here $G \equiv I_{hv}/I_{hh}$ is an instrumental factor determined experimentally. Fluorescence life times $\tau_{life}$ of TMA-DPH in the solutions at 45 °C was measured with a FluoroCube fluorescence spectrometer (Horiba Ltd., Japan) equipped with a diode laser ($\lambda$ = 375 nm). The emission was monitored at 450 nm. The $\eta v$ value, where $\eta$ is the viscosity of the fluorophore environment and $v$ the effective volume of the fluorophore, was obtained from $r$ and $\tau_{life}$ using the Perrin−Weber equation [27]:

$$\frac{1}{r} = \frac{1}{r_0}\left(1 + \frac{k_B T \tau_{life}}{v\eta}\right) \tag{4-2}$$

Here $r_0$ is the intrinsic fluorescence anisotropy. For TMA-DPH, $r_0$ was reported to be 0.39 [28].

Solutions for analysis were prepared as follows. An ethanol solution of 0.5 mM TMA-DPH (purchased from Life Technologies, CA, USA), was added to water−MeOH mixture solutions of PIPOZ-7k-*b*-PNIPAM-9k of $\phi_{MeOH}$ = 0, 0.2, and 0.3. The solutions were stirred for at least 18 h and filtered through a 0.5 μm pore size into a quartz (10 mm × 10 mm) cell at room temperature. The concentrations of PIPOZ-7k-*b*-PNIPAM-9k and TMA-DPH in the solutions were 5 × 10$^{-4}$ g/cm$^3$ and 0.5 μM, respectively. Visual

examination confirmed that the solutions were turbid at 45 °C.

## 4. 3. Results and Discussion

**Turbidity.** Changes with temperature in the transmittance of PIPOZ-7k-*b*-PNIPAM-9k solutions with a polymer mass concentration $c = 1.0 \times 10^{-3}$ g/cm$^3$ in water and in water−MeOH mixtures are presented in Figure 4-1. From the sigmoidal transmittance vs temperature curves, we determined the temperature at which the transmittance starts to decline $T_{onset}$ and the cloud point temperature, $T_{CP}$, defined here as the inflection point of the transmittance vs temperature curve (Table 4-1). The $T_{CP}$ of the diblock copolymer may be influenced slightly by the presence of the quaternary ammonium group that is included in the linker between the two blocks. However, previous studies indicate that the effect of a single charge along an amphiphilic polymer chain on the chain hydrophilicity is usually weak and much smaller than the effect of a charged end group [29]. Both $T_{onset}$ and $T_{CP}$ decrease as the volume fraction of methanol, $\phi_{MeOH}$, increases from 0 to 0.2. The transmittance with temperature curve becomes broader as $\phi_{MeOH}$ increases. The turbidity curve for the PIPOZ-7k-*b*-PNIPAM-9k solution of $\phi_{MeOH}$ = 0.2 exhibits two components: a first drop in transmittance from 100% to 80% with $T_{onset}$ = 34.0 °C and $T_{CP}$ = 34.8 °C, followed by a gradual decrease to 5% transmittance with $T_{CP} \sim 40.2$ °C.

The trend toward lower transition temperatures is reversed as $\phi_{MeOH}$ exceeds 0.2. As observed in Figure 4-1 (diamonds for $\phi_{MeOH}$ = 0.3 and squares for $\phi_{MeOH}$ = 0.4), the turbidity curves are smooth and their temperature span increases markedly as $\phi_{MeOH}$ increases, with concomitant increase in $T_{CP}$. Transmittance vs temperature curves were recorded also for solutions in water and in water−MeOH mixtures of the homopolymers PIPOZ-7k and PNIPAM-10k (see the chemical structures in Chart 4-1), used as model compounds for each block of the copolymer. In the case of PIPOZ-7K solutions, both $T_{onset}$ and $T_{CP}$ increase with increasing $\phi_{MeOH}$, in agreement with the trends reported for PIPOZ in water−ethanol mixed solution [20]. Solutions of PNIPAM-10k exhibit the cononsolvency characteristics of PNIPAM as reported previously [30]. Values of $T_{onset}$ and $T_{CP}$ for all solutions are compiled in Table 4-1.

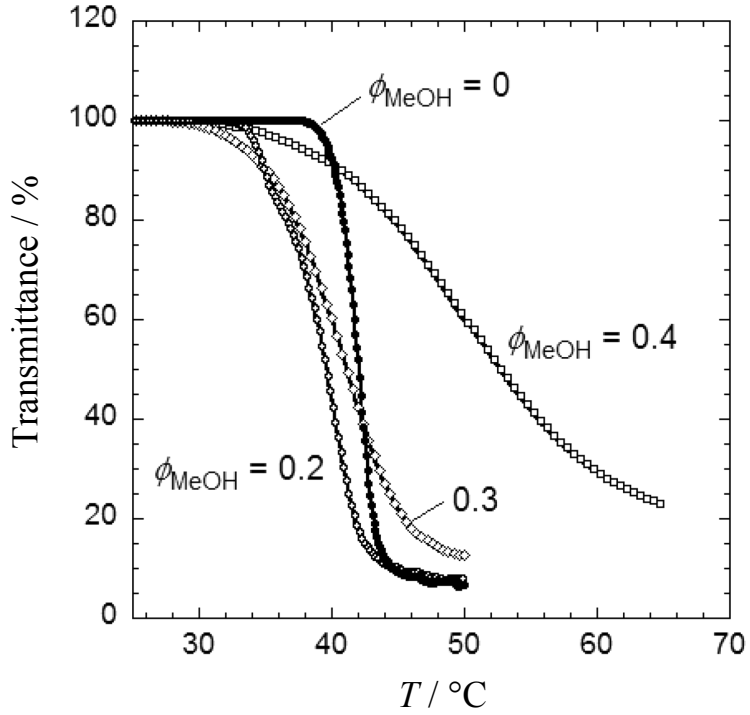


**Figure 4-1.** Temperature dependence of the transmittance of PIPOZ-7k-*b*-PNIPAM-9k in water and water−MeOH mixtures. The polymer mass concentration = $1 \times 10^{-3}$ g/cm$^3$; heating rate = 0.2 °C/min; the digits on the curves are the $\phi_{MeOH}$ values of the mixed solvents.

From the turbidity data, we drew the phase diagrams of PIPOZ-7k-*b*-PNIPAM-9k, PIPOZ-7k, and PNIPAM-10k in water−MeOH mixtures at $c = 1.0 \times 10^{-3}$ g/cm$^3$ (Figure 4-2). The cloud points of the copolymer and PIPOZ-7k in water ($\phi_{MeOH} = 0$) are nearly identical (42.0 °C vs 40.5 °C), but the cloud point of PNIPAM-10k in water is significantly lower (30.7 °C). This discrepancy may not be an intrinsic feature of the copolymer phase transition. It may reflect the sensitivity of the $T_{CP}$ values of low molar mass PNIPAM to the chemical structure of the chain ends [24]. In the following, therefore, we focus on the differences in the general trends of the $T_{CP}$ variation as a function of $\phi_{MeOH}$. The phase diagram of PNIPAM-10k presents a deep minimum ($T_{CP} \sim 12$ °C), corresponding to $\phi_{MeOH} = 0.40$. In the case of PIPOZ-7k, the cloud point continuously increases with increasing $\phi_{MeOH}$. The phase diagram of PIPOZ-7k-*b*-PNIPAM-9k displays a shallow minimum ($T_{CP} \sim 39$ ° C) for $\phi_{MeOH} = 0.25$. However, the trend is mitigated by the fact that in the $0.1 \leq \phi_{MeOH} \leq 0.2$ range, the turbidity curves exhibit a two-step transition. The inflectionpoint temperatures of the first-step minor transition for PIPOZ-7k-*b*-PNIPAM-9k at $0.1 \leq \phi_{MeOH} \leq 0.2$ are plotted with triangles in Figure 4-2.

**Table 4-1. Characteristics of Turbidity and DSC Curves for PIPOZ-7k-*b*-PNIPAM-9k, PIPOZ-7k, and PNIPAM-10k in Water−MeOH Mixture of Different $\phi_{MeOH}$ Values**

| | | turbidity | | DSC | |
|---|---|---|---|---|---|
| polymer | $\phi_{MeOH}$ | $T_{onset}$[b]/°C | $T_{CP}$[b]/°C | $T_M$[b]/°C | $\Delta H$/kJ mol$^{-1}$ |
| PIPOZ-*b*-PNIPAM | 0 | 39.0 | 42 | 45.2 | 4.89 |
| | 0.1 | 36.0 | 37.5, 41.2 | 43.2 | 3.11 |
| | 0.2 | 34.0 | 34.8, 40.2 | 42.7 | 2.58 |
| | 0.3 | 30.0 | 41 | 33.3 | 1.38 |
| | 0.4 | 33.0 | 51.5 | – | – |
| PIPOZ | 0 | 39.4 | 40.5 | 42.6 | 5.80 |
| | 0.1 | 41.0 | 42.2 | 43.5 | 3.20 |
| | 0.2 | 43.1 | 44.3 | 45.6 | 2.20 |
| | 0.3 | 48.3 | 51.5 | – | – |
| PNIPAM | 0 | 29.2 | 30.7 | 33.5 | 5.86 |
| | 0.1 | 26.8 | 28.2 | 31.2 | 4.07 |
| | 0.2 | 21.6 | 22.9 | 28.6 | 3.17 |
| | 0.3 | 14.2 | 16.0 | – | – |
| | 0.4 | 8.8 | 11.2 | – | – |

[a]Results obtained for solutions with $c = 1.0 \times 10^{-3}$ g/cm$^3$. [b]See the text for the definition of $T_{onset}$, $T_{CP}$, and $T_M$.

**Differential Scanning Calorimetry (DSC).** The temperature dependence of the heat capacity at constant pressure $C_P$ for solutions of the homopolymers PIPOZ-7k and PNIPAM-10k at a concentration $c = 1.0 \times 10^{-3}$ g/cm$^3$ is presented in Figure 4-3a for solutions in water (full circles) and in mixed water−MeOH solutions of various $\phi_{MeOH}$ (open symbols). The temperatures $T_M$ corresponding to the endotherm maxima for PIPOZ-7k and PNIPAM-10k differ by ∼10 °C, similarly to the $T_{CP}$ values, most likely as a consequence of the differences in end-group structures. The transition enthalpies ($\Delta H$) of the two homopolymers are similar, as reported earlier [24,31]. The endotherms of the homopolymers in mixed water−MeOH solutions decrease in intensity with increasing $\phi_{MeOH}$. They are too weak to be recorded reliably with the microcalorimeter employed for $\phi_{MeOH} >$ 0.30. The enthalpy data recovered from the endotherms indicate that the phase transition and dehydration of the two polymers are affected significantly by the presence of MeOH [32]. The $T_M$ values undergo strong shifts, toward lower temperatures in the case of PNIPAM-10k

and toward higher temperatures in the case of PIPOZ-7k (see Table 4-1). These trends corroborate the observations of changes in solutions turbidity displayed in the phase diagrams shown in Figure 4-2.

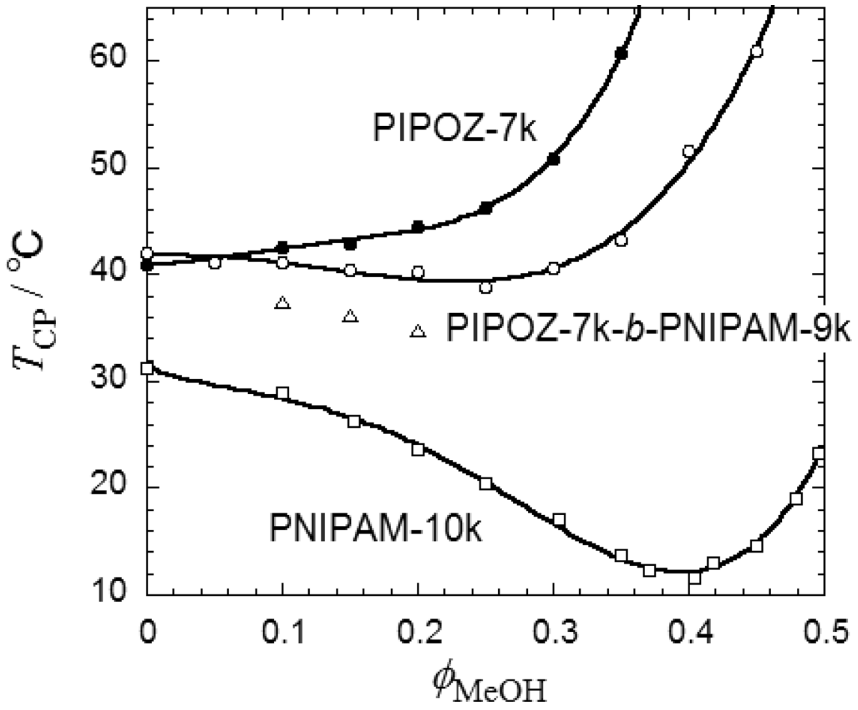


**Figure 4-2.** Phase diagrams of PIPOZ-7k, PNIPAM-10k [30], and PIPOZ-7k-*b*-PNIPAM-9k in water−MeOH mixtures of methanol volume fraction $\phi_{MeOH}$ ranging from 0 to 0.5. Polymer concentration = $1.0 \times 10^{-3}$ g/cm$^3$; data points are $T_{CP}$ obtained from turbidity measurements. Triangles indicate the temperature of the inflection-point of the first-step minor transition for PIPOZ-7k-*b*-PNIPAM-9k.

Thermograms of the diblock copolymer PIPOZ-7k-*b*-PNIPAM-9k, dissolved in water and in water−MeOH mixtures of $\phi_{MeOH}$ = 0.2, 0.3, and 0.4 are presented in Figure 4-3b. The corresponding $T_M$ and $\Delta H$ values are listed in Table 4-1. The thermogram of the diblock copolymer in water (full circles) presents a single isotherm with a weak shoulder on the low temperature side. The $T_M$ value of the main endotherm (45.2°C) is slightly higher than the $T_M$ values of either PNIPAM-10k or PIPOZ-7k in water. The enthalpy associated with the copolymer transition is significantly weaker than the values recorded for homopolymer solutions (Table 4-1). These features of the thermogram of PIPOZ-7k-*b*-PNIPAM-9k in water imply (i) that the interactions between the PNIPAM block and water molecules are strengthened by the presence of the linked PIPOZ chain (higher $T_M$ value) and (ii) that the linked chains of the two blocks dehydrate and collapse cooperatively. This behavior is

different from that exhibited by aqueous solutions of the doubly thermosensitive copolymer PIPOZ-*b*-PEOZ, which exhibit a bimodal endotherm [18], but similar to the DSC behavior for aqueous solutions of a doubly thermosensitive copolymer poly(*N*-isopropylacrylamide)-*b*-poly(*N*-vinylcaprolactam), recently reported by Hou and Wu [12].

The endotherm of PIPOZ-7k-*b*-PNIPAM-9k in a mixed solution of $\phi_{MeOH}$ = 0.2 (open circles in Figure 4-3) presents a broad band with a maximum at 41 °C and a weak shoulder around 33−34 °C, indicating that dehydration takes place in two steps. The former value is similar to the inflection point of the high-temperature sigmoid of the turbidity curve, while the latter temperature is close to the $T_{onset}$ value recorded for this solution. The endotherm recorded for PIPOZ-7k-*b*-PNIPAM-9k in a mixed solution of $\phi_{MeOH}$ = 0.3 (diamonds in Figure 4-3b) is weak and shifted toward lower temperature ($T_M$ ~ 33 °C). It is asymmetric, suggesting the occurrence of two-step dehydration. The enthalpogram of PIPOZ-7k-*b*-PNIPAM-9k in a mixed solution of $\phi_{MeOH}$ = 0.4 (squares in Figure 4-3b) is small and broad, spanning from ~ 40 to ~ 70 °C. It is too small for accurate determination of $T_M$ and $\Delta H$.

**Heat-Induced Phase Separation of PIPOZ-7k-*b*-PNIPAM-9k Solutions.** Figure 4-4 displays photographs of solutions of PIPOZ-7k-*b*-PNIPAM-9k ($c$ = 0.2 g/cm$^3$) in water−MeOH mixtures of $\phi_{MeOH}$ = 0, 0.2, and 0.3 (from left to right) kept at 40 °C for 4 h. The samples with $\phi_{MeOH}$ = 0 and 0.3 are milky, as a consequence of the dehydration and the phase separation of the copolymer. Upon cooling to room temperature, both solutions recovered their limpidity. The $\phi_{MeOH}$ = 0.2 sample kept at 40 °C for 4 h consists of two clear liquid layers, indicating that in this water−MeOH mixture, the dehydration of the copolymer is accompanied by the formation of polymer-rich liquid droplets, which coalesce in a single liquid phase of higher density than the continuous phase.

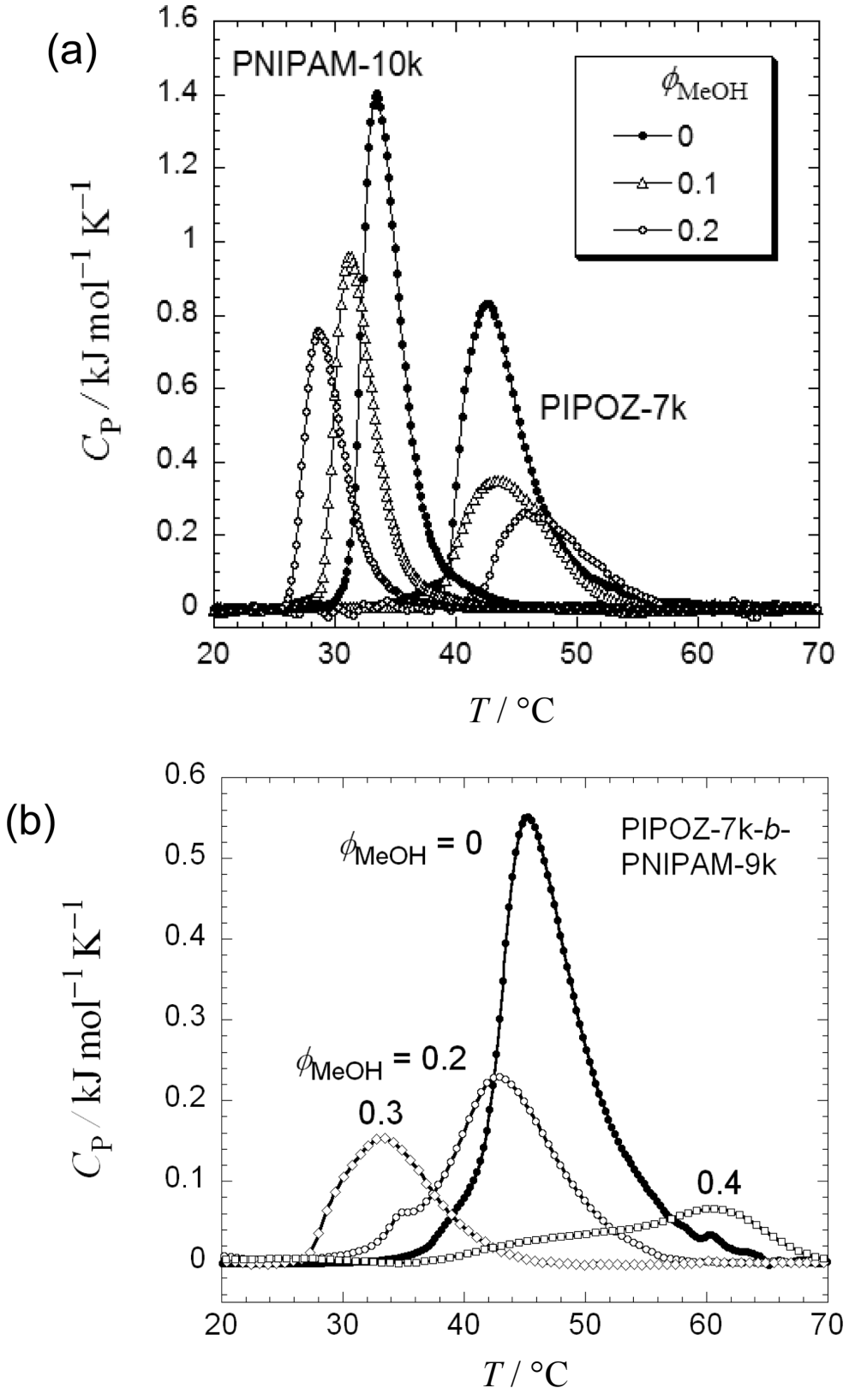


**Figure 4-3.** DSC thermograms for PNIPAM-10k and PIPOZ-7k homopolymers (a) and for PIPOZ-7k-*b*-PNIPAM-9k (b) in water and water−MeOH mixtures: $\phi_{MeOH}$, MeOH volume fraction; polymer concentration, $1.0 \times 10^{-3}$ g/cm$^3$.

**Microviscosity on the Droplets Interface in Phase-Separated Solutions Determined by Fluorescence Depolarization.** The fluorophore TMA-DPH is often used to assess the local microviscosity of inhomogeneous amphiphile solutions. It tends to reside preferentially on the interface between hydrophobic and hydrophilic domains [33]. In fact, the fluorescence of TMA-DPH-containing PIPOZ-7k-*b*-PNIPAM-9k solutions with $\phi_{MeOH}$ = 0, 0.2, and 0.3 kept at room temperature was very weak, as anticipated for TMA-DPH dissolved in polar solvents such water or methanol [33]. However, the emission intensity was strongly enhanced as the solution temperature exceeds 40 °C, an indication that TMA-DPH is anchored to the interface between the droplets of the coexisting concentrated phase and the continuous polymer-poor phase.

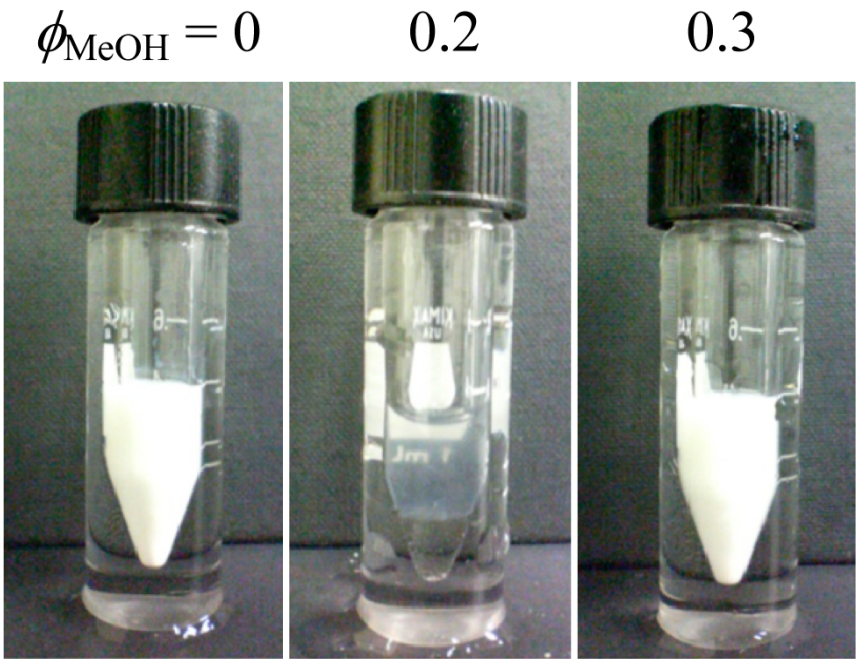


**Figure 4-4.** Photographs of concentrated solutions of PIPOZ-7k-*b*-PNIPAM-9k with $c$ = 0.2 g/cm$^3$ and $\phi_{MeOH}$ = 0, 0.2, and 0.3 after being kept at 40 °C for 4 h.

Figure 4-5 presents the changes as a function of $\phi_{MeOH}$ of the product of the effective molecular volume $v$ of TMA-DPH by the local viscosity $\eta$ surrounding TMA-DPH derived from fluorescence depolarization and fluorescence lifetime measurements carried out on phase separated copolymer solutions heated to 45 °C using eqs 4-1 and 4-2. While the bulk solvent viscosity increases with increasing $\phi_{MeOH}$ (for $\phi_{MeOH}$ < 0.45), the ratio $\eta v$ decreases with increasing $\phi_{MeOH}$ as seen in Figure 4-5, an indication that the surface of the coexisting concentrated-phase droplets becomes more fluid with increasing $\phi_{MeOH}$.

The hydrophilicity at the interface of colloidal particles affects the stability of the

particles in opposite manners. On the one hand, a hydrophilic interface stabilizes colloids in aqueous solutions, as seen in the case of phase-separated aqueous solutions of the diblock copolymer consisting of a PNIPAM block and a hydrophilic poly(*N*-vinyl-2-pyrrolidone) (PNVP) block, where concentrated-phase droplets are stabilized by PNVP block chains on the droplet interface [19]. On the other hand, a hydrophilic interface also promotes the flocculation of colloidal particles, as demonstrated previously in a study of the macroscopic liquid/liquid phase separation of aqueous PIPOZ-*b*-PEOZ solutions heated to a temperature at which PIPOZ-*b*-PEOZ is amphiphilic [18]. The flocculation may be induced by the viscoelastic effect during the collision of colloidal particles [18,34−37].

As shown in Figure 4-4, macroscopic two-phase separation occurred in a PIPOZ-7k-*b*-PNIPAM-9k solution with $\phi_{MeOH}$ = 0.2 at 40 °C, but not in a solution with $\phi_{MeOH}$ = 0.3 also at 40 °C. These results can be related to the hydrophilicity of the concentrated-phase-droplet interface, which induces both stabilization and flocculation of colloids. By increasing the amphiphilicity of the block copolymers, the flocculation effect seems to appear first, and the stabilization effect becomes important.

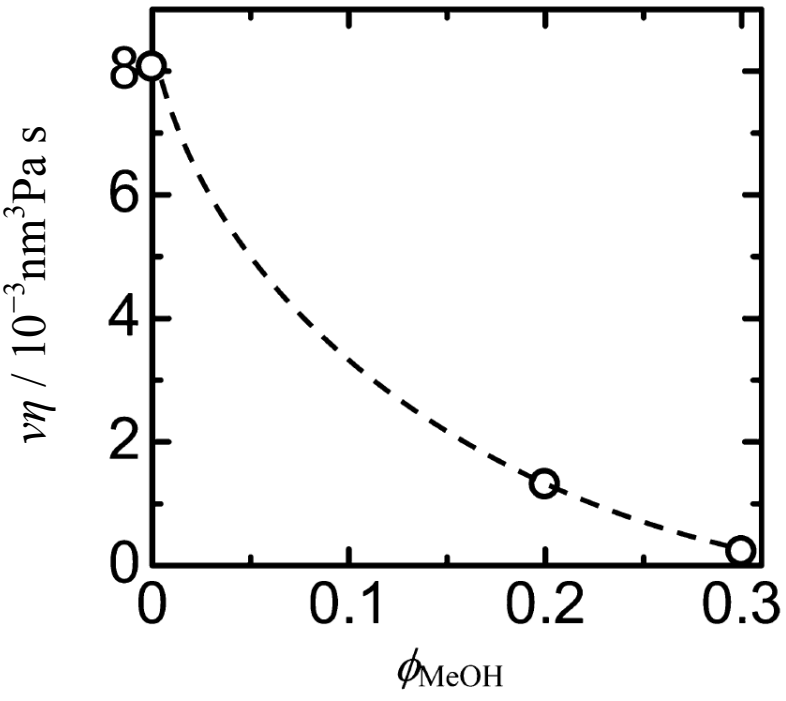


**Figure 4-5.** Changes of the product of the effective molecular volume $v$ of TMA-DPH by the local viscosity $\eta$ sensed by TMA-DPH obtained by fluorescence depolarization measurements for phase-separated solutions of PIPOZ-7k-*b*-PNIPAM-9k in water−MeOH mixtures of different $\phi_{MeOH}$; temperature = 45 °C. The concentrations of PIPOZ-7k-*b*-PNIPAM-9k and TMA-DPH in the solutions were $5 \times 10^{-4}$ g/cm$^3$ and 0.5 μM,

respectively.

**SAXS Profiles.** Profiles recorded by SAXS measurement on solutions of PIPOZ-7k-*b*-PNIPAM-9k in water and water−MeOH mixtures with $\phi_{MeOH}$ = 0.2, 0.3, and 0.4 ($c$ = 0.02 g/cm$^3$) are presented in Figure 4-6. At 25 °C, where all the solutions were transparent, the scattering function intensities $I(k)$ of all solutions exhibit the same pattern, characterized by a plateau for small scattering vector $k$, followed by a decay for $k \geq 0.3$ nm$^{-1}$, although a weak upturn is observed in the low $k$ region for the aqueous solution ($\phi_{MeOH}$ = 0). In contrast, at 40 and 70 °C, where all the solutions were turbid all $I(k)$ are strongly decaying functions at low $k$. For the solutions with $\phi_{MeOH}$ = 0 and 0.2 at 40 °C, as well as for those with $\phi_{MeOH}$ = 0, 0.2, and 0.3 at 70 °C, the functions obey the power law dependence, $I(k) \propto k^{-4}$ in the low $k$ region. At higher $k$, however, the $k$ dependence of $I(k)$ on the solvent composition is weaker, indicating that the solutions contain large and small scattering components, predominantly contributing to $I(k)$ at low and high $k$, respectively. It is noted that the shapes of $I(k)$ for solutions with $\phi_{MeOH}$ = 0−0.4 at 40 °C at the high $k$ resemble those at 25 °C.

It can be seen from Figure 4-3 that dehydration does not occur in the PIPOZ-7k-*b*-PNIPAM-9k solutions with $\phi_{MeOH}$ = 0−0.4 at 25 °C. Thus, we can expect that the copolymer chain is molecularly dispersed in the solutions at 25 °C. The excess scattering intensity $I(k)$ for such solutions is given by [38,39]

$$I(k) \equiv \frac{K'_T(\bar{v}\Delta\rho_e)^2 \zeta c M_1 P(k)}{1 + 2A_2 c M_1 P(k)} \tag{4-3}$$

where $K'_T$ is the SAXS instrument constant, $\bar{v}$ is the partial specific volume of the copolymer, $\Delta\rho_e$ is the excess electron density of the copolymer, $\zeta$ is the correction factor of the selective adsorption in the mixed solvent, and $M_1$, $P(k)$, and $A_2$ are the molecular weight, particle scattering function, and second virial coefficient of the copolymer sample, respectively. We assumed that the electron densities of the PIPOZ and PNIPAM blocks are identical, because they are structural isomers. All SAXS measurements were performed in the same SAXS facility with the same capillary cell, so $K'_T$ should be identical for all solutions.

The excess electron density $\Delta\rho_e$ in water−MeOH mixtures can be calculated by

$$\Delta\rho_e = \frac{n_{e,0} N_A}{\bar{v} M_0} - \frac{N_A (x_H n_{e,H} + x_M n_{e,M})}{\bar{v}_s (x_H M_H + x_M M_M)} \tag{4-4}$$

where $N_A$ is the Avogadro constant, $\bar{v}_s$ is the specific volume of the water−MeOH mixture, and $n_{e,i}$, $M_i$, and $x_i$ are the number of electrons, molar mass, and mole fraction of the

component $i$ (= 0 for the monomer unit, H for water, and M for MeOH), respectively. To calculate $\Delta\rho_e$, we have used $\bar{v}$ = 0.9 cm$^3$/g (the value for PNIPAM in water [40] and for PIPOZ-*b*-PNIPAM at $\phi_{MeOH}$ = 0.2), literature values for $\bar{v}_s$, and $w_M = 1 - w_H = (\rho_M/\rho_H)\phi_{MeOH}/[1 + (\rho_M/\rho_H - 1)\phi_{MeOH}]$ with densities of water ($\rho_H$) and MeOH ($\rho_M$). The correction factor $\zeta$ of the selective adsorption is unity for the single solvent system ($\phi_{MeOH}$ = 0), but less than unity if MeOH is selectively adsorbed onto the copolymer chain in water−MeOH mixtures.

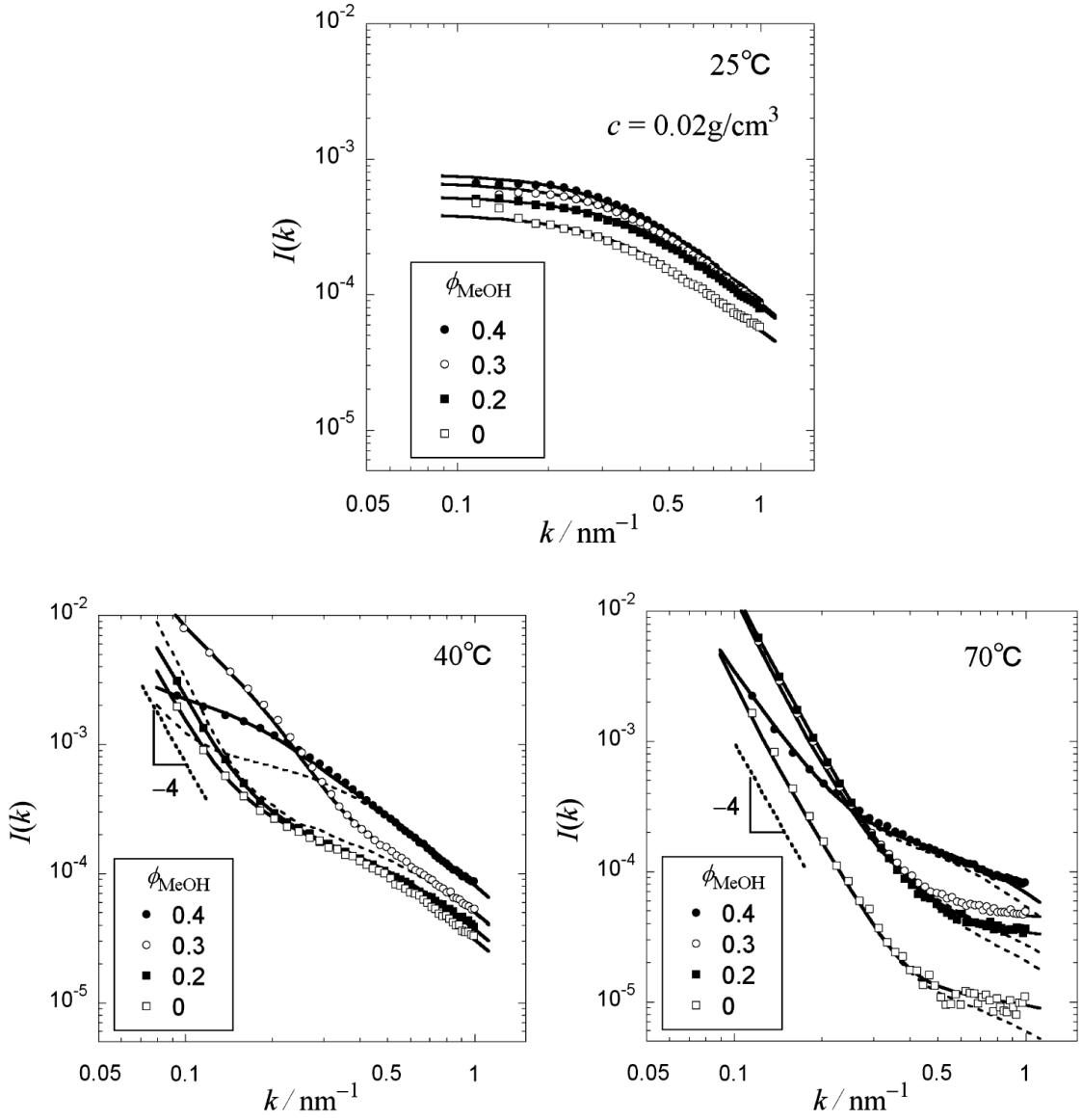


**Figure 4-6.** Double logarithmic plots of the excess scattered intensity $I(k)$ vs the magnitude of scattering vector $k$ for PIPOZ-7k-*b*-PNIPAM-9k solutions with different $\phi_{MeOH}$ at 25, 40, and 70 °C ($c = 2.0 \times 10^{-2}$ g/cm$^3$). Solid and thin dashed curves indicate theoretical values explained in the text and Tables 4-2−4.

The scattering functions at 25 °C are fitted using $M_1 = 2.0 \times 10^4$ (see above) and the following Debye function [41] for $P(k)$

$$P_{\text{chain}}(k) = 2 \times \frac{\exp(-k^2\langle S^2\rangle_{\text{chain}}) - 1 + k^2\langle S^2\rangle_{\text{chain}}}{(k^2\langle S^2\rangle_{\text{chain}})^2} \tag{4-5}$$

with the mean square radius of gyration $\langle S^2\rangle_{\text{chain}}$ of the copolymer chain. Fitting results are shown by solid curves at 25 °C in Figure 4-6, and values of $\zeta$, $\langle S^2\rangle_{\text{chain}}^{1/2}$, and $A_2$ chosen are listed in Table 4-2. Kubota et al. [42] reported the molecular weight dependence of $\langle S^2\rangle_{\text{chain}}^{1/2}$ for PNIPAM in water at 20 ° C: $\langle S^2\rangle_{\text{chain}}^{1/2} = 0.0224 M_1^{0.54}$ nm. Their relation gives $\langle S^2\rangle_{\text{chain}}^{1/2} = 4.7$ nm at $M_1 = 2.0 \times 10^4$, that is comparable with $\langle S^2\rangle_{\text{chain}}^{1/2}$ of the copolymer in water and water−MeOH mixtures. Values of $A_2$ in Table 4-2 are also comparable to those for PNIPAM in water [42].

**Table 4-2. Parameters Used for Fitting the Scattering Functions at 25 °C**

| parameters | $\phi_{\text{MeOH}} = 0$ | $\phi_{\text{MeOH}} = 0.2$ | $\phi_{\text{MeOH}} = 0.3$ | $\phi_{\text{MeOH}} = 0.4$ |
|---|---|---|---|---|
| $\Delta\rho_e$/nm$^{-3}$ | 334 | 463 | 527 | 598 |
| $\zeta$ | 1 | $0.81_5$ | 0.82 | 0.79 |
| $\langle S^2\rangle_{\text{chain}}^{1/2}$/nm | 4.1 | $3.6_5$ | $4.0_5$ | $4.3_5$ |
| $A_2/10^{-4}$cm$^3$g$^{-2}$mol | 1.0 | 0.3 | 0.9 | 1.2 |

The DSC thermograms shown in Figure 4-3 indicate that in water and in water−MeOH mixtures PIPOZ-7k-*b*-PNIPAM-9k is partially and fully dehydrated at 40 and 70 °C, respectively, which may induce liquid−liquid phase separation in the copolymer solutions. The separated concentrated phase may exist as polydisperse spherical particles (large scattering component) while copolymer chains in the dilute phase may be molecularly dispersed or slightly aggregated (small scattering component). The scattering function for such a system is calculated by [18,19]

$$\begin{aligned} I(k) &= K_T'(\bar{v}\Delta\rho_e)^2 \xi c M_1 [w_{chain} m_{chain} P_{chain}(k) \\ &+ w_{sphere} \int \mathrm{d}m m P_{sphere,m}(k) w(m) \end{aligned} \tag{4-6}$$

where $w_{\text{chain}}$ and $w_{\text{sphere}}$ (=1 − $w_{\text{chain}}$) are the weight fractions of the chain and sphere, $m_{\text{chain}}$ is the aggregation number of the chain, $P_{\text{sphere,m}}(k)$ is the particle scattering function of the sphere with the aggregation number $m$, and $w(m)$ is the aggregation number distribution

function expressed in terms of the weight fraction. We have neglected the interparticle interference effect, because the solvents become poor at 40 and 70 °C. Using the mass concentration $c_c$ of the coexisting concentrated phase, the radius $R_m$ of the sphere with the aggregation number $m$ is calculated by

$$R_m = \left( \frac{3mM_1}{4\pi N_A c_c} \right)^{1/3} \tag{4-7}$$

and the particle scattering function $P_{\mathrm{sphere,m}}(k)$ by

$$P_{\mathrm{sphere},m}(k) = \left[ 3 \times \frac{\sin(kR_m) - kR_m \cos(kR_m)}{(kR_m)^3} \right]^2 \tag{4-8}$$

We assume that the size distribution of the concentrated-phase droplets obeys the general log-normal distribution:

$$w(x)\mathrm{d}x = \frac{1}{\sqrt{\pi}} \exp(-x^2)\mathrm{d}x \tag{4-9}$$

Here $x$ is defined by

$$x \equiv \frac{\ln[m / (m_{\mathrm{sphere,w}} m_{\mathrm{sphere,n}})^{1/2}]}{2\ln(m_{\mathrm{sphere,w}} / m_{\mathrm{sphere,n}})} \tag{4-10}$$

with $m_{\mathrm{sphere,w}}$ and $m_{\mathrm{sphere,n}}$ being the weight and number-average aggregation numbers of the polydisperse spheres, respectively.

In Figure 4-6, the scattering functions for the copolymer solutions for all $\phi_{\mathrm{MeOH}}$ at 40 °C have slopes similar to those for $I(k)$ at 25 °C at $k > 0.3$ nm$^{-1}$, indicating that the small scattering component in the copolymer solutions at 40 °C resembles the single chain at 25 °C. In fact, eq 4-6 can fit to the experimental $I(k)$ for all $\phi_{\mathrm{MeOH}}$ at 40 °C in the high $k$ region where $P_{\mathrm{sphere,m}}(k)$ tends to zero, using $M_1 = 2.0 \times 10^4$, $m_{\mathrm{chain}} = 1$, and $P_{\mathrm{chain}}(k)$ given by eq 4-5, along with suitable values for $w_{\mathrm{chain}}$ and $\langle S^2 \rangle_{\mathrm{chain}}^{1/2}$ and the values of $\Delta\rho_e$ and $\zeta$ determined at 25 °C (being ignored their temperature dependences). Moreover, eq 4-6 can fit to the experimental $I(k)$ in the low $k$ region at 40 °C at $\phi_{\mathrm{MeOH}} = 0$ and 0.2, which obey the $k^{-4}$ dependence, using $P_{\mathrm{sphere,m}}(k)$ and $w(m)$ calculated by eqs 4-7−10. The solid curves for $\phi_{\mathrm{MeOH}} = 0$ and 0.2 at 40 °C in Figure 4-6 indicate the theoretical values, calculated with parameter values listed in Table 4-3, which perfectly fit to the experimental results. Among the fitting parameters, $m_{\mathrm{chain}}$ and $\langle S^2 \rangle_{\mathrm{chain}}^{1/2}$ affect $I(k)$ mostly in the high $k$ region, while $m_{\mathrm{sphere,w}}$, $m_{\mathrm{sphere,w}}/m_{\mathrm{sphere,n}}$, and $c_c$ predominantly affect $I(k)$ n the low $k$ region. Therefore, the fitting parameter values were determined almost uniquely.

However, it was impossible to fit $I(k)$ in the low $k$ region for $\phi_{MeOH}$ = 0.3 and 0.4 at 40 °C, where $I(k)$ does not obey the $k^{-4}$ dependence, with the equations above. Although the DSC thermograms of PIPOZ-7k-*b*-PNIPAM-9k at $\phi_{MeOH}$ = 0.3 and 0.4 in Figure 4-3 are not bimodal, the phase separation temperatures of PIPOZ and PNIPAM homopolymers are, respectively much higher and much lower than 40 °C, at $\phi_{MeOH}$ = 0.3 and 0.4, such that the amphiphilicity of PIPOZ-7k-*b*-PNIPAM-9k may be quite strong. Consequently, we may expect that the critical micellar concentration (CMC) of the copolymer in solutions of $\phi_{MeOH}$ = 0.3 and 0.4 at 40 °C becomes lower than the copolymer concentration of the coexisting dilute phase in the phase separated mixture. In such a case, molecularly dispersed copolymer chains and star-like micelles may coexist in the dilute phase. The scattering function for such a solution is calculated by

$$I(k) = K_T'(\bar{v}\Delta\rho)^2 \xi c M_1 \times [w_{chain} m_{chain} P_{chain}(k) + w_{micelle} m_{micelle} P_{micelle}(k) + w_{sphere} \int \mathrm{d}m m P_{sphere}(k) w(m)] \quad (4\text{-}11)$$

with $w_{micelle}$, $m_{micelle}$, and $P_{micelle}(k)$ being the weight fraction, aggregation number, and particle scattering function, respectively, of the star-like micelle. The scattering function $P_{micelle}(k)$ is calculated according to Pedersen and Gerstenberg using equations given in the Supporting Information of ref 18 where adjustable parameters are the aggregation number $m_{micelle}$, the radius of gyration of the corona chain $\langle S^2 \rangle_{corona}^{1/2}$, and the concentration inside the hydrophobic core $c_{core}$ of the micelle. The radius of the core is calculated by $[3m_{micelle}M_{PNIPAM}/(4\pi N_A c_{core})]^{1/3}$ where $M_{PNIPAM}$ is the molar mass of the PNIPAM block chain. The fitting results are shown by the solid curves for the corresponding solvent conditions (Figure 4-6), and the parameters chosen are listed in the fourth and fifth columns of Table 4-3. We also tried to fit $I(k)$ in the low $k$ region for $\phi_{MeOH}$ = 0.3 and 0.4 at 40 °C by a vesicle model. To keep high $I(k)$ in the low $k$ region, we had to select high aggregation numbers of the vesicle comparable to $m_{sphere,w}$ listed in Table 4-3, but such high aggregation numbers of the vesicle gave huge radii of gyration ($\sim 10^4$ nm), which are inconsistent with light scattering results (not reported here).

For PIPOZ-7k-*b*-PNIPAM-9k solutions, molecularly dispersed copolymer chains were observed by SAXS in the coexisting dilute phase for all $\phi_{MeOH}$ at 40 °C. This is a contrast with the aqueous PIPOZ-*b*-PEOZ solution, where only star-like micelles with $m_{chain} \approx 10$ were detected by SAXS in the coexisting dilute phase of the phase-separated aqueous solution [18]. The different association properties of the two copolymers are consistent with the weaker amphiphilicity of PIPOZ-7k-*b*-PNIPAM-9k, compared to PIPOZ-*b*-PEOZ, which leads to an enhanced CMC in the dilute phase, such that molecularly dispersed copolymer chains become

detectable by SAXS.

**Table 4-3. Parameters Used for Fitting the Scattering Functions at 40 °C ($c$ = 2.0 × $10^{-2}$ g/cm$^3$)**

| parameter | $\phi_{MeOH} = 0$ | $\phi_{MeOH} = 0.2$ | $\phi_{MeOH} = 0.3$ | $\phi_{MeOH} = 0.4$ |
|---|---|---|---|---|
| $w_{chain}$ | 0.50 | 0.36 | 0.33 | 0.40 |
| $m_{chain}$ | 1 | 1 | 1 | 1 |
| $\langle S^2 \rangle_{chain}^{1/2}$/nm | 3.6 | 3.1 | 3.0 | 2.8 |
| $w_{sphere}$ | 0.50 | 0.64 | 0.55 (0.67[b]) | 0.42 (0.60[b]) |
| $m_{sphere,w}$ | $6.3 \times 10^6$ | $1.6_5 \times 10^7$ | $6.5_5 \times 10^6$ | $1.5 \times 10^7$ |
| $m_{sphere,w}/m_{sphere,n}$ | 4.5 | 4.3 | 4.8 | 4.5 |
| $c_c$/g cm$^{-3}$ | 0.48 | $0.48_5$ | 0.38 | 0.20 |
| $R_w$/nm[a] | 400 | 550 | 430 | 710 |
| $w_{micelle}$ | 0 | 0 | 0.12 (0[b]) | 0.18 (0[b]) |
| $m_{micelle}$ | | | 55 | 11 |
| $\langle S^2 \rangle_{corona}^{1/2}$/nm | | | 3.4 | 3.0 |
| $c_{core}$/g cm$^{-3}$ | | | 0.41 | 0.29 |

[a]Weight-average radius of the concentrated-phase droplets calculated by

$$R_w^3 = \frac{3 m_{sphere,w} M_1}{4\pi N_A c_c} \left( \frac{m_{sphere,n}}{m_{sphere,w}} \right)^{1/3}$$

[b]Values used to draw thin dashed curves at 40 °C in Figure 4-6.

For all $\phi_{MeOH}$, the radius of gyration $\langle S^2 \rangle_{chain}^{1/2}$ of the single copolymer chain in the dilute phase at 40 °C is smaller than that at 25 °C, due to the reduction of the solvent quality upon heating. The mass concentration inside the molecularly dispersed copolymer chain $c_{in,chain}$ may be calculated by

$$c_{in,chain} = \frac{3 m_{chain} M_1}{4\pi N_A \left( \frac{5}{3} \langle S^2 \rangle_{chain} \right)^{3/2}} \tag{4-12}$$

The values of $c_{in,chain}$ calculated using the results in Table 4-3 are lower than 0.17 g/cm$^3$, indicating that copolymer chain shrinkage 40 °C is not so much, in agreement with the fact noted earlier that the copolymer chain remains partially hydrated at 40 °C (see Figure 4-3).

At 70 °C, the scattering functions, except in the case of solutions with $\phi_{MeOH}$ = 0.4,

obey the $k^{-4}$ dependence over a wide range of $k$, which indicates an increase in $w_{sphere}$. In fact, fits of $I(k)$ at 70 °C in the low $k$ region by eqs 4-5–10, indicated by solid curves in Figure 4-6 at 70 °C, were obtained using $w_{sphere}$ larger than those at 40 °C (cf. Table 4-4). However, the best fits (the solid curves) gives us too small $\langle S^2 \rangle_{chain}^{1/2}$, which leads to unrealistically high $c_{in,chain}$ ($\approx 2 - 30$ g/cm$^3$) from eq 4-12. Assuming $c_{in,chain}$ to be identical with the bulk density of the copolymer ($\approx 1/\bar{v}$ = 1.1 g/cm$^3$), which may be the maximum value, we must choose the values of $\langle S^2 \rangle_{chain}^{1/2}$ in parentheses in Table 4-4. We then obtain the thin dashed curves in Figure 4-6 at 70 °C, which fit $I(k)$ data in the high $k$ region less satisfactorily. This may be due to the finite thickness (or the radial distribution of the electron density) of the copolymer chain [43], which is not considered by eq 4-5, although it was difficult to uniquely determine $\langle S^2 \rangle_{chain}^{1/2}$ and the chain thickness. It is noted that the finite thickness effect may not be important at 25 and 40 °C, because the copolymer chain in the dilute phase does shrink very much at these temperatures. Its large dimension provides the predominant $k$ dependence at high $k$. Because of the strongly attractive interaction at 70 °C, the copolymer chains aggregate in the dilute phase at $\phi_{MeOH} = 0.4$. (A similar fitting to the data at $\phi_{MeOH}$ = 0.4 at 70 °C was obtained by using eq 4-11 with $w_{chain} + w_{micelle} = 0.05$, but it was difficult to determine $w_{chain}$ and $w_{micelle}$ separately by this fitting because of the small amount of the small scattering component.)

**Table 4-4. Parameters Used for Fitting the Scattering Functions at 70 °C ($c$ = 2.0 × 10$^{-2}$ g/cm$^3$)**

| parameter | $\phi_{MeOH} = 0$ | $\phi_{MeOH} = 0.2$ | $\phi_{MeOH} = 0.3$ | $\phi_{MeOH} = 0.4$ |
|---|---|---|---|---|
| $w_{chain}$ | 0.025 | 0.065 | 0.067 | 0.05 |
| $m_{chain}$ | 1 | 1 | 1 | 4.5 |
| $\langle S^2 \rangle_{chain}^{1/2}$/nm | 0.7 (1.5[a]) | 0.5 (1.5[b]) | 0.5 (1.5[b]) | 2.1 (2.5[a]) |
| $w_{sphere}$ | 0.975 | 0.935 | 0.933 | 0.95 |
| $m_{sphere,w}$ | $9.3 \times 10^7$ | $1.2 \times 10^6$ | $1.0 \times 10^6$ | $7.6 \times 10^7$ |
| $m_{sphere,w}/m_{sphere,n}$ | 4.4 | 4.5 | 4.5 | 4.4 |
| $c_c$/g cm$^{-3}$ | 0.71 | 0.75 | 0.60 | 0.53 |
| $R_w$/nm[b] | 860 | 200 | 200 | 890 |

[a]Values calculated from $1/\bar{v}$ = 1.1 g/cm$^3$ and used to draw thin dashed curves in Figure 4-3.

[b]See the footnote of Table 4-2.

From the lever rule, we can calculate the copolymer mass concentration $c_d$ in the

coexisting dilute phase by

$$c_{\mathrm{d}} = \frac{c_{\mathrm{c}} c w_{\mathrm{chain}}}{c_{\mathrm{c}} - c(1 - w_{\mathrm{chain}})} \tag{4-13}$$

where $c$ is the copolymer mass concentration in the original solution before phase separation. Figure 4-7 shows a phase diagram, where the phase-separation temperature is plotted against $c_{\mathrm{d}}$ and $c_{\mathrm{c}}$, for PIPOZ-7k-*b*-PNIPAM-9k solutions with different $\phi_{\mathrm{MeOH}}$. In spite of limited number of data points for each $\phi_{\mathrm{MeOH}}$, the phase diagrams seem to be typical ones for polymer−poor solvent systems. It is noted that the phase gap $c_{\mathrm{c}} - c_{\mathrm{d}}$ becomes narrower with increasing $\phi_{\mathrm{MeOH}}$ = 0.3 and 0.4. This may correspond to the gradual decreases in the transmittance observed in the turbidity measurements at $\phi_{\mathrm{MeOH}}$ = 0.3 and 0.4 shown in Figure 4-1.

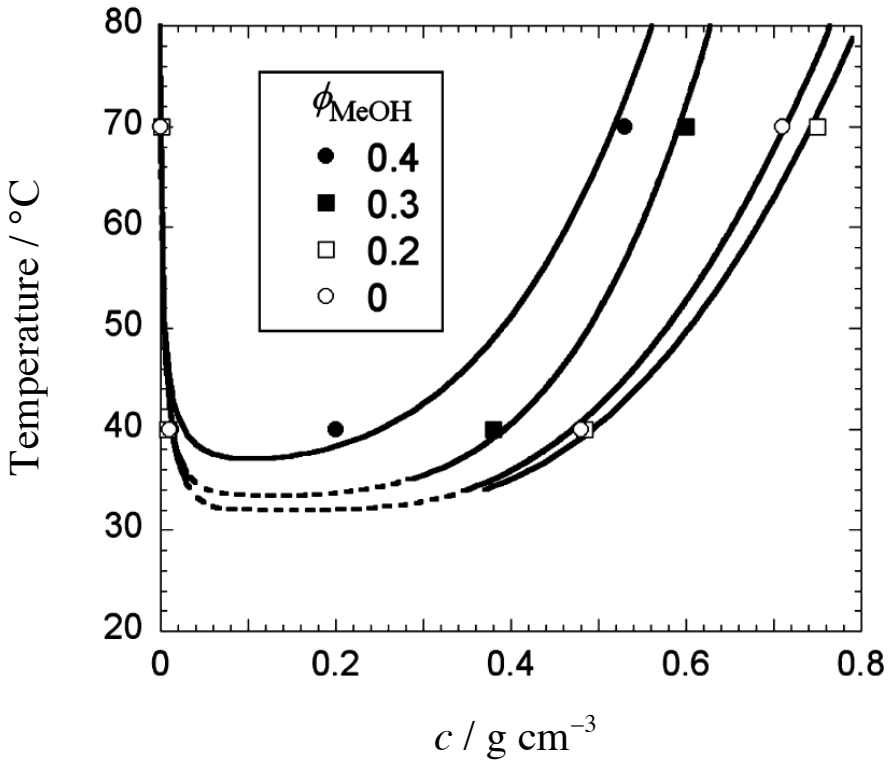


**Figure 4-7.** Temperature−concentration phase diagram for PIPOZ-7k-*b*-PNIPAM-9k solutions with different $\phi_{\mathrm{MeOH}}$.

## 4. 4. Conclusion

The heat-induced dehydration and self-association of the doubly thermosensitive block copolymer PIPOZ-*b*-PNIPAM were examined for solutions in water and water−MeOH

mixtures. Although the difference in the dehydration temperatures of PIPOZ and PNIPAM homopolymers is enhanced with increasing the MeOH volume fraction $\phi_{MeOH}$ up to 0.3, the DSC thermograms of block copolymer solutions in mixed water−MeOH solution indicate that the dehydration processes of the two block do not occur independently. This may be due to the interference of the cononsolvency effect of the PNIPAM block and the cosolvency effect of the PIPOZ block. As a result, the amphiphilicity of PIPOZ-*b*-PNIPAM in water−MeOH mixtures is not strengthened, and, consequently, the micellization of the copolymer does not occur as readily as, for example, in the case PIPOZ-*b*-PEOZ solutions in water heated to a temperature at which water becomes a selective solvent. However, we provide evidence that micellization of PIPOZ-*b*-PNIPAM takes place in water−MeOH mixtures of $\phi_{MeOH}$ = 0.3 and 0.4 at 40 °C, under relatively strong amphiphilicity conditions. Micelles only form in phase separated systems, when the CMC is lower than the polymer concentration in the coexisting dilute phase. Possibly the CMC of PIPOZ-*b*-PNIPAM in water−MeOH mixtures in the phase-separation temperature region may be higher than that of PIPOZ-*b*-PEOZ in water under comparable temperature conditions. Dehydration induces a liquid−liquid phase separation of water−MeOH mixed solutions of PIPOZ-*b*-PNIPAM upon heating. When the copolymer solutions with $\phi_{MeOH}$ = 0, 0.2, and 0.3 were kept at 40 °C for a long time, macroscopic two phase separation took place only in the solution with $\phi_{MeOH}$ = 0.2. Results of fluorescence depolarization of an amphiphilic fluorophore indicate that, at 45 °C, the interface of the concentrated-phase droplets softens with increasing $\phi_{MeOH}$, which may be the driving force toward macroscopic two phase separation at $\phi_{MeOH}$ = 0.2. However, at $\phi_{MeOH}$ = 0.3, the stronger amphiphilicity of PIPOZ-*b*-PNIPAM stabilizes the droplets. The amphiphilicity of the block copolymer affects the colloidal stability of concentrated-phase droplets in the phase separated solutions delicately.

**References**

[1] Y. Mai, A. Eisenberg, Chem. Soc. Rev. **41,** 5969−5985 (2012).

[2] J. Virtanen, S. Holappa, H. Lemmetyinen, H. Tenhu, Macromolecules **35,** 4763−4769 (2002).

[3] S. Yusa, Y. Shimada, Y. Mitsukami, T. Yamamoto, Y. Morishima, Macromolecules **37,** 7507−7513 (2004).

[4] R. Motokawa, M. Annaka, T. Nakahira, S. Koizumi, Colloids Surf. B **38,** 213−219 (2004).

[5] R. Motokawa, K. Morishita, S. Koizumi, T. Nakahira, M. Annaka, Macromolecules **38,** 5748−5760 (2005).

[6] T. Tang, V. Castelletto, P. Parras, I. W. Hamley, S. M. King, D. Roy, S. Perrier, R.

Hoogenboom, U. S. Schubert, Macromol. Chem. Phys. **207,** 1718−1726 (2006).
[7] R. Hoogenboom, H. M. L. Lambermont-Thijs, M. J. H. C. Jochems, S. Hoeppener, C. Guerlain, C.-A. Fustin, J.-F. Gohy, U. S. Schubert, Soft Matter **5,** 3590−3592 (2009).
[8] H. M. L. Lambermont-Thijs, R. Hoogenboom, C.-A. Fustin, C. Bomal-D'Haese, J.-F. Gohy, U. S. Schubert, J. Polym. Sci., Part A **47,** 515−522 (2009).
[9] L. T. Trinh, H. M. L. Lambermont-Thijs, U. S. Schubert, R. Hoogenboom, A.-L. Kjøniksen, Macromolecules **45,** 4337−4345 (2012).
[10] M. M. Bloksma, S. Hoeppener, C. D. Haese, K. Kempe, U. Mansfeld, R. M. Paulus, J.-F. Gohy, U. S. Schubert, R. Hoogenboom, Soft Matter **8,** 165−172 (2012).
[11] Z. Quan, K. Zhu, K. D. Knudsen, B. Nyström, R. Lund, Soft Matter **9,** 10768−10778 (2013).
[12] L. Hou, P. Wu, Soft Matter **10,** 3578−3586 (2014).
[13] Y. Matsuda, Y. Shiokawa, M. Kikuchi, A. Takahara, S. Tasaka, Polymer **55,** 4757−4764 (2014).
[14] I. Dimitrov, B. Trzebicka, A. H. E. Müller, A. Dworak, C. B. Tsvetanov, Prog. Polym. Sci. **32,** 1275−1343 (2007).
[15] I. Szleifer, V. V. Tsukruk, M. Urban, F. M. Winnik, S. Zauscher, I. Luzinov, S. Minko, Nature Mater. **9,** 101−113 (2010).
[16] C. Weber, R. Hoogenboom, U. S. Schubert, Prog. Polym. Sci. **37,** 686−714 (2012).
[17] Y. Zhao, Macromolecules **45,** 3647−3657 (2012).
[18] R. Takahashi, T. Sato, K. Terao, X.-P. Qiu, F. M. Winnik, Macromolecules **45,** 6111−6119 (2012).
[19] T. Sato, K. Tanaka, A. Toyokura, R. Mori, R. Takahashi, K. Terao, S. Yusa, Macromolecules **46,** 226−235 (2013).
[20] H. M. L. Lambermont-Thijs, H. P. C. van Kuringen, J. P. W. van der Put, U. S. Schubert, R. Hoogenboom, Polymers **2,** 188−199 (2010).
[21] C. Diab, Y. Akiyama, K. Kataoka, F. M. Winnik, Macromolecules **37,** 2556−2562 (2004).
[22] M. Ciampolini, N. Nardi, Inorg. Chem. **5,** 41−45 (1966).
[23] X.-P. Qiu, F. M. Winnik, Macromolecules **40,** 872−878 (2007).
[24] X.-P. Qiu, T. Koga, F. Tanaka, F. M. Winnik, Sci. China Chem. **56,** 56−64 (2013).
[25] E. Korchgiva, X.-P. Qiu, F. M. Winnik, Macromolecules **46,** 2341−2351 (2013).
[26] L. Aureli, G. Cruciani, M. C. Cesta, R. Anacardio, L. De Simone, A. J. Moriconi, Med. Chem. **48,** 2469−2479 (2005).
[27] F. J. Perrin, Phys. Radium **7,** 390−401 (1926).

[28] B. R. Lentz, Chem. Phys. Lipids **50,** 171−190 (1989).

[29] J. E. Chung, M. Yokoyama, T. Aoyagi, Y. Sakurai, T. Okano, J. Controlled Release **53,** 119−130 (1998).

[30] F. Tanaka, T. Koga, H. Kojima, N. Xue, F. M. Winnik, Macromolecules **44,** 2978−2989 (2011).

[31] R. Obeid, F. Tanaka, F. M. Winnik, Macromolecules **42,** 5818−5828 (2009).

[32] H. G. Schild, D. A. Tirrell, M. Muthukumar, Macromolecules **24,** 948−952 (1991).

[33] F. G. Prendergast, R. P. Haugland, P. J. Callahan, Biochemistry **20,** 7333−7338 (1981).

[34] H. Tanaka, Macromolecules **25,** 6377−6380 (1992).

[35] V. O. Aseyev, H. Tenhu, F. M. Winnik, Adv. Polym. Sci. **196,** 1−85 (2006).

[36] V. O. Aseyev, H. Tenhu, F. M. Winnik, Adv. Polym. Sci. **242,** 29−89 (2011).

[37] G. Zhang, C. Wu, Adv. Polym. Sci. **195,** 101−176 (2006).

[38] O. Glatter, O. Kratky, Small Angle X-ray Scattering. In Academic Press: London, 1982.

[39] T. Sato, Y. Jinbo, A. Teramoto, Polym. J. **31,** 285−292 (1999).

[40] K. Kobayashi, S. Yamada, K. Nagaoka, T. Kawaguchi, M. Osa, T. Yoshizaki, Polym. J. **41,** 416−424 (2009).

[41] P. Debye, J. Phys. Colloid Chem. **51,** 18−32 (1947).

[42] K. Kubota, S. Fujishige, I. Ando, Polym. J. **22,** 15−20 (1990).

[43] Arakawa, S.; Terao, K.; Kitamura, S.; Sato, T. Polym. Chem. **3,** 472−478 (2012).

# Chapter 5. Summary and Conclusions

The self-assembly behavior of two kinds of block copolymer systems in dilute solution with changing the amphiphilicity of the block copolymers under varing conditions was investigated. As discussed in Chapter 1, we may observe the competition between the phase separation and micellization and also the morphology transition of the micelle with changing the amphiphilicity of the block copolymer in solution. The control of the formation and dissociation of the polymer micelle, as well as the morphology of the polymer micelle is basically important, when block copolymers are utilized as nano-carriers such as the drug delivery system.

In Chapter 2, the self-assembly in dilute aqueous solutions of a mixture of an anionic-neutral block copolymer (AP) and a cationic-neutral block copolymer (MP) (cf. Figure 1-8) by changing the added sodium chloride (NaCl) concentration $C_S$ or electrostatic interactions among oppositely charged blocks has been investigated by direct observation, optical and electron microscopies, and SAXS. The ratio of the charged to neutral block chain lengths was ca. 10, and the total copolymer concentration and the mixing ratio (the mole fraction of the MP charge unit in the total charge units) of AP and MP were fixed to be 0.005 g/cm$^3$ and 0.6, respectively. With decreasing $C_S$ from 2 M to 0 M, we have found reentrant one-phase, two-phase, one-phase transitions in the aqueous solution of the AP-MP mixture. The two-phase to one-phase transition at $C_S \sim 0.5$ M arises from the competition between the macroscopic phase transition and micellization, which is the first observation in dilute block copolymer solutions. Moreover, we have found a micelle morphology transition from the bilayer vesicle to the cylindrical micelle with further decreasing $C_S$ from 0.5 M to lower than 0.05 M.

The mixing ratio dependence of the morphology of the polyion complex micelle formed by AP and MP in 0.1 M aqueous NaCl solution was investigated in Chapter 3 by using SAXS, ELS, and ITC, under the condition that the anionic and cationic block chains are much longer than the neutral block chains. When the anionic and cationic monomer units in the solution are nearly equi-molar, the net charge of the polyion complex micelle is close to zero, and the bilayer vesicle is formed. However, when the anionic or cationic monomer units in the solution are richer than the other, the polyion complex micelle is charged by including the excess block copolymer component to form the smaller spherical micelle. The morphology transition between the vesicle and spherical micelle can take place reversibly by adding AP or MP into the micellar solutions. The electrostatic energy of the micelle may induce the morphology transition.

In Chapter 4, the dehydration and self-assembly of a novel thermosensitive block copolymer consisting of poly(2-isopropyl-2-oxazoline) and poly(*N*-isopropylacrylamide) (PIPOZ-*b*-PNIPAM) (cf. Figure 1-7) upon heating were studied in water and water-methanol (MeOH) mixtures by DSC, turbidimetry, SAXS, and fluorescence depolarization. Although the difference of the phase-separation temperatures of the PIPOZ and PNIPAM homopolymers solutions is enhanced as the MeOH content in the mixed solvent increases, the DSC thermograms of PIPOZ-*b*-PNIPAM in water-MeOH mixtures are not bimodal, which indicates that the dehydration of each block does not occur independently. As a result, the amphiphilicity of this copolymer is so weak in the amphiphilic condition that the solution undergoes a temperature-induced liquid-liquid phase separation, but the micellization was difficult to occur.

In sum, the present thesis work demonstrated that block copolymers can change the morphology of their self-assembly or micelle formed in dilute solution, as shown in Figure 1-2, by altering various solution conditions or the interaction among the two block chains and the solvent. It is important to control the self-assembly morphology of block copolymers in solution, when the self-assemblies are used for applications such as drug delivery systems. This work provides basic knowledge to control the self-assembly morphology of block copolymers.

# LIST OF PUBLICATIONS

[1] R. Takahashi, X.-P. Qiu, N. Xue, T. Sato, K. Terao, F. M. Winnik, "Self-Association of the Thermosensitive Block Copolymer Poly(2-isopropyl-2-oxazoline)-*b*-poly(*N*-isopropylacrylamide) in Water-Methanol Mixtures", Macromolecules **47,** 6900 (2014). (Chapter 4)

[2] R. Takahashi, T. Sato, K. Terao, S. Yusa, "Intermolecular Interactions and Self-Assembly in Aqueous Solution of a Mixture of Anionic−Neutral and Cationic−Neutral Block Copolymers", Macromolecules **48,** 7222 (2015). (Chapter 2)

[3] R. Takahashi, T. Sato, K. Terao, S. Yusa, "Reversible Vesicle−Spherical Micelle Transition of a Polyion Complex Micellar System Induced by Changing the Mixing Ratio of the Copolymer Components", Macromolecules **49,** 3091 (2016). (Chapter 3)

**Related publications**

[1] R. Takahashi, T. Sato, K. Terao, X.-P. Qiu, F. M. Winnik, "Self-Association of a Thermosensitive Poly(alkyl-2-oxazoline) Block Copolymer in Aqueous Solution", Macromolecules **45,** 6111 (2012).

[2] T. Sato, K. Tanaka, A. Toyokura, R. Mori, R. Takahashi, K. Terao, S. Yusa, "Self-Association of a Thermosensitive Amphiphilic Block Copolymer Poly(*N*-isopropylacrylamide)-*b*-poly(*N*-vinyl-2-pyrrolidone) in Aqueous Solution upon Heating", Macromolecules **46,** 226 (2013).

[3] K. Uramoto, R. Takahashi, K. Terao, T. Sato, "Local and Global Conformations of the Flower Micelle and Flower Necklace Formed by an Amphiphilic Alternating Copolymer in Aqueous Solution", Polym. J., in press (doi:10.1038/pj.2016.49).